Florida State University Libraries

2011

Polyelectrolytes in Optoelectronics and Biomaterials

Lara A. Al-Hariri

THE FLORIDA STATE UNIVERSITY

COLLEGE OF ARTS AND SCIENCES

POLYELECTROLYTES IN OPTOELECTRONICS AND BIOMATERIALS

By

LARA A. AL-HARIRI

A Dissertation submitted to the
Department of Chemistry and Biochemistry
in partial fulfillment of the
requirements for the degree of
Doctor of Philosophy

Degree Awarded:
Summer Semester, 2011

The members of the committee approve the dissertation of Lara A. Al-Hariri defended on June 17, 2011.

_____

Joseph B. Schlenoff
Professor Directing Dissertation

_____

Rufina G. Alamo
University Representative

_____

Alan Marshall
Committee Member

_____

Oliver Steinbock
Committee Member

Approved:

_____

Dr. Joseph B. Schlenoff, Chair, Chemistry and Biochemistry Department

The Graduate School has verified and approved the above-named committee members.

*I dedicate this dissertation to
my parents,
Abdul Salam and Kayrieyeh
and to my brothers Mustafa,
Mazen, Mohamad for their endless
support and encouragement.*

*"Not everything that counts can be counted, and not everything that can be
counted counts"
Sign hanging in Einstein's office at Princeton*

ACKNOWLEDGEMENTS

discussions we had. I would like to thank Ali Lehaf in particular for all the high caffeine coffee cup moments over the years.

I feel so blessed to have the everlasting love of the most wonderful parents in the universe Abdul Salam Al-Hariri and Kayrieyeh Al-Hariri. Thank you Dad and Mom for all the hard work you did for me all these years and for your endless and unconditional love. I would never have been able to be standing here today without your hard work and scarifies. My dear three brothers Mustafa, Mazen and Mohamad you're the best brothers in this world. I cannot really find a word to show my love and gratitude for all of you. My dearest aunt Latifeh, or as you like to be called "Lolo", I am sorry for not being there for you during your latest hard days while fighting hard for life. May your soul rest in peace.

A special thank for Rana Jisr and Hasan Rifai for all the help they offered. I consider both of you to be family. Rasha Hamdan, Zahraa Khamis, Zahra Alghoul, Imad Ahmad, Abdulkader Baroudi thank you all for everything.

At a personal level I would like to thank Dr. Steve Acquah for being there during all those stressful days and for all the support you showed. Thank you Steve for drawing a smile on my face and believing in me when I myself lost hope. Cassie Smith and Luna Schmid I thank you for everything. You are among the best friends I've met through my journey in Tallahassee.

This dissertation is the summary of a journey both scientific and personal. It's now time for this journey to end and I look forward to the start of the next one, fully equipped with the skills and knowledge to progress as a Doctor of Philosophy.

Lastly, I would like to thank FSU for the opportunity. It is an honor to be a graduate from Florida State University.

Lara Al-Hariri
June, 17, 2011

TABLE OF CONTENTS

LIST OF TABLES

LIST OF FIGURES

xiii

ABBREVIATION

ALG	Alginate
AFM	Atomic Force Microscopy
A7R5	Smooth Muscle Cell Line
ATR-FTIR	Attenuated Total Internal Reflection
CMC	Carboxymethyl cellulose
CHI	Chitosan
CFU	Colony Forming Unit
DBS	Dodecyl benzene sulfonate
DMF	Dimethylformamide
DMS	Dimethyl sulfide
DNA	Deoxyribonucleic acid
ETL	Electron Transport Layer
FTIR	Fourier Transform Infra red
HTL	Hole Transport Layer
HA	Hyaluronan
ITO	Indium tin oxide
LB	Langmuir-Blodgett
LB	Luria Bertani
LBL	Layer-by-layer
LED	Light Emitting Diode
LCD	Liquid Crystal Display
MEH-PPV	2-methyoxy-5-(2-ethylhexyloxy)-1,4-phenylenevinylene)
O.D.	Optical Density
OLED	Organic Light Emitting Diode
OSRW	Orthogonal Space Random Walk
PA	Poly(acetylene)
PAA	Poly(acrylic acid)
PAH	Poly(allylamine hydrochloride)

PDAD	Poly(diallyldimethyl ammonium)
PE	Polyelectrolyte
PEG	Poly(ethylene glycol)
PEI	Poly(ethylene imine)
PEGNOPS	Poly(ethylene glycol)-4-nonylphenyl-3-sulfoproply ether
PEMU	Polyelectrolyte Multilayer
PL	Photoluminescence
PMA	Poly(methyacrylate)
PMPA	Poly((N-methyl-pyridinium-2-yl) acetylene)
PPV	Poly(phenylene vinylene)
PSS	Poly(styrene sulfonate)
PSP	Poly(sodium phosphate)
PTAA	Poly(thiophene-3-acetic acid)
PVBCl	p-poly(vinylbenzyl chloride)
PVBDMS	Poly(vinyl benzyl dimethyl sulfonium)
PVBTMA	Poly(vinyl benzyl trimethyl ammonium)
PVBTMP	Poly(vinyl benzyl trimethyl phosphonium)
PV4MP	Poly(vinyl-4-methyl pyridine)
PXDMS	Poly(xylylidene dimethylsulfonium)
PXT	Poly(xylydiene tetrahydrothiophene)
QCM	Quartz Crystal Microbalance
RGD	arginine-glycine-aspartic acid
SAM	Self-Assembled Monolayer
SDS	Sodium Dodecyl Sulfate
SEC	Size Exclusion Chromatography
SPAn	Sulfonated poly(aniline)
SPR	Surface Plasmon Resonance
SMRCA	Six Member Ring Cyclic Anhydride
THT	Tetrahydrothiophene
TMP	Trimethyl phosphine
TMA	Trimethyl amine

ECM   Extracellular Matrix (ECM)

ES   Ethane sulfonic sodium

EL   Electroluminescence

ABSTRACT

Polyelectrolyte multilayers are built by the alternating deposition of oppositely charged polymers from solutions onto a substrate. The physical and chemical properties of the multilayers can be controlled by the polyelectrolyte combination, the build up, and the post-build up conditions. The demands of novel material coatings that could be used at the surface of biomedical devices and nano-assemblies that can be used in optoelectronic devices are the trigger for material scientist to explore the new research areas. Polyelectrolyte multilayers are investigated in an aim to fulfill the spectrum of needs ranging from biomaterial to optoelectronic field.

In this dissertation, the thermal elimination of a water soluble poly(xylylidene) precursor to poly(phenylene vinylene) (PPV) is investigated using small and macro-counterion. The aqueous route to PPV is investigated to yield high photoluminescence efficiency at low elimination temperature. The polyelectrolyte multilayers terminated with different heteroatom polycations interaction with cells is investigated for application as a coating for stent.

Fluorescence, UV-vis and Fourier transform infra red spectroscopy were used in order to investigate the optical properties of PPV. PPV elimination was accomplished in air at 80 °C using the macro-counterion poly(ethylene glycol)-4-nonylphenyl-3-sulfoproply ether (PEGNOPS). The route to PPV using PEGNOPS was low on carbonyl content, with a possible contribution from PPV chain separation. The PEGNOPS precursor showed no carbonyl formation on long term storage in contrast to other counterions.

Orthogonal Space Random Walk (OSRW) was performed to understand the exceptionally low temperature (80 °C) required for thermal conversion of PPV precursor containing PEGNOPS. Simulations of the solvent free-system converged for starting points where the backbone was expanded or compressed. The simulation revealed the ability of PEGNOPS to partially pre-order the precursor chain in a conformation that favors the E2 elimination.

The elimination mechanism of poly(xylydiene tetrahydrothiophene) (PXT), precursor to PPV, in assembly in polyelectrolyte multilayers was investigated using FT-IR. PXT assembly with poly(styrene sulfonate) (PSS) and poly(acrylic acid) (PAA) as a polycation were investigated.

The heteroatom effect on polyelectrolyte multilayer assembly was explored. Polycations having the same charge density, molecular weight, and molecular weight distribution were employed for multilayer assembly. The polycations differed only in the heteroatom on which the positive charge resided. The three multilayers terminated with the three different polycations poly(vinyl benzyl trimethyl ammonium) (PVBTMA), poly(vinyl benzyl trimethyl phosphonium) (PVBTMP) and poly(vinyl benzyl dimethyl sulfonium) (PVBDMS) had similar build up characteristics, hydration and wettability. The interaction of the smooth muscle cells (A7r5) with the PVBTMA, PVBTMP and PVBDMS terminated multilayers was investigated. The PVBTMA and PVBTMP are cytophobic to A7r5 cells whereas the PVBDMS multilayer is cytophilic. The effect of UV sterilization of the PVBDMS multilayer on cell interaction was explored.

CHAPTER 1

INTRODUCTION

1.1 Polyelectrolyte Definitions and Applications

Polyelectrolytes are macromolecules that have many ionizable side chain groups. A polyelectrolyte (PE) can be natural (polysaccharide, protein and deoxyribonucleic acid (DNA)), naturally modified (carboxymethyl cellulose) or synthetic. The PEs can also be cationic, anionic or amphophilic (has combination of positive and negative charge on the same or different monomer). Synthetic PEs can be synthesized either from the charged monomer unit (e.g. polymerization of styrene sulfonate) or by modifying a pre-existing polymer (e.g. sulfonation of polystyrene). Naturally modified PEs are obtained via modification of the naturally occurring polymer. The solubility of PEs (natural or synthetic) are different than that of their corresponding neutral polymer; which can be soluble in polar solvents whereas its neutral form is non soluble in polar solvents. They are sensitive to ionic strength; as the ionic strength increases the charges on the PE are shielded by the salt, decreasing repulsion between the same charge which results in contraction of the extended PE chain that exists at low ionic strengths. The three main classes of polycations are ammonium ($1°$, $2°$, $3°$ and quaternary), sulfonium and phosphonium. The fact that most of these PEs are used in industrial products reduced the number of publications on their synthesis and applications because research is typically withheld in highly competitive laboratories. Synthetic and naturally modified polycations gained a lot of interest due to their intrinsic properties that made them candidates for water and wastewater treatment from the dyeing industry,[1,2] soaps,[3] cosmetics,[1, 3, 4] paper,[4] and food industry.[4] The most industrially used polyanion is carboxymethyl cellulose (CMC). Being non-toxic and non-allergic, CMC is used to increase the viscosity of drinks, stabilizing emulsion in ice creams, and is used with cement as a fluid-loss control additive. A new era began when research focused on using these polyelectrolytes in their film-solid form. This work focuses on the nanoscale thin film form of polyelectrolytes in both optoelectronic and

biomaterial fields. In optoelectronics, the electroluminescent polymer precursor route is subjected to extensive research to enhance the photoluminescence of the polymer. The intrinsic properties of the polyelectrolyte films that affect their interaction with cells and bacteria have been a step toward cytophobic anti-bacterial coatings.

1.2 Polyelectrolyte Multilayer (PEMU) Films

Langmuir-Blodgett (LB) films, invented by Langmuir and Blodgett,[5,6] and the self-assembled monolayer (SAM), invented by Nuzzo and Allara,[7] were the early techniques developed for immobilization of proteins and cells for applications in drug delivery and tissue engineering field. The disadvantages of LB technique are the films limited stability due to the weak physical interaction, the requirement of expensive instrumentation, amphiphilic requirement of molecules, and long fabrication time.[8] The drawbacks of the SAM technique are the instability of the film under ambient conditions, limited substrate choice (thiol adsorbs onto noble metal only), and its ability to form only one layer.[8] Thus there was a need for a simpler, versatile surface modification method in which a broad spectrum of molecules can be involved. Layer-by-layer (LBL) assembly was first described by Decher et. al. in 1992 as an alternating assembly of oppositely charged PEs to form ultrathin films.[9,10] In the last decade, LBL assembly has been used to construct multilayers from almost anything: PE, uncharged polymers (via hydrogen bonding),[11,12] inorganic (divalent metal phosphate),[11] nanoparticles (quantum dots),[13] and natural PE (protein, DNA).[13] LBL films simplicity of construction, the film stability (at physiological salt and pH, film decomposes at 2.5 M KBr), and the high efficiency in producing a uniform film are some of LBL technique advantages. The films formed using the simple LBL assembly technique offers a control over the composition and architecture at the nanoscale level for films that can be used by itself or as a coating for another material to alter its properties for a better performance in potential applications. The ability to integrate diverse functionality without significant alteration of their chemical or electrical properties to the assembly broadens the spectrum of potential applications for the films. Currently, PEMU are used in optoelectronic,[14] separation,[15-17] anti-fouling,[13, 18] and corrosion applications, and have been used for years.[13,14] The

ability to precisely build PEMU films with control over film thickness, morphology and functionality on the outmost layer provides the opportunity for these films to be used in the fields of biomedical research, biotechnology, and drug delivery.

In the PEMU field the most used polycations for ammoniums poly(diallyldimethyl ammonium (PDAD), poly(vinyl-4-methyl pyridine) (PV4MP), poly(allylamine hydrochloride) (PAH), for sulfonium (poly(xylylidene tetrahydrothiophenium) (PXT), poly(xylylidene dimethylsulfonium) (PXDMS)) and for phosphonium DNA is the only polycation used in PEMU field (Figure 1.1). Although DNA is expensive, it was used for biotechnology application and as a proof of concept that even naturally occurring PE can be integrated in PEMU.[19] Ranging from primary to quaternary, poly(ethylene imine) (PEI) is mainly used as an anchoring pre PEMU build step on substrates since it was proved to enhance PEMU assembly.[20] PXT and PXDMS gained their importance from the fact that they are precursors for the electroluminescent conjugated polymer poly(phenylene vinylene) (PPV) that is used in optoelectronic applications (organic light emitting diode (OLED), solar cells). The most commonly used polyanions are poly(styrene sulfonate) (PSS), poly(acrylic acid) (PAA) and CMC. PSS with a sulfonate functional group is used as strong base (pH independent), PAA (weak base, pH dependent), and CMC.

The availability of well developed thin films characterizing techniques for both in-situ and ex-situ methods made it possible to enhance developments in field of the thin films. To name some of these techniques: Quartz Crystal Microbalance (QCM), Surface Plasmon Resonance (SPR), Atomic Force Microscopy (AFM), Attenuated Total Internal Reflection Fourier Transform spectroscopy (ATR-FTIR), Ellipsometry and UV-vis spectroscopy.

Figure 1.1 The common polyelectrolytes used in multilayers the polyanions (PAA, CMC, PSS) and polycations (PDADMA, PXT, PXDMS, PAH, PV₄MP, PLL and PEI).

1.3 Mechanism of Polyelectrolyte Multilayer Build up

The LBL process involves the dipping of the charged substrate into solutions of a polycation and a polyanion for a certain time. During each dip, the polyelectrolyte is adsorbed on the oppositely charged surface and the charge is mitigated and the surface charge is altered. Three rinse steps are done after each polyelectrolyte step to remove any excess loosely attached polyelectrolyte (Figure 1.2). The excess charges on the surface are compensated by counterions; reversing the surface charge was proven by surface force measurements and zeta potentials.[17, 21-23] The PEMU assembly is driven by the entropy gained from the release of ions upon the association between the polycation and the polyanion. In PEMU, the association is mainly governed by electrostatic forces. The PE adsorption is kinetically irreversible on the time scale of assembly unless one of the PEs used is of relatively small molecular weight (Mw of less than 10,000) or the interaction between PEs is weak due to relatively high salt concentration. The PEs, used in PEMU, have the ability to inter-diffuse to varying level to the other layers therefore the PEMU has rather a fuzzy non-stratified nature. PEMU in which the PEs are locked (non inter-diffusable) are known to follow the linear growth regime, the labile PEs (inter-diffusable) follow the exponential regime.[24] The rearrangement of the PEMU bulk is possible by inducing extrinsic sites inside it; e.g: addition of salt. Extrinsic sites are the association of polyelectrolyte in a PEMU with small counterion of salts (e.g: Na^+, Cl^-); intrinsic sites are the association of oppositely charged PE in the PEMU. The addition of salt to the PEMU is represented by the following equilibrium.

$$Pol^+ Pol^-_m + y\, Na^+_{aq} + y\, Cl^-_{aq} \rightleftharpoons (1\text{-}y)\, Pol^+ Pol^-_m + y\, Pol^+ Cl^-_m + y\, Pol^- Na^+_m \qquad (1.1)$$
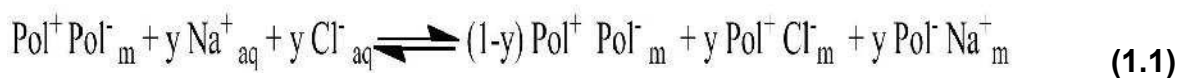
The term Pol^+Pol^- represents the intrinsically charge compensated PEs, ($Pol^+ Cl^-$) and ($Pol^- Na^+$) are PEs extrinsically compensated by salt counterions and "m" is used to refer to a multilayer. As Equation (1.1) implies, the addition of salt breaks part of the

intrinsic sites, consequently inducing the mobility of the PEs. The mobility of the PE, in PEMU, perpendicular to the substrate is known as interdiffusion [24] and that parallel to the surface is known as PEMU smoothing.[25]
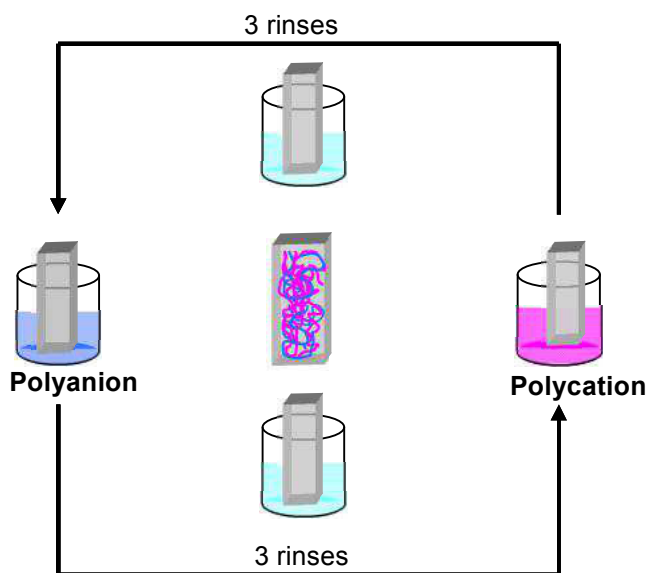
Figure 1.2   A representation of the formation of a PEMU on a charged surface. The fuschia and blue correspond to the polycation and polyanion, respectively.

1.3.1 PEMU Mode of Growth: Linear and Exponential

The two modes of growth of PEMU are linear and exponential.[18] As the name indicates, linear growth is referred to PEMU in which the thickness increases linearly with the number of deposited layers and the thickness increment is constant for each deposition. This mode is typically due to the limited interpenetration of the PE in PEMU, in which the PE is able to interpenetrate only to its neighboring layers. In the exponential growth mode, the thickness increment is not constant for each deposition and is expected to be higher than that with linear growth. In the exponential mode, at least one of the PE has the ability to interdiffuse through the PEMU.[26] The exponential growth is usually observed for polyaminoacids, polysaccharides (poly(L-lysine) (PLL), hyaluronan (HA), alginate (ALG)) and poly(acrylic acid) (PAA) PEMU.[18, 27] It was observed that even linear growth can be altered to an exponential one upon the

6

increase in temperature or NaCl concentrations.[28,29] Recently, Cini et. al. described for the first time a concentration (of the PE) dependent regime mode growth PEMU built of short poly(sodium phosphate) (PSP) and PAH. The PSP/PAH PEMU follows a linear growth regime at low concentration (10^{-5} and 10^{-4} M) and an exponential growth regime at 10^{-3} M.[30]

1.3.2 Salt Concentration Effect on PEMU

The addition of salt to the build up solution, of the PEs, results in the breakage of the electrostatic cross-links between PEs in the PEMU. The extent of the cross-links breakage depends on the salt concentration, extent of hydration and the hydrophobicity of the PEs. The less hydrated the salt, the higher its ability to break the cross-links, which is known as the doping effect. The more hydrated the salt, the more it will be subject to a higher entropy when losing the water to pair with one of the PE pairs.[31] The more hydrophobic the PE pairs in the assembly the harder to be doped e.g. PSS/PAH.[31] Schlenoff et. al. reported the swelling of PEMU with extensive list of salts.[31] The ability to alter the thickness of the PEMU and its elastic modulus in a straightforward method, by the addition of salt, is an advantage of PEMU in many applications.

1.3.3 Molecular Weight (Mw) Effect on PEMU

At high Mw (Mw > 10,000) the effect on PEMU characteristics is minimal.[32] Few studies on the effect of the Mw, especially for natural PE, on PEMU characteristics are available in literature due to the difficulty of finding a mono disperse naturally occurring PE.[32] An increase in PEMU thickness was recorded with the increase of the Mw of CHI and HA. For synthetic PEs, Lynn et. al. reported that PEMUs of PAH/PAA approached an exponential growth as the Mw of PAA decreased.[33] Sui et. al. showed that construction of PEMU from low Mw (as low as 10,000) of PSS and P4VP caused stripping of the quasisoluble complex formed on the surface and resulted in a decrease in the thickness.[32] PEMU from the same PE but higher Mw resulted in a higher thickness PEMU.

1.3.4 Effect of pH on PEMU Buildup

Since PEs in PEMU are electrostatically bonded, the degree of ionizability of the PEs (charge on the PE) has an effect on the strength of association and the characteristics of the PEMU. The pH effect is more pronounced for weak acid or base PE (e.g. PAA, PMA and PAH). In case of partially charged PAA and PAH a non-linear growth was observed.[34] It was found that the thickness of the PEMU of weak polyacid and polybase combination dramatically depends on pH.[35]

1.3.5 Temperature Effect on PEMU

Salomäki et. al. showed the effect of temperature on the assembly of the PEMU.[29] A 5% increase in the mass deposited was observed per 1 °C increase near room temperature.[29] The changes in temperature during the build up also have a pronounced effect on the mode of growth. The PEMU buildup is independent of the temperature change for the primary layers (the first 3 layers).[29]

1.4 Background on Biomaterials

Biomaterials are defined as materials implanted into the body to replace an organ or imitate the function of an organ that interacts positively with the biological systems (e.g: eye contact lens, artificial hip replacement). Biomaterials have a tremendous importance in saving lives, enhancing the quality of human life and have significant economic implications. The two major requirements for a successful biomaterial are: 1- The match between the mechanical properties (strength of material) of the implant and that of the organ to be replaced depending on its role in the body e.g: hip implant should have a high modulus. 2- The biocompatibility of the implant which is the positive response of the body to the implant. The biocompatibility mainly depends on the surface properties of the implant. Therefore, it is critical to understand how different materials interact with the body. Since the field of biomaterials is developing at a quick pace, the definition of biocompatibility is dynamic. Biocompatible materials were first defined as materials that do not leach biologically toxic substances when implanted into the body. The most recent definition extends to materials that have a synergistic response to bodily functions. The body responds almost similarly to all materials (non toxic leaching

materials) by what is known to be the "foreign body reaction". The foreign body reaction is a series of cascade reactions that takes place when a material is implanted in the body which results in an implant encapsulated in an acellular, avascular collagen bag (Figure 1.3).[36] This encapsulation prevents the interaction between the implant and the surrounding tissue which may seriously affect its performance in the body. The first reaction in that series is the non specific protein adsorption on the surface of the implant, that occurs via various kinds of bonding (electrostatic, hydrophobic and hydrogen bonding). Unlike the specific protein adsorption that usually takes place during normal wound healing, the non-specific adsorption involves conformational changes of the protein and reversible adsorption to the surface. In a scenario where a wound is produced, the macrophage cells clean the wound (bacteria and damaged cells) by phagocytosis followed by activation of the healing cell types (fibroblast). In the case of the implant, the body identifies these proteins as invaders and the macrophages adhere to the implant trying to phagocytose it which is hampered by the size of the implant in most of the cases. At this stage, the macrophages fuse as one big cell to engulf the implant resulting in the formation of a collagen capsule around it. Therefore, the inhibition of the non-specific adsorption of proteins may help in enhancing the ability of the body to identify the implant as part of it. In light of the above, the anti-fouling surfaces that prevent non-specific protein adsorption proved attractive to researchers in biomaterial and biomedical field.
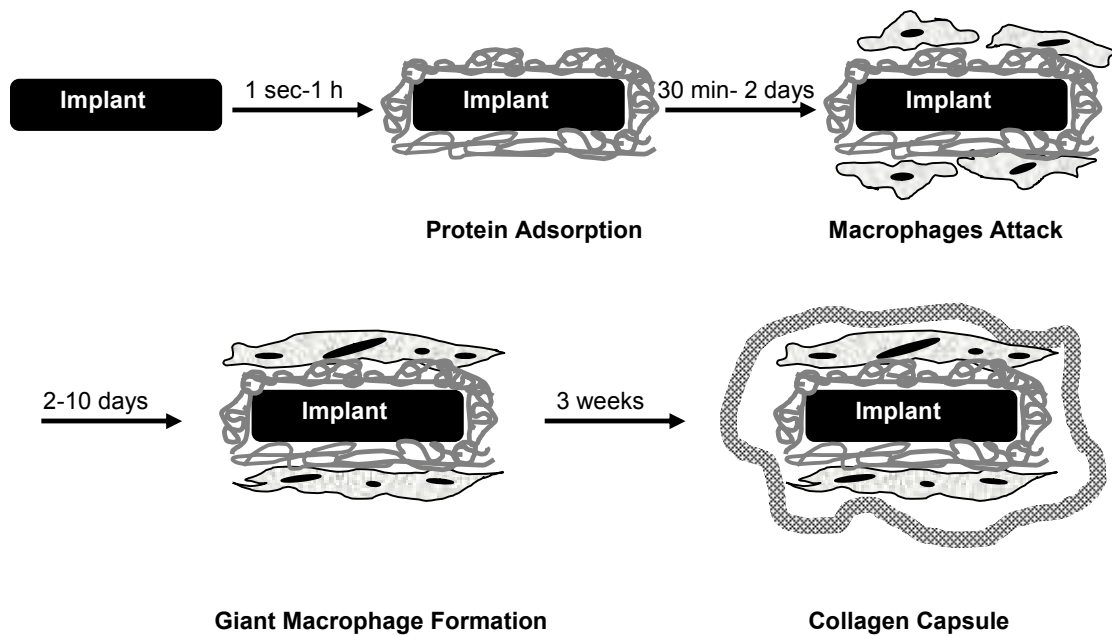
Figure 1.3 Schematic diagram illustrating the foreign body reaction against an implanted material from 1 sec to 3 weeks.

1.4.1 PEMUs in Biomaterials

Since the surface of the material is the first contact for the interaction between biomaterials and the body, considerable research has been dedicated to modify surface properties of materials to render it more biocompatible. Work has been done to figure out the critical variables that make the PEMU either cytophobic or cytophilic without excluding those that may render the PEMU anti-bacterial. The cytophobic films are used to enhance the biocompatibility of the implant while cytophilic coatings are developed for potential use in tissue engineering to enhance cell growth. In addition to their use in both tissue engineering and enhancing biocompatibility of materials, PEMU was found to be useful as a reservoir for DNA delivery.[33] The effect of the bulk and surface properties of the PEMU on the cell interaction have been studied: the surface charge of the PEMU,[37] the roughness, the stiffness,[38-40] the nature of PE (synthetic or natural), and the hydrophilicity.[41] Olenych et. al. reported that A7r5 cells adhere to the negatively charged PEMU rather than positively charged and zwitterionic ones.[37] Many reports assured that cells prefer stiff films compared to low modulus ones (mainly gel-like). The

stiff films are achieved by photo or chemical cross-linking of the film.[18] Another study by Salloum et. al. showed that A7r5 cells prefer hydrophobic surfaces compared to the hydrophilic one. Anti-bacterial PEMUs have been developed by employing two methods: 1- PEMU terminated with PE with anti-bacterial activity (most polycations have anti-bacterial activity) 2- Complexing the PEMU with one of the well known anti-bacterial agents (eg: Ag nanoparticles, Ag^+ ions, hydrophobic polypeptides).[42,43] One of the challenges in the biomedical field is the blood coagulation on catheters during surgeries or implants in contact with blood (artificial arteries). The PEMUs terminated with chitosan and heparin possessing anti-thrombogenicity effect showed improved anti-coagulation properties when used as coatings on stainless steel coronary stents.[44] Therefore the field has expanded to the exploration of higher performance anti-bacterial cytophobic and cytophilic PEMUs for biomaterial field.

1.5 Background on Optoelectronics

In 1977 a collaboration between Shirakawa and Heeger yielded the first conducting polymer, poly(acetylene) (PA), via p-type doping.[45] The reported PA was achieved by a mistake in the ratio of the Ziegler Natta reaction. Following that work, an explosion of research on synthesis, characterization and application of conjugated polymer was done. In 1990, Burroughes et. al. wrote a letter to "Nature" about poly(phenylene vinylene) (PPV), the conjugated polymer: "*The response of the system to electronic excitation is nonlinear-the injection of an electron and a hole on the conjugated chain can lead to a self-localized excited state which can then decay radiatively, suggesting the possibility of using these materials in electroluminescent devices*".[46] The above discovery introduced a new class of conjugated polymers known as electroluminescent polymers defined as conjugated polymer that emits in the visible region of light when subjected to electric field. The discovery of electroluminescent polymers shifted the field of conjugated polymers from their applications in non-metallic semiconductors to a competitive candidate in the optoelectronic field especially light emitting diodes (LEDs).

LEDs are classified based on the material used in their emissive layer: inorganic semiconductors (eg: gallium phosphide, zinc sulfide), organic small molecules (fluorescent and phosphorescent dyes), and polymers. The last two kinds are known as OLEDs. The first efficient LED using small organic molecules was prepared by Tang et. al. in 1987.[47] OLEDs are nano-electronic electroluminescence devices, 100 to 500 nm thickness (Figure 1.4). OLEDs are self luminous devices in which light is emitted by applying an electric field without the need for a backlight. OLEDs can be used in many display applications example computers, mp3 players, etc. Unlike Liquid Crystal displays (LCDs) which needs a backlight, OLEDs usually composed of an anode, cathode, emissive layer, hole transport and electron transport layers (Figure 1.4). The OLEDs have superior properties to that of LCDs being thinner, having a wider angle field of view, lighter in weight, brighter in color, easier to be applied to larger areas, and fewer processing techniques.

LEDs function along the same principle. When an electric field is applied, electrons are injected from the cathode through the electron transport layer (ETL) under the effect of the applied electric field (Figure 1.5). The holes (positive charges) are injected from the anode and move toward the emissive layer through the hole transport layer (HTL). Both electrons and holes combine to form a neutral excited state called an exciton. The life time of an exciton depends on its band gap, or the energy difference between the HOMO and the LUMO energy levels. The energy released from exciton formation excites the emissive layer which releases this energy depending on the band gap of the molecules emissive layer. Part of this energy is released as the displayed light of the emitting device which is in the visible region.
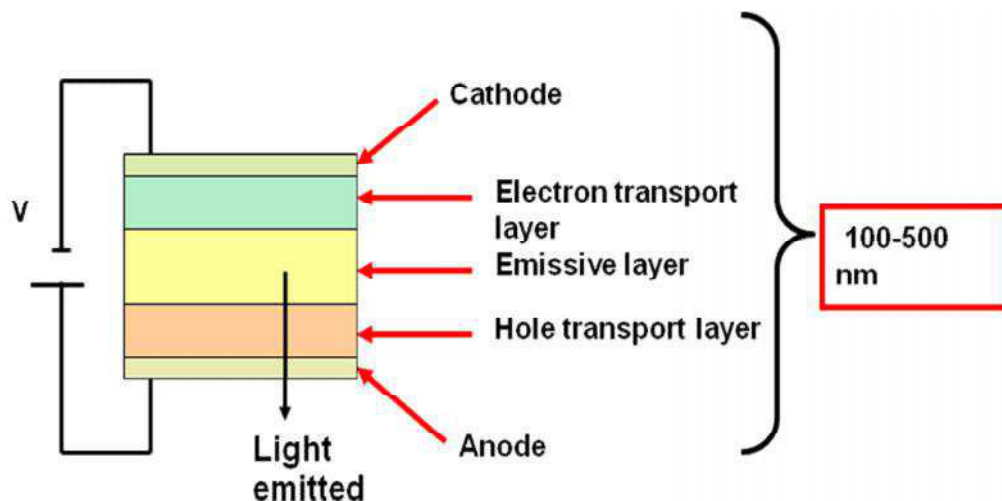
Figure 1.4   Schematic representation of OLED which consists of cathode, an electron transport layer, an emissive layer, a hole transport layer and an anode.
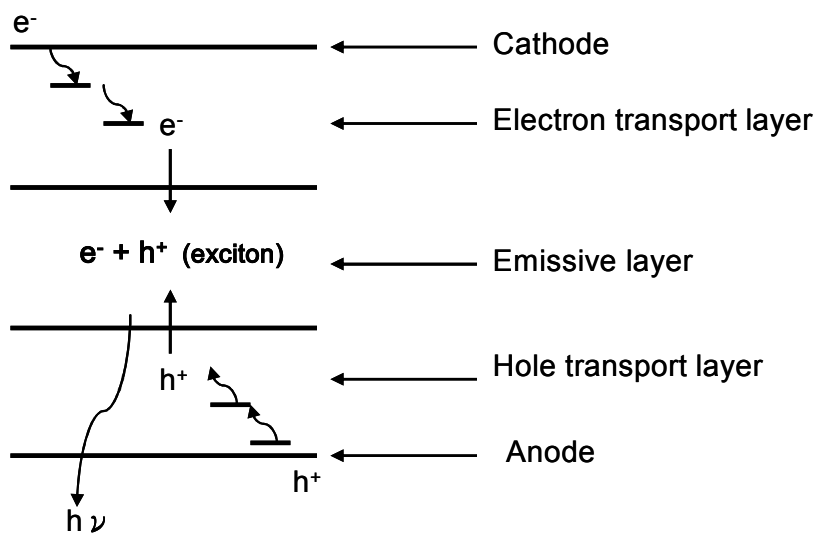
Figure 1.5   Schematic representation of how an OLED works.

A critical step in OLED assembly is the deposition of the emissive layer. Vapor deposition and solution coating (casting) are ways to deposit the emissive layer. The vapor deposition method requires an oxygen and humidity free blanket during the deposition of the organic molecules that is sometimes hampered by the crystallization of

the molecules which affects OLED efficiency. Another drawback of the vapor deposition is the lack of reliability of the deposited film thickness. The solution coating method requires polymer to be soluble which is not the case for most conjugated polymers.

The processability of the conjugated polymers can be improved by using one of the following strategies:

1-Using oligomers of the conjugated polymers results in a reduced electroluminescent emission due to the shorter length of conjugation.[48]

2-Adding soluble side chains to the conjugated backbone e.g: 2-methyoxy-5-(2-ethylhexyloxy)-1,4-phenylenevinylene (MEH-PPV).[49]

3-Using a polyelectrolyte (polyanion or polycation) conjugated polymer eg: poly(thiophene-3-acetic acid) (PTAA), sulfonated poly(aniline) (SPAn), poly((N-methyl-pyridinium-2-yl) acetylene) (PMPA).[50]

4-Precursor route in which the conjugated polymer is obtained in situ by thermal annealing of the film e.g: poly(xylyidene tetrahydrothiophene) (PXT).

The aqueous route is the most studied one and the PXT precursor has been the most promising one. As a proof of concept Ferreira et. al. successfully fabricated, by LBL assembly, different combinations of polycations/polyanions that include conjugated/conjugated polyions, conjugated/nonconjugated, and precursor polymer/conjugated polyions. For simplicity, the emissive layers' optical properties have been studied separately without the whole OLED assembly. The LBL method allows the control over the electrode interface and of the combination zone which is critical for the device performance.[51-52] For example, Onitsuka et. al. reported a higher efficiency of the device when the polyanion (insulating layer) was in contact with the Al electrode rather than the light emitting polymer (PPV).[51]

1.5.1 PXT Synthesis and Elimination

1.5.1.1 PXT Synthesis

Although it is not the only method, poly(phenylene vinylene) (PPV) is usually prepared from the thermal annealing of one of its precursors. Although all of them have the same backbone and differ only in the leaving group, PXT is not the only precursor to PPV e.g: dimethyl sulfide, alkyl sulphonyl and alkyl sulphinyl.[53] The monomer of PXT is freshly prepared (Figure 1.6 A) from bis (tetrahydrothiophenium-p-xylene) chloride. The

shelf time of A is short due to the presence of tetrahydrothiophene (THT) a good leaving group. The polymerization reaction mechanism is not known but in literature reports suggest either radical or anionic mechanism.[54] Figure 1.6 shows the anionic mechanism of PXT synthesis. The polymerization is usually quenched by an acid, the conjugate base of which is the counterion of PXT. Using this method high molecular weight PXT is formed, around 100 KDa, the gel formed during polymerization is broken by mechanical stirrer.
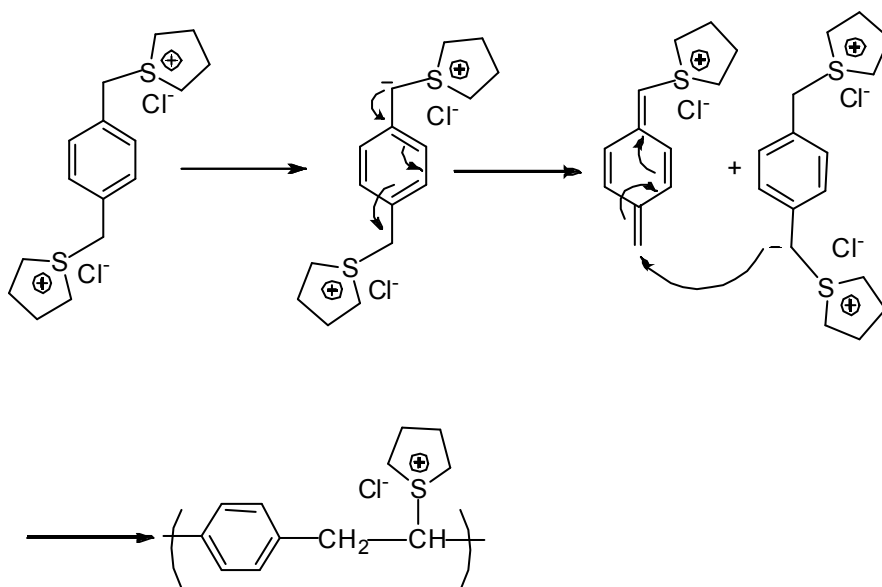
Figure 1.6   Shows the anionic mechanism for PXT synthesis from its monomer.

Impurities are excluded through purification by dialysis e.g: salt, monomer and oligomers of PXT. Figure 1.7 shows some of the possible chemical defects that could be formed prior to and after thermal annealing of PXT and/or the PPV backbone. Since THT is a good leaving group it can be substituted by Cl⁻ and OH⁻ ions which are good nucleophile (unit c and b Figure 1.7 respectively). Hydroxide is usually added to initiate polymerization whereas Cl⁻ is from HCl that is added to quench the polymerization. The defects (units b and c Figure 1.7) cause the break in conjugation in case their elimination temperature is higher than that of PPV thermal annealing. These defects can be removed by undergoing the reaction at higher temperature. Carbonyl defect (unit a Figure 1.7) will be discussed in details in Chapter 3.

15
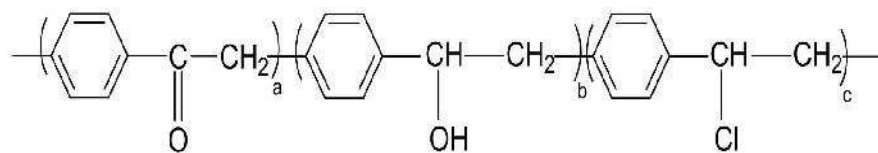
Figure 1.7 Possible chemical defects on PPV formed prior to, during or after thermal annealing of the PXT precursor. a) backbone oxidation to yield carbonyls b) hydroxide substitution during synthesis c) chloride substitution during storage.

1.5.1.2 PXT Elimination

The preparation of PPV from PXT is achieved by thermal annealing (Figure 1.8). The temperature at which the elimination is performed is critical to avoid defect formation (mainly carbonyl) in the backbone and be suitable to the materials, assembled with PXT in optoelectronics that may be affected by temperature. The optical properties of the PPV, prepared via the aqueous route, depend on the percentage of elimination (length of conjugation) where many factors are involved. The inter-chain and defect quenching are two factors that dramatically affect PPV optical properties. These two factors are shaped by the orientation of the conjugate segments, the extent of disorder of the backbone, the temperature of elimination, the elimination environment (under vacuum, inert gas blanket), and the counterion. The mechanism of elimination is discussed in Chapter 4. Details about the different factors that influence optical properties are discussed in Chapter 3, 4 and 5.
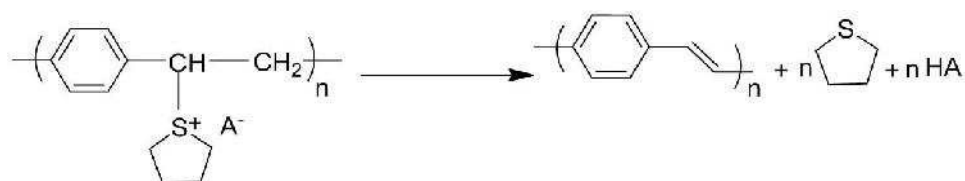
Figure 1.8 The precursor route to PPV.

1.6 Dissertation Outline

Details on the instruments and the techniques used in this work are described in Chapter 2. The experimental details of the methods and chemicals used are provided in each subsequent Chapter.

In Chapter 3, the thermal elimination of a water soluble precursor (PXT) to PPV is studied and films of PXT with different counterions are assembled. The optical properties of these films are studied using FT-IR, UV-vis and Fluorescence spectroscopy. The effect of counterions on the stability of PXT during storage is addressed. A defect free and low temperature conversion route to PPV is achieved by using the macro-counterion poly(ethylene glycol)-4-nonylpheny-3-sulfo-propyl ether (PEGNOPS) in the processing.

In Chapter 4, a coordinated experimental and simulation molecular dynamic are performed to understand the exceptionally low temperature thermal conversion of PPV starting from PXT-PEGNOPS. The ability of the macro-counetrion to partially pre-order the precursor chain in a confirmation that favors the E2 elimination pathway is discussed.

In Chapter 5, multilayers of PXT with a carboxylate and sulfonate polyanion are fabricated and their optical properties are examined. The differences in the mechanism of elimination of PXT to PPV using these two polyanions are discussed.

In Chapter 6, the synthesis of polyelectrolytes having the same charge density, molecular weight, and molecular weight distribution and differ only in the heteroatom on which the positive charge resided are performed. The characterization and stability of the polycations are done by NMR and FT-IR. The differences between polyoniums are explored by following their layer-by-layer assembly with two polyanions. The dry and wet thickness, wettability and roughness of the films are reported.

In Chapter 7, the effect of the polyonium terminated multilayers on the adhesion of smooth muscle cells A7r5 is studied using live cell imaging. The bacteria adhesion to the polyonium multilayers is studied using the Live/Dead assay. The cytoxicity of the polyonium solutions on both A7r5 and bacteria are evaluated using alamar blue assay.

CHAPTER 2

INSTRUMENTATION AND EXPERIMENTAL METHODS

2.1 Polyelectrolyte Multilayers Build up

All multilayers were assembled by using a robot (StratoSequence V, Nanostrato Inc.) (Figure 2.1). The substrates that were used to build up multilayers on are either silicon wafer or quartz slide. The robotic platform holds the beakers containing the polyelectrolyte solutions and the water rinsing solutions (Figure 2.1). The platform moves up and down dipping the substrate in the solution in a known automated order for a controlled dipping time. The substrate was dipped in the first polymer solution for 10 minutes followed by three consecutive rinses in water each for one minute. Then the substrate was dipped in the second polymer solution for another 10 minutes followed by another three consecutive rinses of water (Figure 1.2). The build up of a bilayer (two layers of oppositely charged polyelectrolyte) took a total of 26 minutes. The details about each polymer solution concentration are mentioned in the Experimental Section of each chapter. All substrates (silicon wafers, quartz slides and sapphire round slides), unless mentioned somewhere else, were subjected to a cleaning step before any coating using piranha (7/3 H_2SO_4 (36 M)/H_2O_2: piranha is a very strong oxidizing agent handle it with caution) for 20 min, rinsed with distilled water to get rid of piranha traces then dried using a gentle stream of nitrogen. For all the multilayers throughout this work the substrate was primed with a layer of poly(ethylene imine) (PEI) by dipping it for 20 min in 10 mM solution, rinsed with water and dried with stream of nitrogen before any further multilayer build up.
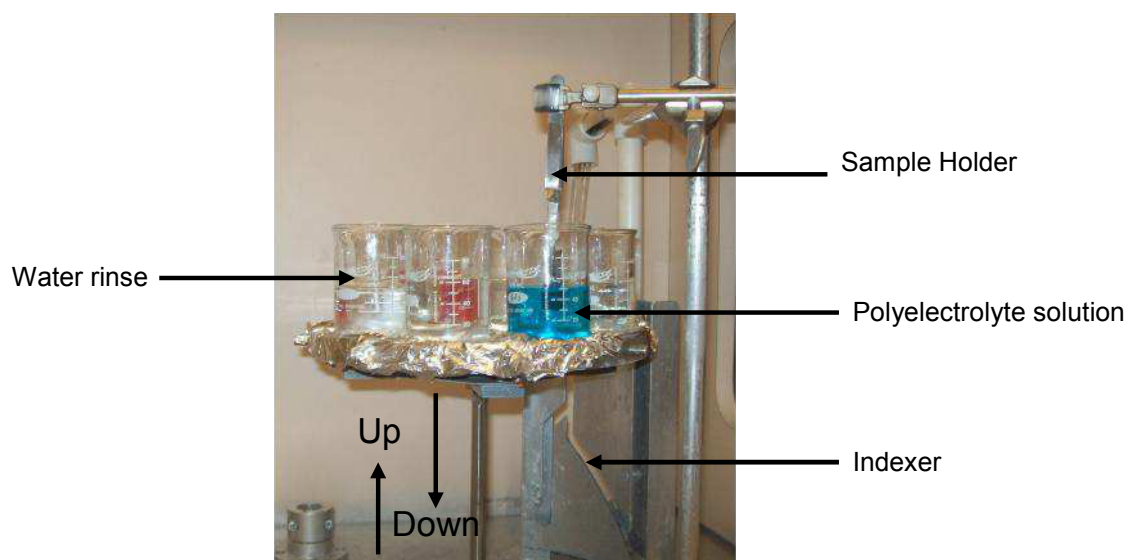
Figure 2.1 The NanoStrata sequence V Robot used for polyelectrolyte multilayers assembly.

2.2 Multilayer Thickness Measurements

Ellipsometry[55] is a non-destructive optical technique to measure the refractive index and indirectly the thickness of an ultrathin film ranging from 1 Å to 1µm. Ellipsometry is based on the fact that the light reflected from a surface experiences a change in its polarizability.[56] The polarizability of an elliptically polarized light is analyzed after it is reflected from the sample surface. The change in the polarizability is a characteristic of the surface structure and the material of the film. Ellipsometry usually measures the change of the amplitude (ψ) and the relative phase change ($\triangle$), which is the change between the orthogonal and the parallel vectors of the polarized light of a certain wavelength and angle of incidence. ψ is the measure of the change of the absolute values of the reflection coefficient of the orthogonal and the parallel vectors.

The thickness and refractive index of the polyelectrolyte multilayer (PEMU) was measured by a Gaertner Scientific L116S auto gain variable Stokes ellipsometer with a He-Ne laser of 632.8 nm wavelength and at a fixed incident angle 70º. A StokesMeter[TM] with four stationary detectors is used to analyze the laser beam and give the ψ and $\triangle$

values. The LGEMP software calculates the thickness and refractive index of the sample using Equation 2.1.

$$\frac{r_{TM}}{r_{TE}} = \tan\psi \; e^{i\Delta}$$

(2.1)

Where r_{TM} is the reflectivity of the magnetic field that is perpendicular to the direction of propagation, r_{TE} is the reflectivity of the electric field that is perpendicular to the direction of propagation.

2.3 Surface Analysis Techniques

2.3.1 Dynamic Contact Angle (DCA)

The contact angle[57] of a material (film) with a liquid gives an idea about the material wettability which is an attribute of films. The contact angle is defined geometrically as the intersection angle between solid, liquid and gas when a liquid droplet is sitting on top of the film (Figure 2.2). A contact angle higher than 90º indicates that the surface is of low wettability. If the contact angle is lower than 90º the surface is of high wettability, a zero contact angle indicates a complete wetting of the surface.
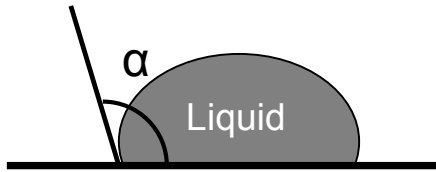
Figure 2.2   The contact angle (α) of the surface with the liquid.

The dynamic contact angle is done using the ThermoCahn dynamic contact angle analyzer using the force tensiometry. The instrument is consisted of a sensitive balance, moving sample holder and a stage that holds the liquid container used in the test. The sample that will be subjected to dynamic contact angle measurement is hooked to the sample holder and tarred. While the sample is moving in and out of the liquid, the force (Fwet) is measured by the balance. The buoyancy force and the weight

of the sample are canceled by extrapolating to zero depth and tarring, respectively. The contact angles are calculated using Equation 2.2.

F_{total} = Wetting force+ Weight of probe - Buoyancy

$F_{wet} = \gamma\ P\cos(\alpha)$ **(2.2)**

γ is the surface tension of the liquid, usually measured using the Wilhelmy plate. For water, the surface tension is 72.3 mN m^{-1}. P is the perimeter of the sample (width and length). The advancing angle is the maximum angle measured when the sample touches the liquid (Figure 2.3). The receding angle is the minimum which is measured when the sample is withdrawn from the liquid (Figure 2.3).
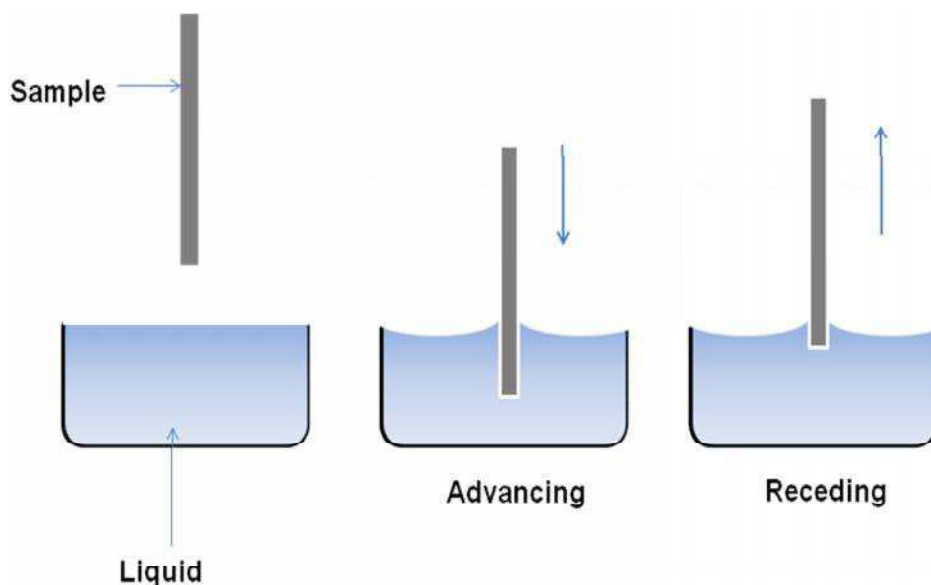
Figure 2.3   A scheme of the steps of the dynamic contact angle measurement.

2.3.2 Quartz Crystal Microbalance (QCM)

QCM is a mass sensitive device with the ability to measure very small mass deposition on the quartz crystal in real-time. This ultra sensitive technique is capable of measuring a small change in mass, as small as a fraction of a monolayer. QCM is consisted of a piezoelectric quartz crystal that resonate when a voltage is applied, the deposition of the material on this crystal change the resonance frequency. The change in the resonance frequency is used to measure the mass of the material deposited on

the crystal (Equation 2.3). This change is proportional to the mass adsorbed for rigid films deposited under vacuum and it is described by Sauerbrey Equation 2.3.

$$\triangle f/\nu = -\triangle m/C \tag{2.3}$$

Where C is a constant that depends on the thickness of the crystal, ν the overtone number, $\triangle f$ is the change in the resonance frequency and $\triangle m$ is the mass adsorbed into the crystal.

In case the crystal is in contact with liquid, which is mostly the case in this work, the liquid shear force exerted on the crystal due to the liquid viscosity is taken into consideration. The seven frequencies and dissipation are measured simultaneously to measure the thickness of the visco-elastic films, for which Sauerbrey Equation is not valid. This is usually applicable for adsorption of protein (films containing a lot of water) where accurate thickness cannot be done without several frequencies measurements (Equation 2.4)

$$\triangle f = -f_u{}^{3/2} ((\rho_L \eta_L)/(\pi (\rho_q \mu_q)))^{1/2} \tag{2.4}$$

Where $\triangle f$ is the change in frequency, f_u the unloaded quartz crystal frequency, ρ_L the density of the liquid in contact with the crystal, η_L viscosity of the liquid in contact with the crystal, ρ_q the density of the quartz and μ_q shear modulus of the quartz.

The dissipation frequency, which is the sum of the loss of energy per cycle, measurement has the advantage of determining the amount of water in the film. This is used to determine whether the film is rigid (less water) or soft (rich in water). The crystal can be coated by gold, titanium, silica or stainless steel. The details of the method used are discussed in the Experimental Section of Chapter 6.

2.3.3 Atomic Force Microscopy (AFM)

AFM[55, 58] is a scanning probe microscopy used to measure the roughness, the thickness and modulus of films. It provides a nanoscale profile of the surface by measuring the interaction forces between sample and the probe. The tip used in the measurement is supported on a flexible cantilever which is consisted of a spring. The force between probe and the surface depends on the spring constant of the cantilever and the distance between the tip and the surface. As the tip is repelled or attracted by the surface the laser beam is deflected by the upper side of the cantilever (Figure 2.4).

The two modes of AFM are: the tapping and the contact mode. In the contact mode, the tip is brought in contact with the surface. The tip will bend due to the forces between the sample and the tip. The contact mode is applied to rough samples measurements and it has the advantage of being fast. In the tapping mode, the cantilever oscillates at its resonant frequency (200-400 kHz) and scans across the surface. The advantage of the tapping mode is the high resolution scanning of soft surfaces. The roughness and the thickness, when mentioned in this work, were measured using AFM (Asylum Research Inc., Santa Barbara, CA, Dimension 3001) and Igor Pro software (Wavemetrics, Lake Oswego, OR) in the tapping mode. The details of the experiments are mentioned in the Chapter 6. Force curves were obtained using a MFP-3D unit (Asylum Research Inc., Santa Barbara, CA) and Igor Pro software.
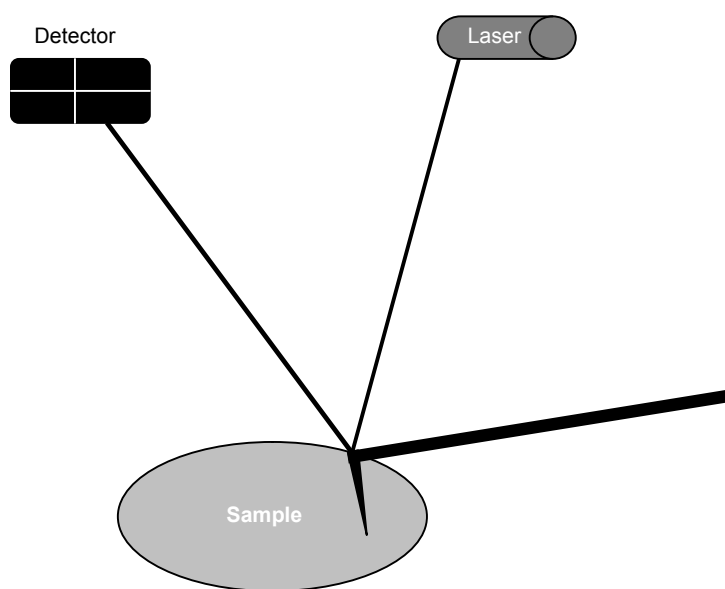
Figure 2.4 Schematic of an AFM instrument showing the laser beam reflected from the tip of the cantilever to the position sensitive photodiode detector.

2.4 Spectroscopy

2.4.1 UV-vis Spectroscopy

UV-vis spectra were done using a double beam mode Varian Cary (Bio 100) UV/VIS/NIR spectrophotometer. The absorption of the solution and the films was done in the linear range of the detector response within Beer's law. The solution absorption was done in a matched quartz cuvette taking the solvent as a background. The absorption of the films was done by assembling PEMU on a fused quartz slides or sapphire which is transparent to the UV-vis region. Sapphire has the advantage of preserving its optical properties at high temperature.

2.4.2 Fluorescence Spectroscopy

Materials absorb the light at a certain wavelength equivalent to the energy gap between its HOMO and the LUMO level of the molecule. The electron relaxes back using different paths (Figure 2.5) most of them are none radiative via inter system crossing from a singlet to triplet and heat dissipation. The path that involves the relaxation from the singlet excited state to the singlet ground state releases the energy in form of light. The light emitted is definitely higher in wavelength than the absorbed one. The difference between the absorbed wavelength and the emitted wavelength is known as Stokes shift which is characteristic of each material. Photoluminescence was taken using a Cary Eclipse Fluorescence spectrophotometer. Samples were excited at different wavelengths of excitation and emission was scanned to 800 nm.
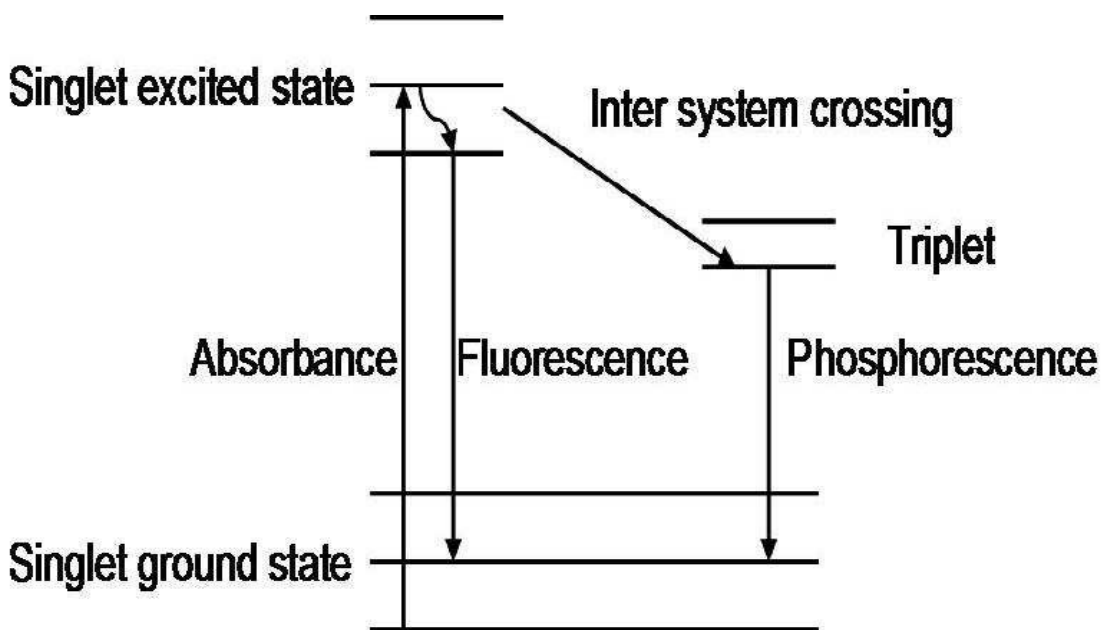
Figure 2.5   Scheme of the different paths of relaxation of the electron back to the ground state

.

2.4.3 Fourier Transform Infrared Spectroscopy (FT-IR)

FT-IR[59] is a widely used qualitative and quantitative technique for identification of compounds. Covalent bonds absorb in the IR region in different vibrational modes: stretching, bending and rocking. The absorption frequency (wavenumber) is a characteristic for each type of bond (single C-C, double C=C or C-O) depending on the reduced mass of the atoms and the strength of the bond.

In this work, FT-IR spectra for films and solid powder were taken using Nicolet Nexus 470 with a DTGS detector. The solid samples were made into a KBr pellets using a Carver Laboratory Press (model C) at 10000 Psi. The films were assembled in a double sided silicon wafer that transmits in the IR region. The film samples were placed in a holder with a 15º tilting to decrease scattering. A background was taken before each sample. For solid samples, KBr background was taken while for films the silicon wafer was taken as a background. All the spectra were taken with 36 scans at a 4 cm^{-1} resolution.

2.5 Cell Culture and Biological Assays

2.5.1 Cell Culture

Cell culture[60,61] is the process of growing cells derived from multicellular eukaryotes (especially animal cells) under controlled condition outside the body (*in vitro*). Cells used in the cell culture are isolated from tissues by enzymatic digestion (collagenase, trypsin or pronase) that breaks the extracellular matrix of the cells or by using the cells that grow out of a piece of tissue that is grown in a growth media. The cells at this stage are called primary cells that usually have a limited lifespan after which they stop dividing. The main challenge of cell culture is to grow the cells healthy without any loss of their characteristics (function and metabolism) and/or ability to divide. Cells obtained from the division of the primary cells are called the cell line. Cell culture has been employed in many fields: biotechnology (production of biological materials), biomaterials (in vitro response of cells to new materials e.g.: coatings, implants) and drugs (cells response to new drugs before going to in vivo studies). For higher level of mimicking the biological systems, three dimensional cell culture growth protocols are recently employed.

Cells in cell culture are grown under tight conditions of temperature (37 °C), gas mixture (5% CO_2 for mammalian cells), growth media and aseptic environment. The temperature and the gas mixture are maintained by keeping the cell culture in a cell incubator. The growth media is a solution of growth factors and essential nutrients (ions and trace elements, glucose, essential amino acids and vitamins) that is added to the cells to maintain their growth. The media growth supplemented differs from one cell line to the other; different cell lines need different constituents, pH, glucose concentration and growth factor. The serum is extracted from animal blood and has high potential for carrying viruses. The fact that the growth media is an optimum environment for bacterial growth that has faster division than mammalian cells dictates that all work must be performed in an aseptic environment and take precautions by sterilizing or using sterile equipment, flasks and workplace (usually using a biosafety hood/laminar flow cabinet), and the addition of antibiotics and anti-fungals to the growth media.

The cells were cultured in a specialized plastic flask at a certain plating density. The plating density defined as number of cells growing per area plays a critical role in the characteristics of the cells in some cell types. Cells can be either grown in suspension or by adhering to the surface. At a certain cell density, usually implied by the aim of the cell culture, cells (adherent type) are detached using trypsin then seeded to two or more flasks (known as splitting). The density and the viability of the cells are done prior to any seeding using Cedex HiRes Analyzer (Roche Innovatis AG). The media is changed upon depletion of nutrient which is usually monitored by a pH indicator added to the media, cells produce acid during the metabolic process that alters the pH.

In this work, the cell line derived from a rat aortic smooth muscle known as A7r5 cell line was used and cultured in Dulbecoo's Modified Eagle Medium (DMEM) supplemented with fetal bovine serum (FBS). A7r5 cell line is an adherent cell line that is usually used in vitro studies due to the role that the smooth muscle cells play in wound healing. A7r5 has the ability to reversibly convert between two phenotypic modes the synthetic proliferative (motile) and the non-motile.[62] The experimental methods details of the cell culture of A7r5 will be discussed in Chapter 7.

2.5.2 Cell Viability Test

The cell density and viability are determined using the Cedex HiRes Analyzer (Roche Innovatis AG) that uses the trypan blue exclusion method. Trypan blue (Figure 2.6) is a diazo dye that is impermeable through the live cell membrane while it is permeable in case of dead cells. Therefore, trypan blue selectively stains dead cells. A 1 µL of the cells suspension is transferred to the cup that is loaded to the tray of the Cedex instrument where trypan blue stain is added automatically. The cells are channeled to a flow cell. The counting is done automatically with the Cedex to avoid any human error. The Cedex detectable cell density range is between 50,000-10,000,000 cells/mL and detectable cell diameter of 8-40 µm.
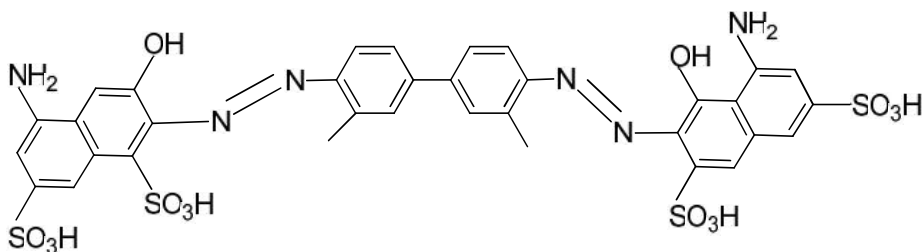
Figure 2.6   The structure of trypan blue dye.

2.5.3 Alamar Blue Assay

The alamar blue assay is a quantitative method to measure the metabolic activity of the cells. The principle of the assay is based on the ability of the healthy cells to uptake Resazurin a non-fluorescent indicator dye. The dye is nontoxic and has no interference with the metabolic activity of the cells. The healthy cells reduce Resazurin continuously from its non-fluorescent form to Resorufin which is fluorescent. Resorufin is a red fluorescent dye that emits light at 590 nm when excited at 530-560 nm (Figure 2.7). Therefore, the metabolic activity of the cells can be monitored by the intensity of fluorescence at 560 nm and has linear relationship with the viability. The assay is also used as in vitro Cytotoxicity assays. The assay does not require any extraction step which makes the method simpler than the others. The alamar blue dye is added in a specific amount to the cell culture which is incubated, with the dye, for 1-4 h at 37 °C after which the fluorescence is measured. The fluorescence can be measured at different time interval using Molecular Devices SpectraMax MicroPlate Reader and SoftMax Pro Software.
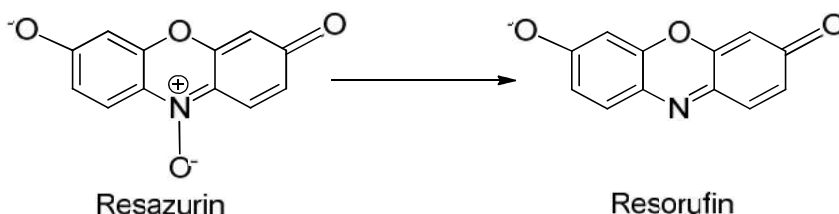
Figure 2.7   The reduction reaction of Resazurin (non-fluorescent dye) to Resorufin (red fluorescent dye) by live cells.

2.6 Bacteria Culture and Biological Assays

2.6.1 Bacteria Culture

Microbiological growth[63] (bacteria growth) is a method to multiply microbial organisms by growing them in a culture media under controlled conditions in the laboratory. Unlike cell culture, bacteria growth is described by the increase of the number of colonies. The division of bacteria occurs by binary fission which is simpler than eukaryotic division. The bacteria growth in fresh media typically has three distinct phases (Figure 2.8): lag, log (logarithmic), stationary and decline phase. The lag phase occurs due to the transfer of the bacteria from one culture (usually frozen glycerol) to another. The lag in the division is associated with physiological adaptation; the bacteria may experience an increase in size with the lack in binary fission. In the log phase, bacteria undergo binary fission in which the number of bacteria increases. In the stationary phase, the increase in bacteria growth and the death of bacteria are in equilibrium due to the limitation in nutrients or toxins released in log phase. Serial dilutions are done to keep the bacteria in their log phase.
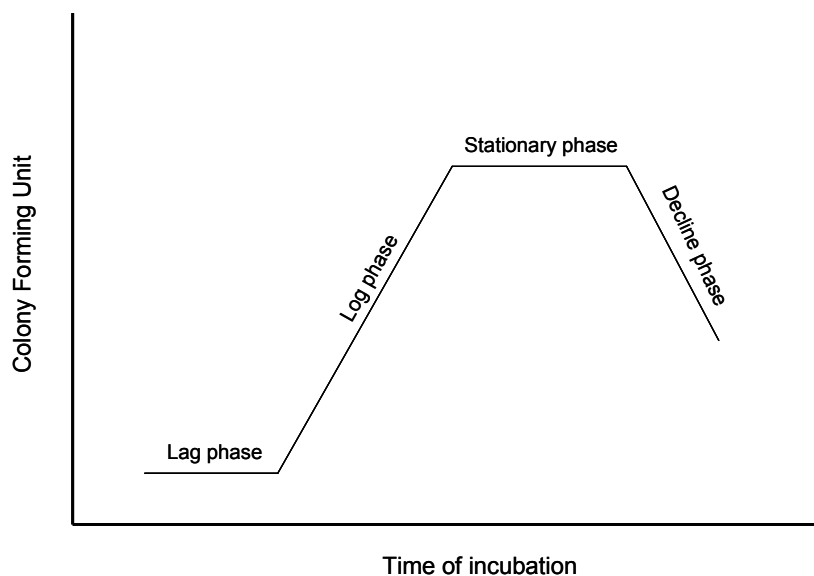
Figure 2.8   A schematic diagram of the bacteria growth modes during time of incubation.

2.6.2 Bacteria Counting

Bacteria growth is described by colony forming unit (CFU) which are estimated by using standard plate counts.[63] The bacteria extract were taken from a frozen glycerol stock and added to 2 mL Luria Bertani (LB) media incubated overnight at 37 ºC at 300 rpm, the media looked turbid indicating that a log phase was attained. Serial dilutions were prepared in a chilled media, to prevent the growth while performing the test. The protocol includes preparation of solution of approximate concentration between 10^2 -10^5 CFU/mL by serial dilution from the stock. The absorbance of the all the prepared solutions at 600 nm were recorded, which is known as optical density (O.D.) (scattering at 600nm which increases as the turbidity of the solution increase). A 0.1 mL of the serial dilutions solutions were plated on an agar plate overnight at 37 ºC. The number of formed colonies were counted and coupled to the O.D. The CFU/mL is the average number of colonies per plate multiplied by dilution factor.

2.6.3 Agar Plate Preparation

The agar plate[63] is a method used to count the number of formed colonies by bacteria. Agar is a commonly used solidifying agent that melts at 95 ºC and solidifies at 42 ºC. It does not have any nutritive role. Nutritive materials (yeast extract, tryptone) are added to the agar during its formation. In 600 mL distilled water all the following are dissolved: 6g NaCl, 3g yeast extract, 6 g tryptone, and 9 g agar. The solution is autoclaved at 121 ºC for 45 min to insure its sterility. The solution is cooled to 37 ºC while stirring and then directly transferred to 100 mm petri dishes before solidifying. The agar petri dishes are left to solidify at room temperature under sterile conditions. The agar plates are stored at 4 ºC for later use in plate counting.

2.6.4 Luria Bertani (LB) Broth

The LB[63] broth is the media used to provide bacteria with essential nutrients. The LB broth is prepared from dissolving the following in 1 L of distilled water: 10 g of NaCl, 5 g of yeast extract, and 6 g tryptone. The media is stored under aseptic techniques after autoclaving it at 121 ºC for 45 min.

2.6.5 Live/Dead Assay

The Live/Dead assay is a method used to assess bacteria viability in a mixed population of dead and live bacteria. The assay is consisted of a mixture of dyes SYTO9 (excitation 480/ emission 500 nm) and propidium iodide stains (excitation 490/ emission 635 nm). SYTO9 is a green nucleic acid fluorescent dye that penetrates both healthy and damaged cell membranes whereas propidium iodide nucleic acid stain can only penetrates bacteria with damaged membranes and stains it red. Under fluorescence microscopy dead bacteria will be stained red or orange while live bacteria will be stained green only. In this work the live/dead assay was used to test the PEMU ability to kill bacteria on contact. The details of the contact killing test will be discussed in Chapter 7.

2.6.6 Inverted Fluorescence Microscopy

Compound microscopes are usually used to view fixed samples (non live samples, deprived from their nutrient media). This kind of microscope is designed with the light source and condenser below the stage, objectives and nosepiece above the stage. A more practical microscope is the inverted one which is useful for viewing live cells, and tissue culture in a container (petri-dish) with the media. Therefore, observing the cells in their natural conditions. As the name indicates an inverted microscope has its condenser, light source and the objective below the stage. Inverted fluorescence microscopy operates using the fluorescence light from the specimen, which is either labeled by fluorescent dyes or it auto fluoresces. The sample is illuminated with a light that matches the excitation wavelength of the sample, an illumination filter is mounted to ensure that the light wavelength matches the required excitation wavelength and the light is more near its monochromatic characteristics (Figure 2.9). The illumination light is reflected by the dichromatic mirror to the specimen. The dichromatic mirror transmits the fluorescent light from the specimen, which has a longer wavelength then the excitation wavelength and it blocks light of shorter wavelength (the illumination light). The combination of the filters and dichromatic mirror is chosen in a way that the excitation filter exhibits a high level of transmission at the wavelength of excitation, the dichromatic mirror reflects wavelengths in the region of the excitation wavelength and

transmitting the lower and higher wavelengths, and the emission filter only transmits the light in the emission wavelength range. The microscope filters can be changed to observe the green, blue and red fluorescence.

In this work, inverted fluorescence microscopy (Nikon Eclipse Intensilight C-HGFI and Cool Snap HQ2 camera from Photometric, NIS-advanced software) was used equipped with 41017 Endow GFP bandpass emission (400-650 nm) and Texas Red (TEXRED) (450-750 nm) (41004) emission filters (Chroma Technology Corp).
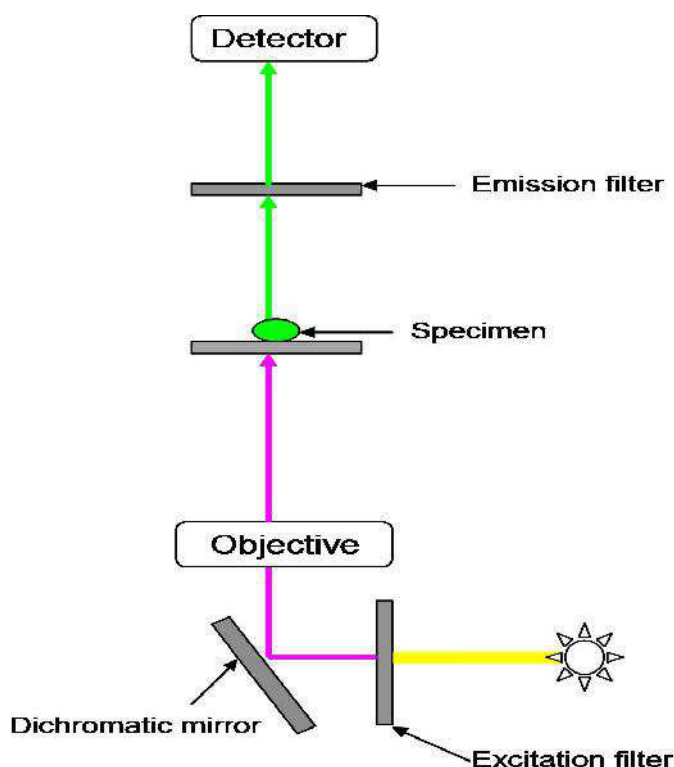
Figure 2.9   Schematic diagram of an inverted fluorescence microscopy.

2.7 Multilayer Nomenclature

In all of this work the following shorthand is used for multilayers: $(A/B)_n$ C@ f MY where A is the first layer in contact with the substrate, which is either a silicon wafer or quartz slide, usually cationic polyelectrolyte, B is the anionic polyelectrolyte, C is the

terminating layer, n is the number of bilayers. M represents the cation and Y is the anion of the salt used during the build up where f is the concentration of the salt during the assembly. For example, $(PXT/PSS)_5$ @ 0.25 M NaCl, represents five bilayers of PXT/PSS with PSS as the terminating layer build at 0.25 M NaCl. The shorthand Z-N when used implies that polyelectrolyte Z is compensated with the counterion N. For example the shorthand PXT-Cl implies that PXT polycation is compensated with chloride as a counterion. The polycations PVBTMA, PVBTMP and PVBDMS are termed ammonium, phosphonium and sulfonium, respectively.

CHAPTER 3

TOWARD DEFECT FREE LUMINESCENT POLY(PHENYLENE VINYLENE) (PPV) FILMS: THE MACRO-COUNTERION AQUEOUS ROUTE

3.1 Introduction

Poly(acetylene) (PA), a conjugated polymer, was widely studied as a good candidate in the semi-conductors field due to its high conductivity. Its very low photoluminescence (PL) excluded it from gaining attention in fields other than that of non-metallic semi-conductors. In 1990, Burroughes et. al. reported the ability of poly(phenylene vinylene) (PPV) which is a conjugated polymer to emit light when an electric field is applied. [64] Conjugated polymers have been subjected to extensive research for use in optoelectronic applications [65-66] including organic light emitting diodes (OLEDs), [65, 67-70] field effect transistors, [65, 71,72] polymer solar cells [70, 73] and flexible electronic devices. [72] OLEDs built from PPV, and its derivatives have demonstrated promising efficiency.[74] The insolubility of PPV, which complicates its processing, [66, 75,76] has been addressed by using lower molecular weight materials, [75] introducing non-conjugated spacers or by adding soluble side chains.[77] Another method to overcome the processing challenge is *via* a precursor route. Figure 3.1 shows a common route, where a water soluble poly(xylylidene) with tetrahydrothiophene (THT) as a good leaving group permits relatively low temperature thermal elimination to yield PPV, the conjugate acid of the counterion and THT.
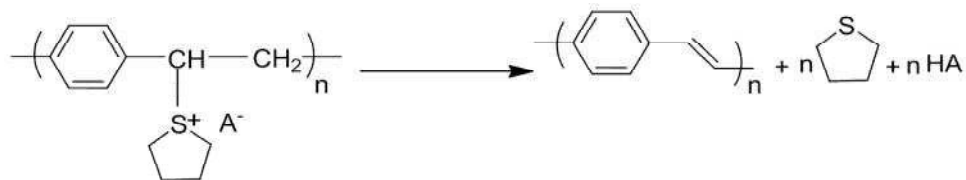
Figure 3.1 The precursor route to PPV.

While the ability to convert PXT to PPV at low temperature has advantages, especially in LED applications in which other, thermally sensitive, materials are involved, the thermal elimination route introduces various defects into the polymer backbone. For example PPV suffers from side reactions which lead to carbonyl groups in the backbone.[78] These carbonyl defects, reported by Murase et. al.,[79] who prepared PPV in air according to Figure 3.1, caused a drop in the electrical conductivity of PPV. The formation of hydroxyl defects on the PPV backbone which is prepared via the same route (Figure 3.1) were reported by Hsieh et. al. [80] When research in conjugated polymers turned to potential OLED applications, it was quickly found that defects, especially carbonyls, severely compromised PL. [81-82] For example, Yan et. al. [83] reported that PL is reduced by a factor of two for every one carbonyl in 400 PPV repeat units. The presence of carbonyl in the backbone of the PPV decreases the LUMO energy level. The mechanism of carbonyl quenching takes place via radiationless electronic transition from the LUMO of PPV without any carbonyl in the backbone to the LUMO of PPV with carbonyl defects in the backbone (Figure 3.2). Such a carbonyl quenching mechanism, which occurs for all derivatives of PPV, and its dramatic effect on PL intensity of PPV, is now well documented. [67, 81, 83-88] OLEDs rely on electroluminescence (EL) to generate light. Since the conversion of excited state energy to light is similar in EL and photoluminescence (PL), the latter is usually employed to gauge the potential maximum efficiency of OLEDs. [81, 89-91]
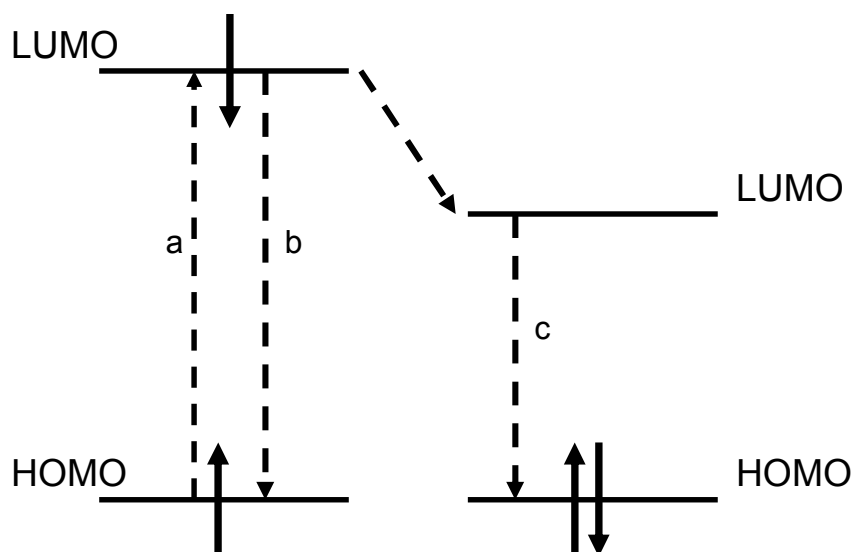
Figure 3.2   Schematic diagram of energy levels of PPV without any defects (left) and PPV with carbonyl defects in the backbone (right). (a) electronic transition via absorption of light from HOMO to the LUMO (b) transition back to the ground state which release light (c) radiationless transition after intersystem crossing to the LUMO of the PPV with defect.

The counterion, A$^-$ in Figure 3.1, was shown to have a significant impact on elimination temperature.[78] PXT with a halide as a counterion is fully eliminated at 200 °C while that with those with acetate must be heated to 350 °C. At this high temperature, carbonyl formation increases, even under high vacuum or under ultrapure argon.[81] Thermal elimination at lower temperatures leaves a significant amount of unconverted precursor, copolymer of PXT-co-PPV, which also yields low PL efficiency. It was reported that PXT with dodecyl benzene sulfonate (DBS) (Figure 3.1) as a counterion can be converted to highly conjugated PPV within 3 min at 115 °C.[92] A significant feature of this work was that conversion occurred under atmospheric conditions without the use of a dynamic vacuum or inert gas. As DBS is a hydrophobic counterion it caused precipitation of PXT on exchange with chloride ions.[92] To prevent precipitation, aliquots of NaCl were added to the PXT-DBS exchange solutions.[92] Treger et. al. reported that using sodium dodecyl sulfate (SDS) as a counterion for PPV derivatives enhances their optical properties and inhibits the photo-oxidation of the films.[93] Using

SDS as a counterion increased the half-life of the degradation of the PPV derivative by 3 fold.

Yan et. al. [94] pointed out the virtues of separating PPV chains which encourage the formation of (emissive) intrachain excitons as opposed to (non emissive) interchain excitons. Diluting PPV derivatives in blends or in solution enhanced intrachain excitons. An alternative approach involves the packing of the PPV chains by intentionally introducing cis inclusions in the backbone or bulky side chains.[95,96] Based on the above approaches we suggested using larger counterions as a separator between PPV chains. The exchange of PXT counterions (small ions e.g. Cl⁻) by macro-counterions is straightforward, which makes this approach easier than those in which synthesis is involved. To maintain the solubility of this precursor in water, A⁻ should be hydrophilic. We were interested in the use of a hydrophilic macroscopic counterion. In particular we were intrigued by a counterion that could enhance solid state ionic conductivity, which might be useful in the light emitting electrochemical cells described by Cao et. al. [97-98] The counterion used in this study was poly(ethylene glycol)-4-nonylphenyl-3-sulfopropyl ether (PEGNOPS) which is a long chain surfactant (Figure 3.3). PEGNOPS has a hydrophilic moiety, twenty ($-O-CH_2-CH_2$) units, that prevents PXT precipitation. We found that a PXT-PEGNOPS precursor required exceptionally low conversion temperatures (as low as 80 °C), yielded low carbonyl formation and PPV with high relative PL.
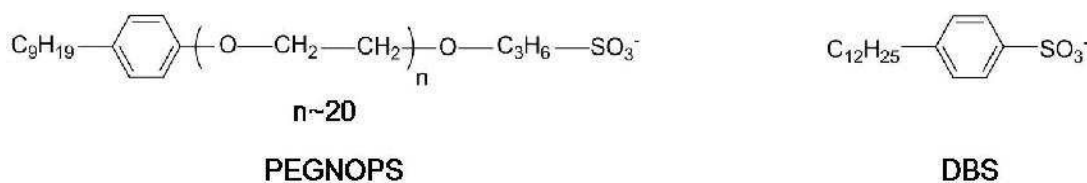
Figure 3.3   Structures of PEGNOPS and DBS.

3.2 Experimental Section

3.2.1 Materials

DBS, PEGNOPS and α, ά-dichloro-p-xylene (98%) were used as received from Sigma-Aldrich.

Monomer synthesis: p-xylylenebis(tetrahydrothiophenium chloride) was prepared by refluxing α, ά -dichloro-p-xylene with tetrahydrothiophene at 80 °C for 20 h in methanol under Argon. The product was purified by evaporating methanol followed by washing with cold acetone.[99] Poly(xylylidene tetrahydrothiophenium chloride) (PXT-Cl) was prepared following a literature procedure.[99] PXT-Cl was purified by dialyzing against distilled water using a 12,000-14,000 molecular weight cutoff dialysis tubing (Spectra/Pro).

3.2.2 Ion Exchange

The chloride ion was exchanged by mixing 10 mM PXT-Cl with 1.42 mM PEGNOPS dissolved in ethanol and dialyzing it against 0.2 M PEGNOPS solution for 24 h, then for 48 h against distilled water. Chloride was exchanged by DBS using the method by Marletta et. al. [92]. Films were cast under atmospheric conditions at room temperature on the relevant substrate. Elemental analysis on the ion exchanged PXT-PEGNOPS (Atlantic Microlab): C 57.05%, H7.87%, S 7.71%, Cl 0.65%; showing that 78% of the chloride was exchanged by PEGNOPS.

3.2.3 Optical Measurements

Infrared (IR) spectroscopy was performed using a nitrogen purged FTIR (Nicolet Nexus 470 with a DTGS detector) spectrometer. The resolution was 4 cm^{-1} with 36 averaged scans on samples, which were prepared on double-sided polished silicon (Si<100>) wafers. The sample holder was held at 15° off perpendicular to avoid interference fringes on the spectra. UV-vis spectra were recorded on a Varian Cary 100 UV-vis double beam spectrophotometer. Samples were prepared on fused quartz slides (GM Associates, 2 mm thick, 1 inch diameter). Photoluminescence was recorded on a

Cary Eclipse Fluorescence spectrophotometer. Samples were excited at different wavelengths.

3.2.4 Thermal Annealing

PXT films were converted to PPV under vacuum on a vacuum line equipped with an oil diffusion pump, or under atmospheric conditions. In both cases, samples were monitored by a thermocouple in direct contact with the substrate on which the film was cast. PXT films with different counterions were converted at 80 °C under atmospheric conditions, then cooled and subjected to characterization. For comparison, PXT-Cl was converted under vacuum for 10 min at 210 °C. [83, 92]

3.3 Results and Discussion

While the aqueous precursor route to PPV (Figure 3.1) enhances processibility, especially film formation, the defects affect optical and electrical properties. The residual impurities from synthesis (e.g: monomers, salt and oligomers) may have more of an effect on PPV films compared to their effect in solution due to the higher density in the film. The removal of impurities from the PPV precursor is done by dialysis. Figure 3.4 shows some of the possible chemical defects that can be formed prior to, during, or after the thermal annealing of PXT. For example, since THT is a good leaving group it can be substituted during synthesis or storage by Cl⁻ and OH⁻ ions which are nucleophiles (unit **c** and **b** Figure 3.4, respectively). Hydroxide is usually added to initiate polymerization where Cl⁻ is from residual HCl that is added to quench polymerization. The defects break conjugation along the backbone, but can be partially removed by elimination at higher temperature. Counterions such as PEGNOPS have a sulfonate, which is a weak nucleophile, and its long chain may also help to decrease the nuleophilicity of the sulfonate group due to steric hindrance. A critical chemical defect that may occur in the backbone of PXT and /or PPV is a carbonyl group (unit **a**, Figure 3.4) that is formed via oxidation. The carbonyl defect is problematic because it is hard to remove at high temperature. In fact, higher annealing temperature promotes carbonyl formation, as does photo-oxidation during storage. Considerable research has focused

on the effect of these chemical defects on PPV. All have emphasized the strong (negative) impact that a carbonyl has on the optical properties of PPV. [67, 81, 83, 85, 88]
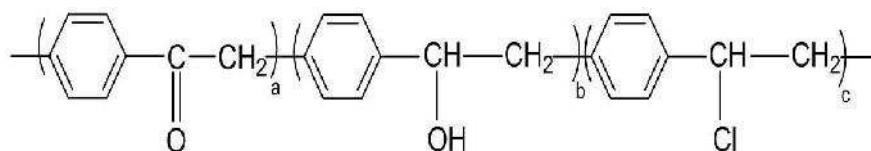
Figure 3.4   Possible chemical defects on PPV formed prior to, during or after thermal annealing of the PXT precursor. a) backbone oxidation to yield carbonyls b) hydroxide substitution during synthesis c) chloride substitution during storage.

Figure 3.5 shows the FT-IR spectrum of PXT-Cl before elimination and PPV prepared from PXT-Cl eliminated at 80 C under atmospheric condition for various time. The relative extent of elimination is estimated by the ratio of a PPV band at 3024 cm^{-1} (*trans* vinylene mode) to the area of 1515 cm^{-1} (in-plane bending of H on a benzene ring).[78, 86]   The latter was found to be approximately constant during elimination. The carbonyl intensity is also normalized to 1515 cm^{-1} peak. Figure 3.6 shows the PL intensity of PPV prepared from PXT-Cl at 80 °C in air in comparison to the amount of carbonyl and extent of elimination in the film. While the extent of elimination increases with the increase time for thermal annealing, the PL intensity, after an initial increase, falls off with further heating. At the same time, the carbonyl content increases, consistent with the decrease in PL efficiency. For efficient PL quenching of the fluorophore (conjugated backbone) the quencher (carbonyl) should be in proximity. The fact that carbonyl is embedded in the backbone unfortunately maximizes quenching, decreasing the quantum efficiency of devices based on PPV.
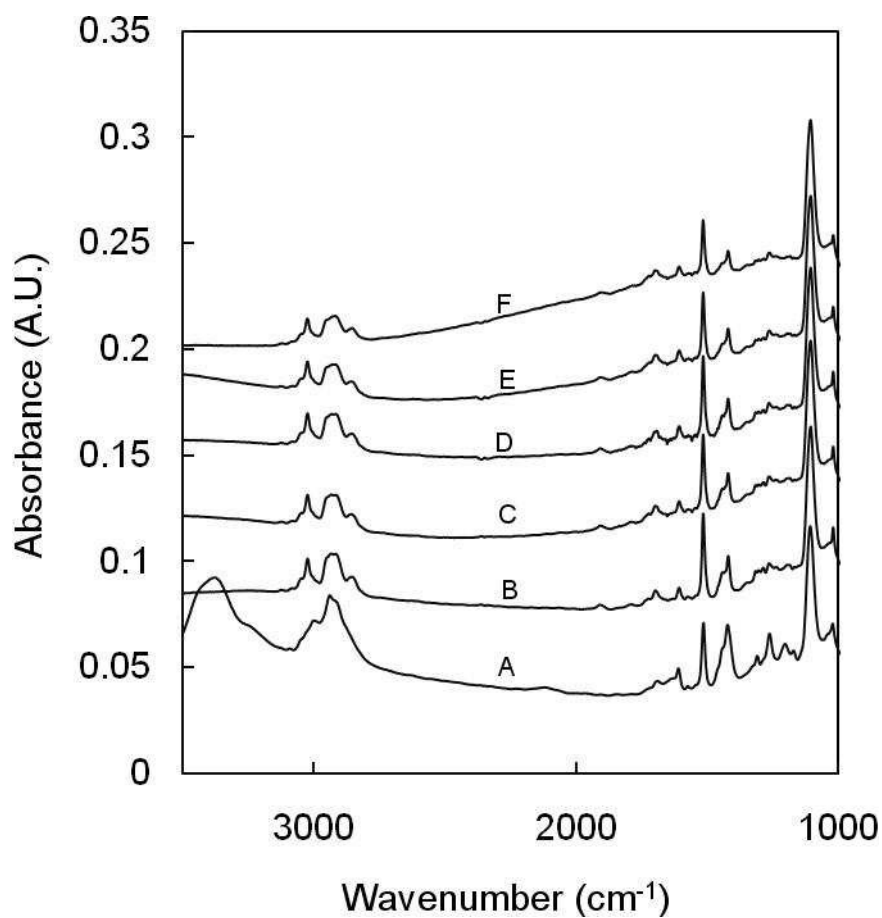
Figure 3.5 Shows the FT-IR spectra of (A) PXT-Cl film before elimination, (B) 60 min, (C) 140 min, (D) 200 min, (E) 320 min, and (F) 380 min of thermal elimination at 80 °C under atmospheric condition.
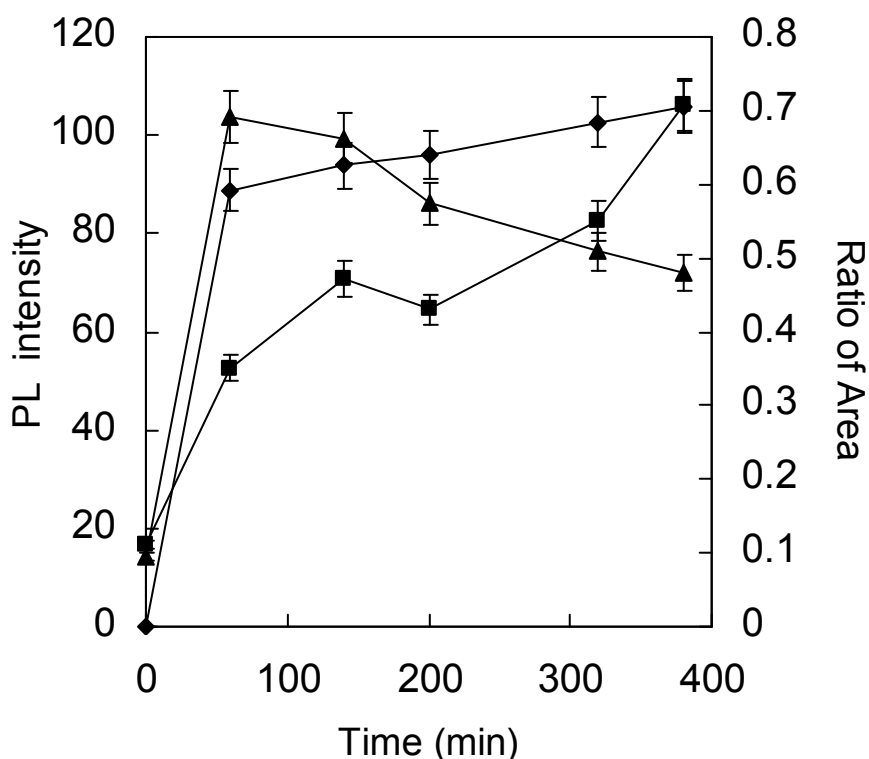
Figure 3.6 PL intensity of PXT-Cl thermally annealed at 80 °C under atmospheric conditions. (▲) PL intensity, in arbitrary units, at λ=525 nm vs. time of thermal annealing at 80 °C in air. (♦) Area of IR peak at 3024 cm^{-1} (*trans* vinylene C-H stretch in PPV) normalized to the 1512 cm^{-1} peak area (in-plane C-H stretch of benzene ring). (■) Normalized IR area of 1690 cm^{-1} band (carbonyl stretch) relative to 1512 cm^{-1} peak.

The problem of carbonyl formation has been tackled by changing thermal annealing and/or storage conditions. For example, thermal annealing was carried out under Ar (99.999%), under high vacuum, or under a blanket of reducing gas (85% nitrogen, 15% hydrogen).[81] However in each case, a significant amount of carbonyl was formed, and in the best case only a 40% reduction was reported.[81] The second approach involves performing the elimination at low temperature which results in a copolymer of PXT-*co*-PPV with low PL intensity.[67] The reactivity of the PPV backbone can be decreased by adding electron withdrawing side groups, such as phenyls or trifluoromethyls,[100] which reduces the oxidation of the PPV backbone.[101] Shielding the PPV backbone by attaching bulky groups as side chains also aids in reducing backbone

oxidation. Finally, the PPV precursor was blended with PEG which improved the atmospheric stability and optical properties of PPV.[102,103]

PXT is typically stored in the dark at low temperatures to minimize photo-oxidation. All synthetic polymers degrade to some extent upon exposure to light. The UV-Vis energy ranges from 290-600 nm (97-48 Kcal/mol) which is enough to break weak chemical bonds (Table 3.1) causing oxidation and scission in the backbone and/or the side chain.[104] Photo-degradation changes the molecular weight, molecular weight distribution, physical and the mechanical properties of the polymers and serves to reduce the utility of the polymer for its application. Upon exposure of the polymer to light, free radicals are formed either in the backbone or side chain, or both depending on which has the weaker type of bond.[104] If oxygen is present, which is typically the case, the ground triplet state of oxygen would react with free radicals to form alkoxy radicals and results in scission on the backbone.[104]

Table 3.1   Energy of chemical bonds.[104]

Chemical bond	Energy in Kcal/mole
C-H	94-99
C-C	77-83
C-O	76-79
C-Cl	82
C-Br	67
O-O	51

Our results showed a significant counterion dependence of defect formation on the storage of the PXT precursor. Figure 3.7 shows the IR spectra of PXT-Cl, PXT-DBS and PXT-PEGNOPS solutions after 30 days of storage under ambient conditions. Both Cl⁻ and DBS precursors formed carbonyls (see stretch at ~1700 cm^{-1}). In comparison, the amount of carbonyl formed for PXT-PEGNOPS under the same conditions was minimal. The normalized area of the carbonyl stretch versus storage time under ambient conditions for the three different counterions is plotted in Figure 3.8. PXT-DBS had a higher tendency to form carbonyls than PXT-Cl over 5 days, which has relatively short

storage time. For PXT-Cl, carbonyl formation was constant after 5 days of storage, whereas carbonyl formation continually increased for DBS. The highest carbonyl ratio that PXT-PEGNOPS reached was 0.017± 0.002 which is 76 times less than PXT-DBS. Even after 14 months of storage, PXT-PEGNOPS had a carbonyl peak ratio 24 times smaller than that of PXT-DBS after 30 days of storage. These results showed the effectiveness of PEGNOPS as a counterion to prevent the premature carbonyl formation of PXT during storage, even under ambient temperature and light.
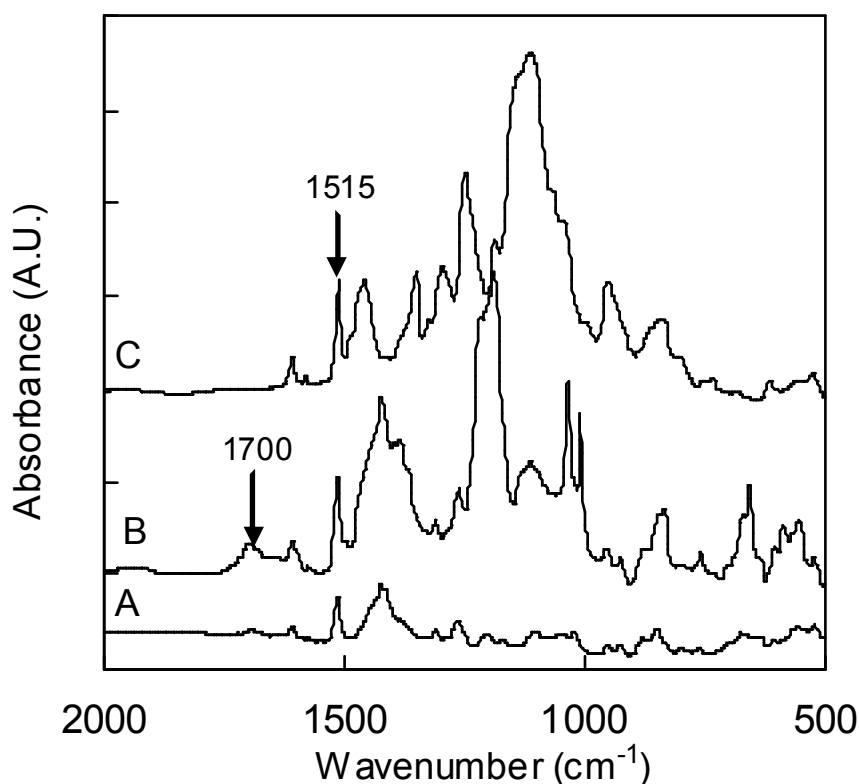
Figure 3.7 IR absorption spectra of cast films of (A) PXT-Cl (B) PXT-DBS (C) PXT-PEGNOPS stored at room temperature in the presence of ambient light for 30 days. The peak at 1700 cm^{-1}corresponds to the carbonyl stretch. The spectra have been normalized to the 1512 cm^{-1} aromatic band. In spectra B and C this band is presented at twice the height of spectrum A to account for the contribution to the band from the counterion.
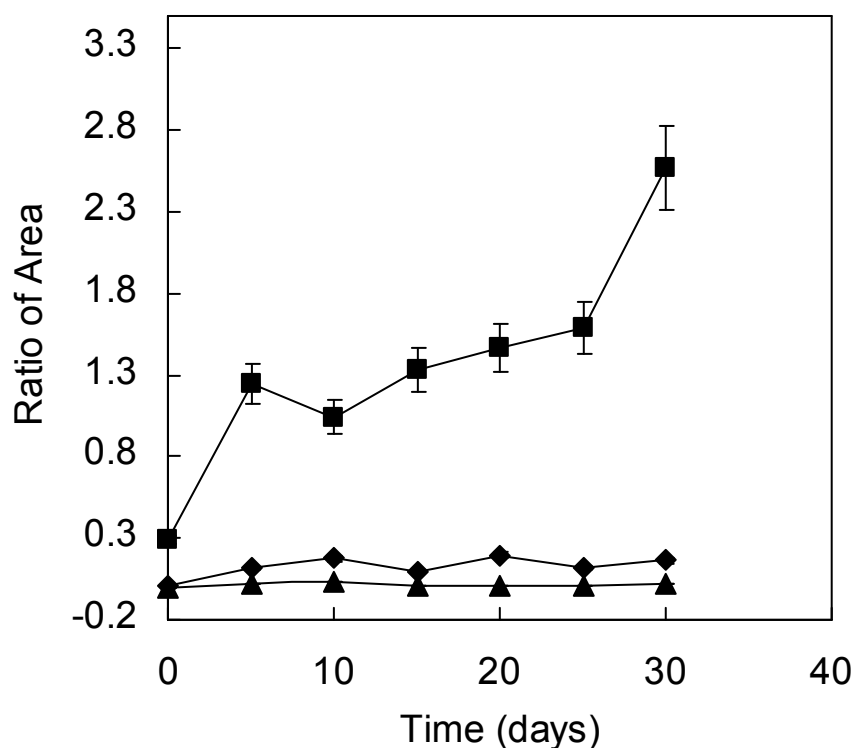
Figure 3.8   Shows ratio of area under the FT-IR peak at 1700 cm^{-1} carbonyl stretch to the area of 1512 cm^{-1} peak in plane stretch of benzene ring C-H for (■) PXT-DBS squares, (♦) PXT-Cl diamonds; and (▲) PXT- PEGNOPS triangles which are stored at room temperature under ambient light.

The maximum conversion of PXT-Cl to PPV films is done at high temperatures, typically 210 °C to 300 °C, under vacuum or a blanket of high purity inert gas. These conditions yield PPV with nominally the most extended conjugation (indicated by the red shifted UV-vis absorption) but also lead to low PL intensity due to carbonyl defects. High temperatures are unfavorable for most PPV applications, since other materials used in conjunction with PPV to make devices can suffer from changes in properties. The elimination of PXT with the PEGNOPS counterion provides the lowest conversion temperature reported and may be performed under atmospheric conditions. Furthermore, the formation of carbonyl groups is significantly suppressed; leading to enhanced PL. Figure 3.9 shows IR spectra of PPV annealed at 80 °C under atmospheric conditions for 20 min. Both Cl and DBS have formed carbonyls during

annealing while PEGNOPS showed relatively few carbonyls. In fact, the normalized area of the carbonyl peak (Spectra C in Figure 3.9) was found to be lower than the area formed after 30 days of room temperature storage of PXT-Cl.
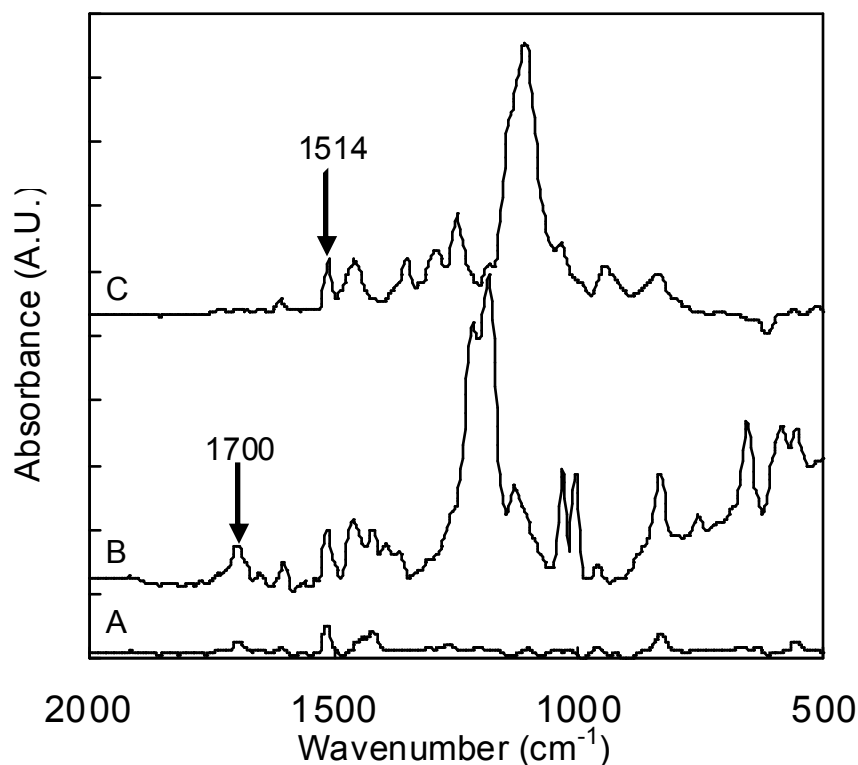
Figure 3.9 IR absorption spectra of (A) PXT-Cl (B) PXT-DBS (C) PXT-PEGNOPS films annealed at 80 °C for 20 min under atmospheric conditions. The peak at 1700 cm^{-1} corresponds to the carbonyl stretch. The spectra have been normalized to the 1512 cm^{-1} aromatic band as in Figure 3.7.

The optimum time of thermal annealing of PXT-PEGNOPS is determined by monitoring the PL which is used since it is more sensitive to defects than absorption, to get a better picture of the properties. PXT-PEGNOPS films were processed at 80 °C under atmospheric conditions Figure 3.10. The highest PL of PXT-PEGNOPS film is obtained when the film is thermally annealed for 20 min at 80 °C. These conditions, reached following extensive experiments varying time and temperature, were found to yield PPV films with the highest PL intensities.
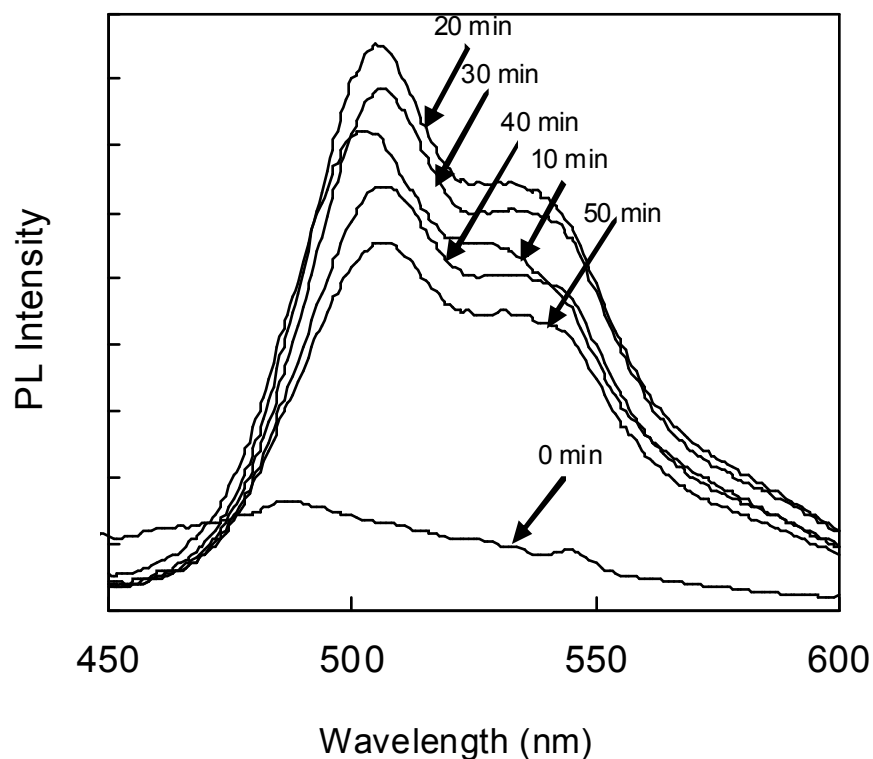
Figure 3.10 Photoluminescence spectra of PXT-PEGNOPS films thermally annealed at 80 °C under atmospheric conditions at various times.

Figure 3.11 depicts PL and UV-vis absorption spectra of PPV prepared from PXT-Cl at 210 °C for 10 min under vacuum compared to PXT-PEGNOPS heated at 80 °C for 20 mins under atmospheric conditions (optimum conditions). The spectra are scaled such that the absorbance at 400-450 nm is the same height, which allows comparison of the relative PL efficiency. Although PPV, when prepared from PXT-Cl is more conjugated, as determined from the red shifting of the absorbance band, it has a lower luminescence intensity compared to PPV prepared from PXT-PEGNOPS under atmospheric conditions. This finding is the result of the lower concentration of carbonyls on the backbone for the latter. The reduction in conjugation is believed to be a result of the residual chloride counterions. Elemental analysis showed that 22% of PXT is compensated by chloride ions. The PXT compensated by PEGNOPS eliminates at 80 °C whereas the chloride compensated required higher temperature (as high as 210 °C) before it was eliminated.
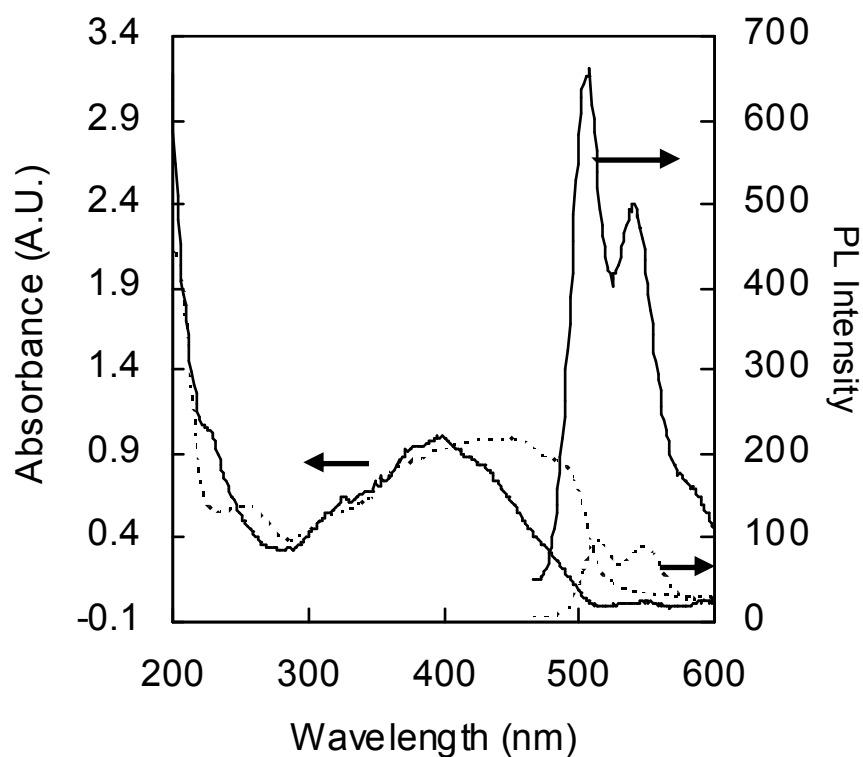
Figure 3.11 UV-vis and normalized (to the 400-450 nm absorption band) PL spectra of (a) PXT-Cl film thermally annealed at 210 °C under vacuum for 10 min (dotted lines) (b) PXT-PEGNOPS film thermally annealed at 80 °C under atmospheric conditions for 20 min (solid lines).

The ability of PEGNOPS to retard PPV oxidation at both room temperature in solution and at slightly elevated temperatures was surprising. The lower content on elimination, even in air, is a clear consequence of the significantly reduced elimination temperature. Molecular dynamic simulations, discussed in Chapter 4, suggest that the bulky polymeric anion actually sets up the PXT backbone for anti-elimination to give *trans*-PPV. An additional role for PEGNOPS could be to slow oxygen diffusion to the oxidation to form peroxide or/and carbonyl. Figure 3.12 shows a known mechanism of PEG oxidation.

Figure 3.12 PEG oxidation reaction.

Figure 3.13 FT-IR spectra of PEGNOPS extracted from a PXT-PEGNOPS film thermally annealed at 80 °C in air.

Figure 3.13 shows the IR spectrum of PEGNOPS extracted by ethanol from a PXT-PEGNOPS film thermally annealed where insoluble PPV stays on the substrate and PEGNOPS ends up in ethanol. The peak at 1729 cm^{-1} (carbonyl stretch) shows that

PEGNOPS plays the role in the sacrificial barrier process that consumes most of the oxygen before reaching the PPV backbone. The peaks at 1114 and 841 cm^{-1} are the C-O stretch peaks in symmetric ether which corresponds to the PEG units in PEGNOPS. The spectrum (Figure 3.14) of PPV left on the silicon wafer after the extraction of PEGNOPS (by ethanol after thermal annealing at 80 °C) shows 3024, 1721, 1695 and 961 cm^{-1}. Both peaks at 3024 and 961 cm^{-1} are those of PPV.
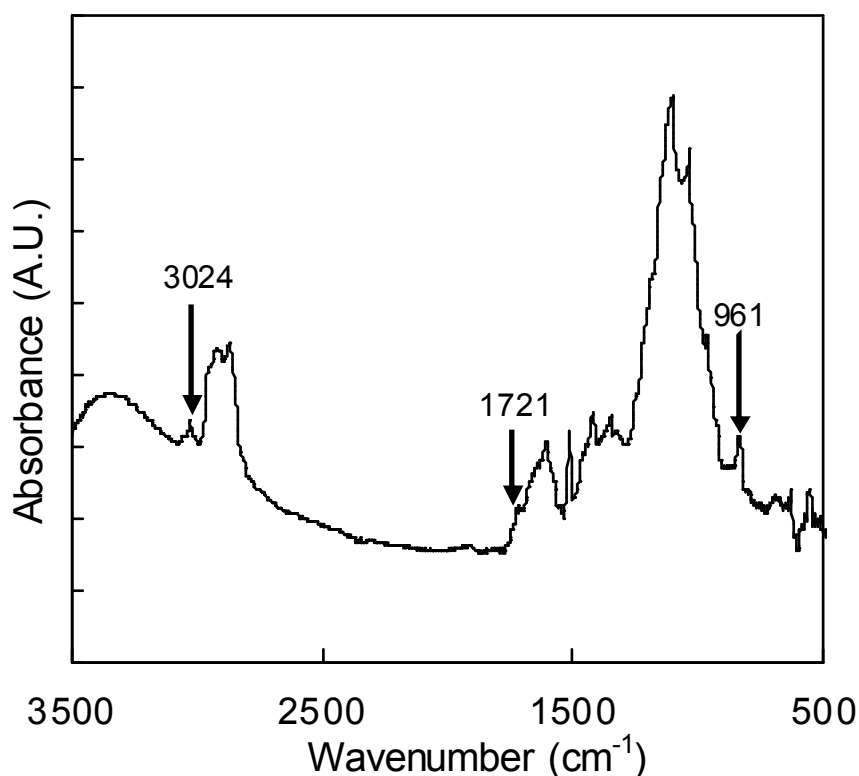
Figure 3.14 FT-IR absorption spectra of cast film of thermally eliminated PXT-PEGNOPS at 80 °C in air after extraction with ethanol.

The emissive layer in OLED is usually deposited on the conductive electrodes. Although Indium tin oxide (ITO) is the most used conductive transparent anode, it is known to be unsuitable for PPV prepared by the aqueous route where Cl$^-$ is used as a counterion. During the conversion of PXT-Cl to PPV, hydrogen chloride is formed as a by-product, and reacts with ITO to form InCl$_3$ (Figure 3.15). This reaction not only causes non-uniformity in the current distribution in OLEDs due to the conductivity of the

formed $InCl_3$ but also leads to the degradation of the OLED in the long term.[105,106] Another advantage of PEGNOPS is the immobility of its acidic form (HA, Figure 3.1 where A=PEGNOPS).

$$InO_2 + 6HCl \longrightarrow 2InCl_3 + H_2O + 2H_2$$

Figure 3.15 Reaction of ITO with HCl.

3.4 Conclusion

The assembly of PEGNOPS and PXT, a PPV precursor, has many benefits. First, the elimination to PPV occurs at a significantly lower temperature when compared to the traditional chloride counterion precursor. Second, the number of carbonyl groups is lower, and the photoluminescence yield is higher, even though elimination is carried out in air. Third, the assembly being rich in polyether units, should be capable of transporting lithium ions for devices that rely on electrochemical excitation of energy for light emission. The PEGNOPS to PPV precursor showed no carbonyl formation on long term storage, in contrast to the precursors with dodecyl benzene sulfonate and chloride counterions, PEGNOPS can be used to increase PXT shelf time.

CHAPTER 4

THERMAL ELIMINATION of PRECURSORS TO POLY(PHENYLENE VINYLENE) WITH A MACRO-COUNTERION VERSUS A SMALL COUNTERION: A COORDINATED EXPERIMENTAL AND SIMULATION

4.1 Introduction

Poly(phenylene vinylene) (PPV) and its derivatives are intensively studied conjugated polymers.[107] In addition to conductivity in the doped state, good thermal stability[108-109] and tunable luminescence in the undoped state have stimulated application of PPVs in optoelectronic[110] devices such as organic light emitting diodes (OLEDs),[109, 111-113] field effect transistors,[109-111] photovoltaic cell[109, 111,112] and polymer lasers.[111,112] To prepare thin films, modification of the PPV backbone with hydrocarbon pendant groups yields soluble derivatives.[49, 114] Alternatively, films may be cast from a high molecular weight water-soluble precursor, which is subsequently converted into the final polymer by thermal elimination (Figure 4.1).
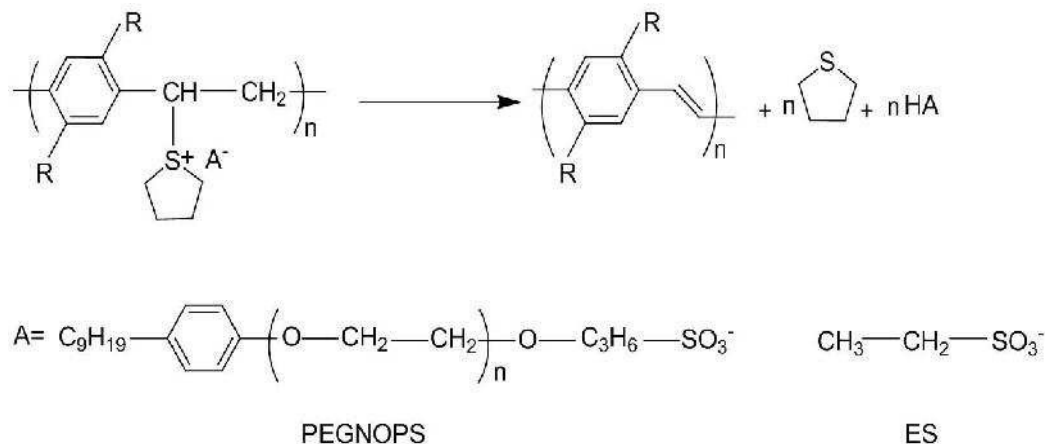
Figure 4.1 Elimination of PXT and structures of PEGNOPS (n ~ 20) and ES counterions.

The optical and electrical properties of PPVs prepared by the thermal elimination route depend on many variables such as processing,[113] temperature of elimination[107, 115] compensating counterion,[116-118] and side chains in the precursor.[53] Such factors control the spatial orientation and intermolecular distance between conjugated segments,[119] the effective conjugation length[108, 115, 119-121] and the extent of order of the backbone (crystallinity).[122,123]

Optical properties of PPV are understood and tuned through interactions of PPV segments. These interactions, leading to the formation of excimers, exiplexes and aggregates that form a new ground state, were shown to decrease photoluminescence (PL). They are enhanced if PPV segments are in proximity. Yan et. al.[124] indicated that amorphous PPV, in which chromophores are separated, have more efficient PL than crystalline PPV, where interchain fluorescence quenching takes place. Since then, there have been various attempts to promote separation between PPV chromophores. Kas et. al.[119] enhanced PL by controlling the distance between conjugated segments of the PPV backbone and controlling orientation by grafting PPV as a side chain on a self assembled α-helical peptide. Another commonly used method is the dilution of PPV segments by another nonconjugated polymer.[125] Son et. al.[122] interrupted the conjugation of PPV by engineering *cis* linkages into the backbone, giving amorphous PPV that suppresses polymer packing and increases PL. Many groups have studied the effect of the length, flexibility, structure and bulkiness of the side chain on the packing of PPV and consequent effects on the PL. [126-129]

For the aqueous elimination route (Figure 4.1), an additional strategy for enhancing the PL efficiency has been to lower the temperature of elimination, which decreases the formation of quenching sites in the backbone of PPV. Convenient variables for modulating the temperature of elimination are choice of the counterion or leaving group (Figure 4.1).[107] It was shown that tetrahydrothiophene (THT) gives a higher effective conjugation length at a lower temperature of elimination than dimethylsulfide as a leaving group.[130] Marletta et. al.[116] reported that PXT films with dodecylbenzenesulfonate (DBS) as a counterion can be efficiently eliminated at 115 °C. In contrast, PPV films processed from PXT using chloride as counterion are prepared at 210 °C. This high temperature is usually explained by the fact that the sulfonium ion is

thermally more stable with a less basic counterion.[116]Small counterions are mostly used in the aqueous routes of PPV such as: Cl⁻, CH$_3$COO⁻, F⁻, Br⁻ [117] and the only two long-chain counterions used have been DBS[116] and perfluorononoate.[131] In spite of the variety of counterion sizes, the emphasis in past work for explaining elimination temperatures has been on the basicity of the counterion. Poly(styrene sulfonate) has been used as a polymeric counterion for poly(xylylidene tetrahydrothiophenium) (PXT).[132,133] Abe et. al.[134] reported that using polymers or polyelectrolytes as additives to the conjugated polyelectrolytes increased the PL by inducing order to the conjugated polyelectrolyte.

In a recent paper by Al-Hariri et. al. it was reported that using poly(ethylene glycol)-4-nonylphenyl-3-sulfopropyl ether (PEGNOPS) as the counterion for PXT enhanced the PL due to the sacrificial and separation role that PEGNOPS played in suppressing carbonyl formation in the PPV backbone and interchain quenching, respectively. The fact that the elimination temperature was only 80 ºC was difficult to explain, but it permitted elimination in air. The use of long-chain counterions brings an interesting dimension into polyelectrolytes such as PXT: the morphology is essentially a bottle-brush, where the length of the side chains is varied simply by changing the counterion. If the chain length of the counterion is long enough, the environment of the backbone is then controlled by the counterion. In an effort to understand the role of this macro-counterion in PXT elimination, complimentary orthogonal space random walk (OSRW) molecular dynamics simulations were done, which suggested that the backbone conformation of PXT is favorably influenced by the ethylene oxide tails of the macro-counterion. To separate between the effects caused by the head group chemistry and by the environment coordinated experiments and theory using a short-chain aliphatic sulfonate were done, which mimics the hydrophilic sulfonate end of PEGNOPS.

4.2 Experimental Section

4.2.1 Materials

Ethane sulfonic sodium salt form (ES), PEGNOPS and *α, α´*-dichloro-*p*-xylene (98%) were used as obtained from Aldrich. PXT-Cl was prepared from *p*-xylylene bis(tetrahydrothiophenium chloride) using a literature procedure.[135] PXT-Cl was purified by dialysis against distilled water using a 12,000-14,000 molecular weight cutoff (MWCO) Spectra/Pro dialysis tubing.

4.2.2 Ion Exchange

PXT-ES preparation by ion exchange: PXT-Cl was dialyzed against a 0.1 M solution of ES for one day then for 48 h against distilled water with a change of water each 8 h. PXT-PEGNOPS: 10 mM PXT-Cl was mixed 1.42 mM with PEGNOPS dissolved in ethanol (to give a several-fold excess of PEGNOPS) then dialyzed against 0.2 M PEGNOPS then against water for 48 h with a change of water each 8 h. Elemental analysis of the ion exchanged PXT-PEGNOPS (Atlantic Microlab): C 57.05%, H 7.87%, S 7.71%, Cl 0.65%, implying that 78% of the chloride was exchanged by PEGNOPS. Films were cast under atmospheric conditions at room temperature on relevant substrates. Films were thermally annealed under atmospheric conditions in a heater fitted with a thermocouple in direct contact with the substrate.

4.2.3 Films Characterization

UV-vis data were obtained using a Varian Cary Bio 100 UV/VIS double beam spectrometer. Samples were prepared on round sapphire slides. Photoluminescence was recorded on a Cary Eclipse Fluorescence spectrometer. Samples were excited at different wavelengths and emission was scanned to 800 nm.

4.2.4 Computational Methods

A recently developed accelerated molecular dynamics simulation method, "the orthogonal space random walk (OSRW) algorithm", was employed.[136] OSRW simulations were preformed in a customized CHARMM program. The two model systems consisted of ten PXT units with ten ES as counterions (190 atoms) or ten PXT units with ten PEGNOPS as counterions (1920 atoms). The initial structure of each

model system was built using the CHARMM Internal Coordinate (IC) facility. Since simulations were done to mimic PXT-ES and PXT-PEGNOPS films that have no water (solvent), simulations were done with no solvent. For each model PXT-PEGNOPS and PXT-ES two initial structures were generated via a restraint-minimization procedure with a PXT chain R_g 7 Å (termed the "compact" initial condition) and 16 Å (termed the "extended" initial condition). Simulations started from the compact and extended initial conditions to confirm that the models were not stuck in local minima during simulations. Similar results, attained independent of initial simulation starting conformation, indicates the robustness of the method.

The simulations were performed at 80 °C (temperature at which the experiments were carried out) using OSRW and canonical ensemble simulations. Langevin dynamics were employed as the thermostat to control temperature with a friction coefficient of 60 ps^{-1} acting on all the heavy atoms. The random forces were set corresponding to the target temperature of 80 °C. The time-step was 1 femtosecond. In all the recursion simulations, Equation 4.1 is employed.

$$F_m(\lambda, U_o) = \sum_i h \exp\left(-\frac{(\lambda - \lambda_i)^2}{2w_1}\right) \exp\left(-\frac{(U_o - U_{o,i})^2}{2w_2}\right) \tag{4.1}$$

Where the height of the Gaussian function h was set to 0.1 kcal/mol; the widths of the Gaussian function, ω_1 & ω_2, were set to 0.01and 4 kcal/mol respectively. In the PXT-PEGNOPS OSRW simulations, the lower bound scaling parameter λ_0 was set to 0.2 due to the fact that its energy landscape is more rugged; in the short surfactant model OSRW simulations, the lower bound scaling parameter λ_0 was set to 0.6. In the metadynamics recursion, $F_m(\lambda, \frac{\partial U_o}{\partial \lambda})$ was updated every 10 time steps; in the scaling parameter space recursion, $f_m(\lambda)$ was updated every 100 time steps. Each of the production simulations was initiated when the radius of the gyration of the target polymer chain converged in the corresponding recursion simulation.

4.3 Results and Discussion

4.3.1 The Elimination Mechanism

Studies on the mechanism of elimination of PXT are controversial. Many mechanisms were suggested, including E1cB, E1 and E2 but none of them is fully consistent with the experimental results.[54, 107, 117, 130, 137,138] E1cB can be discounted because of the following: the unfavorable thermodynamics for formation of the carbanion, lack of stabilizing groups and/or strong base, having THT which is a good leaving group and the fact that E1cB will yield a mixture of *cis* and *trans* PPV[117, 138] whereas reaction from PXT route yields *trans* PPV only.[122, 139] Both Wang et. al.[117] and Shah et. al.[137] attempted to reconcile the controversy regarding the mechanism of elimination by suggesting that E2 occurs at low temperature (100-150 °C) while E1 is the dominant pathway at higher temperatures.

In the literature on elimination mechanisms, only the basicity of the counterion was considered, where most of the counterions used were small.[117] Although Marletta et. al.[116] used (the larger) DBS and perfluorononoate counterions, they did not look into the effect of counterion chain length on elimination. If the final conjugated polymer is charged its photophysical properties may be strongly influenced by the counterion. For example, Abe et. al.[134] explored the effect of polyelectrolyte counterions on the PL of a charged PPV derivative. These authors showed that when polymers and/or polyelectrolytes were used as counterions, PL in the conjugated polyelectrolyte was strongly enhanced.[134] Polyelectrolytes as counterions provide approximately the same mass/charge ratio as do small organic ions. In contrast, PEGNOPS, charged only at one end, provides significantly more mass/charge. The elimination occurs at 80 °C, a temperature region where the E2 mechanism dominates.

4.3.2 The Film Characterization

Figure 4.2 shows absorption and normalized PL spectra of PXT-ES and PXT-PEGNOPS thermally annealed films at 80 ºC in air for 20 min. PPV prepared from PXT-PEGNOPS has a broad UV-vis absorption spectrum due to the wide distribution of conjugation lengths. The absorbance peak centered at 410 nm and extending to 500 nm implies the presence of long conjugated segments in the backbone. On the other

hand, material prepared from PXT-ES has a narrower absorbance band centered at 325 nm and a shoulder at 370 nm. This relatively narrow absorbance indicates that shorter conjugation lengths of PPV result from PXT-ES. Absorption is an instantaneous phenomenon during which no vibrational relaxation takes place, whereas PL originates from the most stable excited vibrational state following spectral diffusion which leads to better-resolved PL peaks.[140] The PL of PXT-PEGNOPS is 4 times higher in intensity and more red shifted than PXT-ES. These significant differences are observed in spite of the fact that the charges on both counterions are aliphatic with the same basicity (same functional group).
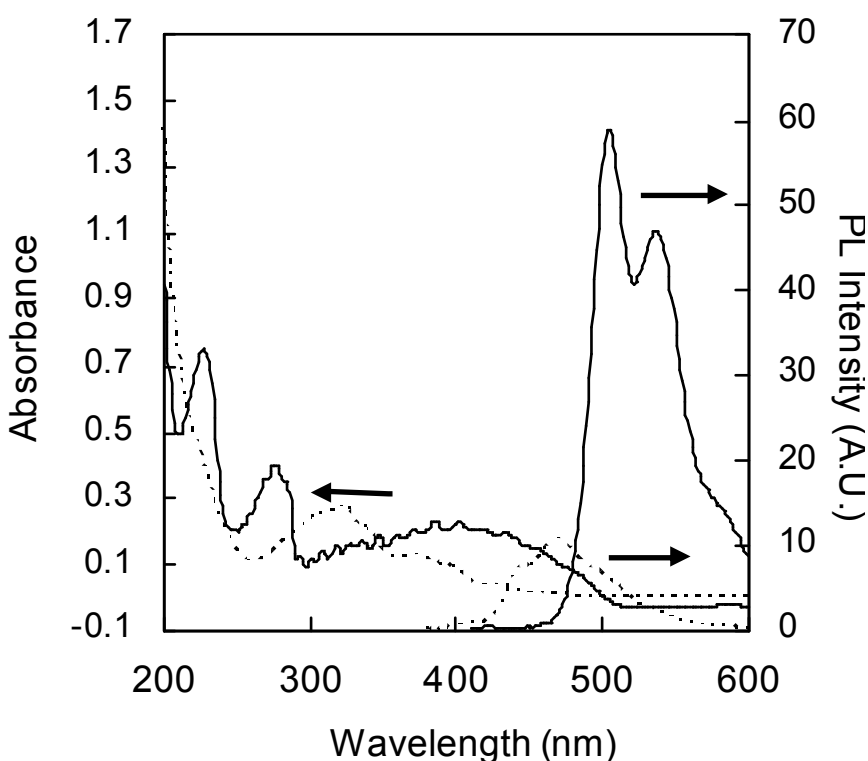
Figure 4.2 UV-vis and PL spectra excited at λ=400 nm for PXT-PEGNOPS film thermally annealed at 80 °C in air for 20 min (solid spectra) and of PXT- ES film thermally annealed at 80 °C in air for 20 min (dotted spectra).

4.3.3 Surface Energy and Molecular Modeling

To gain insight on the reasons for the low temperature elimination, OSRW molecular dynamics simulations[136] were carried out on both PXT-ES and PXT-

PEGNOPS models. Both models consisted of 10 PXT units with 10 PEGNOPS/ES counterions assuming ion exchange is 100%. Figure 4.3 shows the time-dependent evolution of the radius of gyration of the PXT chain for the PXT-ES system starting from two different initial conditions. The convergence of two recursion simulations from two starting structures, the compact one with the radius of gyration of 7.8 Å and the extended one with the radius of gyration of 15 Å, demonstrates the sampling adequacy. In other words, it demonstrates that none of the models are trapped in local minima during simulation and that a global minimum is achieved. Note that only very slight initial compaction was possible, as the final structure is already a compact, random-coil, space-filling structure. Sampling adequacy is also demonstrated in the convergence of the PXT-PEGNOPS simulation in Figure 4.4. It is noteworthy that the recursion simulations on the PXT-PEGNOPS model converged after around 20 ns to the global minimum (R_g=8.8 Å) whereas the PXT-ES model reached the global minimum (R_g=7.8 Å) after 2.5 ns. This is due to the longer chain of PEGNOPS that takes more time to relax. The conformation of PXT-PEGNOPS and that of PXT-ES in their most stable conformations are represented in Figure 4.5. It is clear from the equilibrium R_g values in Figures 4.3 and 4.4 that the PXT chain is slightly more expanded in PEGNOPS compared to ES. The much larger volume occupied by PEGNOPS, which causes this chain expansion, is clearly seen in Figure 4.5. The environment for the polyelectrolyte is controlled by its PEGNOPS counterion.
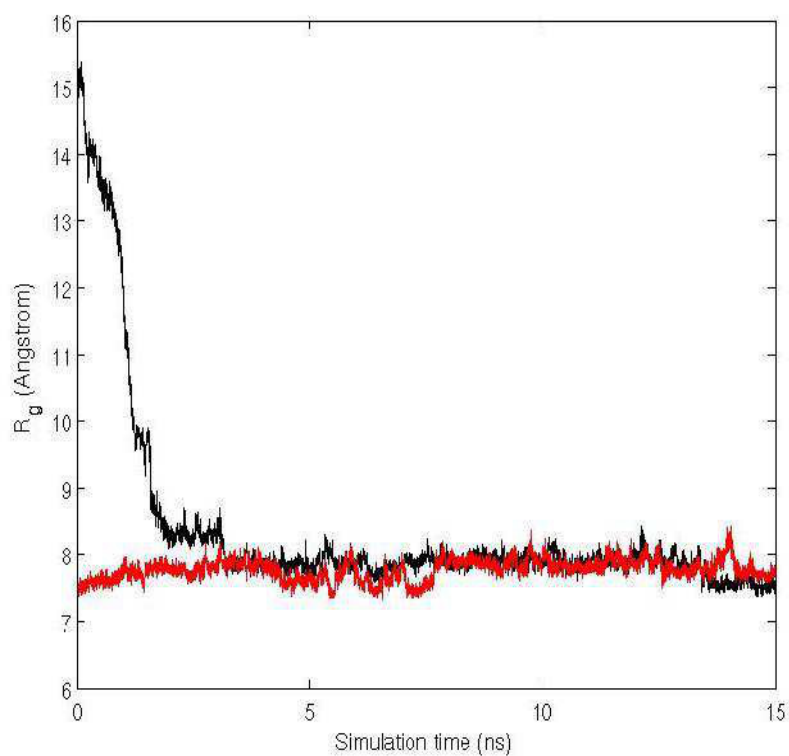
Figure 4.3   Radius of gyration evolution of 10 monomer units of PXT chain of PXT-ES versus time of OSRW simulation at 80 °C.
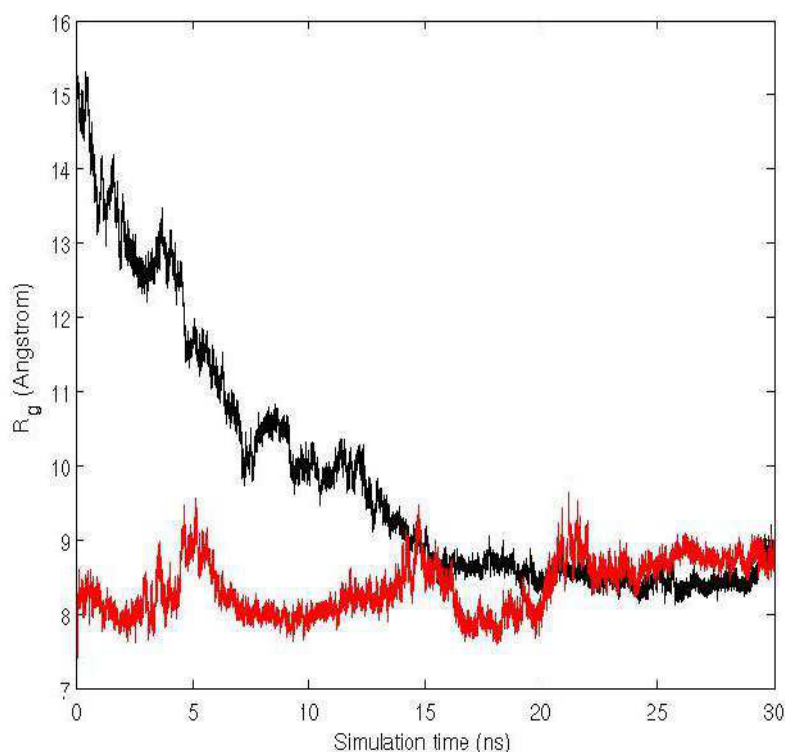
Figure 4.4 Radius of gyration evolution of 10 units of a PXT chain for PXT-PEGNOPS versus time. OSRW simulation done at 80 °C.

Figures 4.6 and 4.7 respectively reveal the free-energy surfaces of the PXT-ES and PXT-PEGNOPS models in the space described by the C-C/C-S dihedral angle (shown in Figure 4.8) and the radius of gyration of PXT. The C-C/C-S dihedral angle describes the relative orientation between the THT and the benzene ring as shown in Figure 4.8.

For PXT-ES the most populated conformational regions are those with C-C/C-S dihedral angles around 0-20, 50-85, and 140-180 degrees (Figure 4.6). In comparison, for PXT-PEGNOPS the conformational region with C-C/C-S dihedral angles from 20-180 degrees are well populated (Figure 4.7). It is well known that for E2 elimination, the leaving group, THT, and one of the hydrogen atoms (Figure 4.8) should be in the *anti* positions, i.e. the H-C/C-S dihedral angle between the two should be around 180 degrees (Figure 4.8). Table 4.1 illustrates examples of the H-C/C-S dihedral angles at which the E2 mechanism is possible; where the THT group and one of the hydrogens

61

(H_a, H_b) is in the *anti* position. The C-S/C-C dihedral angles between 0-120 degree encompass the reactive region (Figure 4.6 and 4.7 red zone in % population), where the E2 reaction is promoted. The region between 120 and 180 degrees is the non-reactive region (Figure 4.6 and 4.7 blue zones in % population).
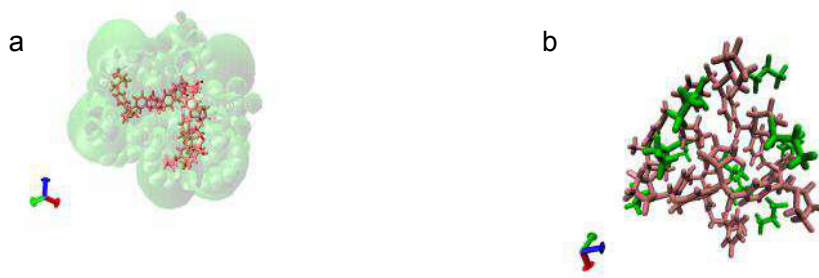
Figure 4.5 Molecular modeling of a) PXT-PEGNOPS in its most stable conformation and b) PXT-ES in its most stable conformation. PXT main chain is brick red and the molecules in green are the counterions.

In the PXT-ES model 42% of the population is in the reactive region (0-120°) whereas for the PXT-PEGNOPS complex the percentage is 55%. Thus, the reactive region in PXT-PEGNOPS is 30.9% more populated than that of PXT-ES; i.e. there is 30.9% more chance to have the hydrogen atom located in the *anti* position in PXT-PEGNOPS than in PXT-ES. This result is consistent with the experiments that showed that PXT-PEGNOPS has higher conjugation length than PXT-ES (Figure 4.2 UV-vis) although both of them are processed under the same conditions.
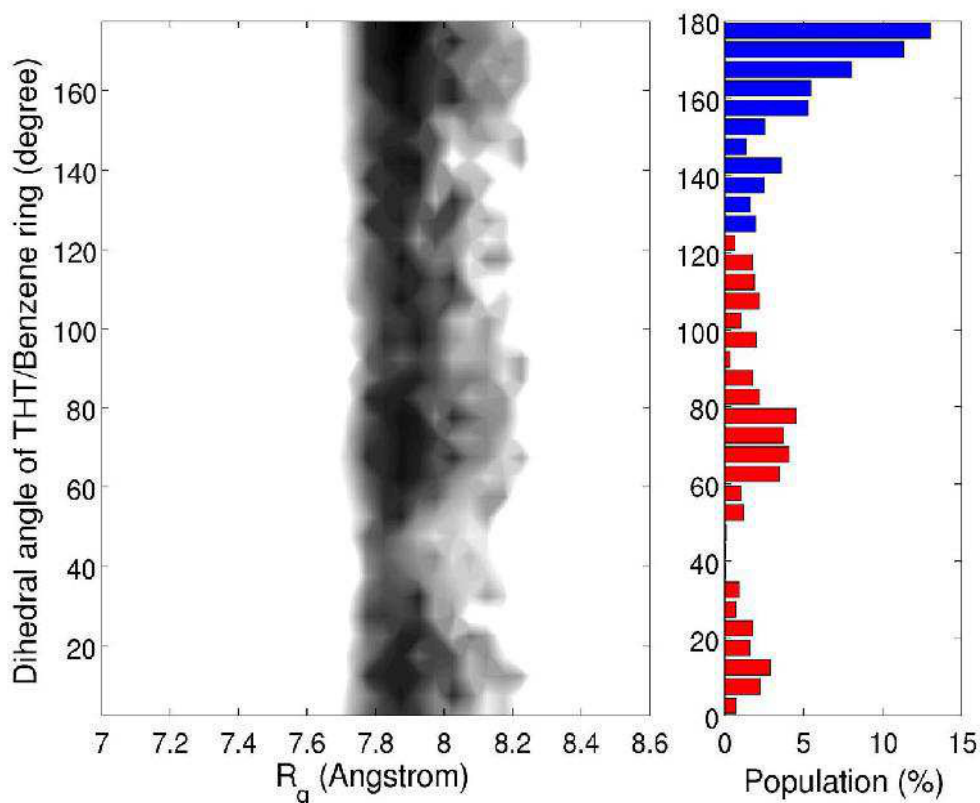
Figure 4.6 Potential of free energy surface of PXT-ES at 80 °C versus Rg. Column on the right shows dihedral angle versus % of population. The red zone in % of population represents the reactive region for *trans* elimination, the blue zone represents the non-reactive region for *trans* elimination.

It appears that the 20 PEG units in the backbone of PEGNOPS form bundles around the PXT chain due to intra- and inter-molecular hydrogen bonding between PEG units (Figure 4.9). Such H-bonding is possible in the absence of water. The bundles organize the PXT chain in a conformation that favors E2 elimination.
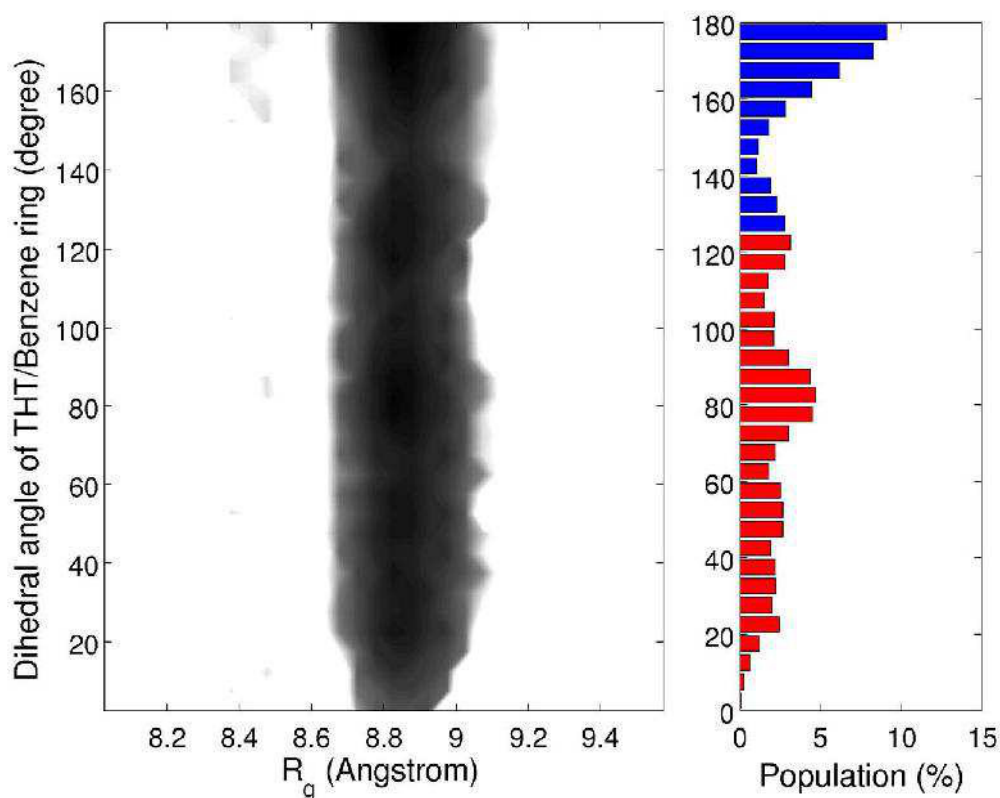
Figure 4.7 Potential of free energy surface of PXT-PEGNOPS at 80 °C versus Rg. Column on the right shows dihedral angle versus % of population. The red zone in % population represents the active region for *trans* elimination, the blue zone represent the non-reactive region for *trans* elimination.
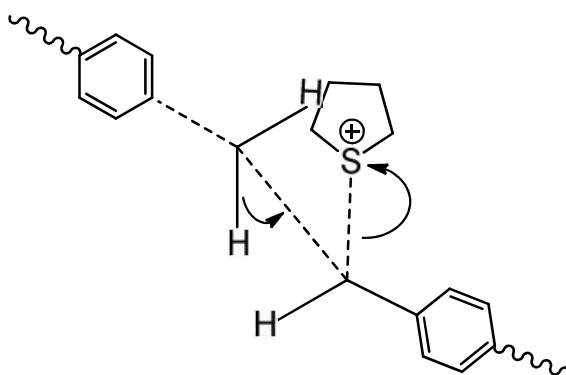
Figure 4.8 The dashed lines are the C-C/C-S dihedral angle optimized for the E2 elimination mechanism shown by the arrows.

Table 4.1 PXT conformations for different dihedral angles and E2 mechanism reactivity at that angle.

THT/Benzene dihedral angle	180 º	60 º
THT/ H_b dihedral angle	60 º	180 º
	Non reactive region	**Reactive region**
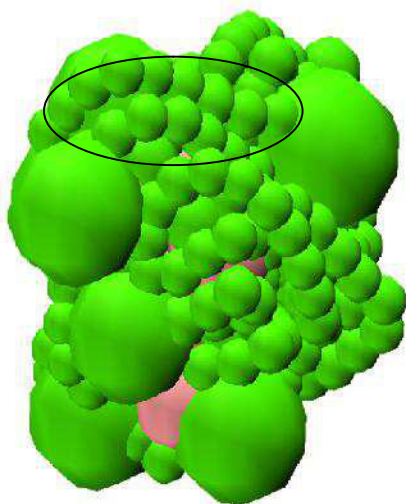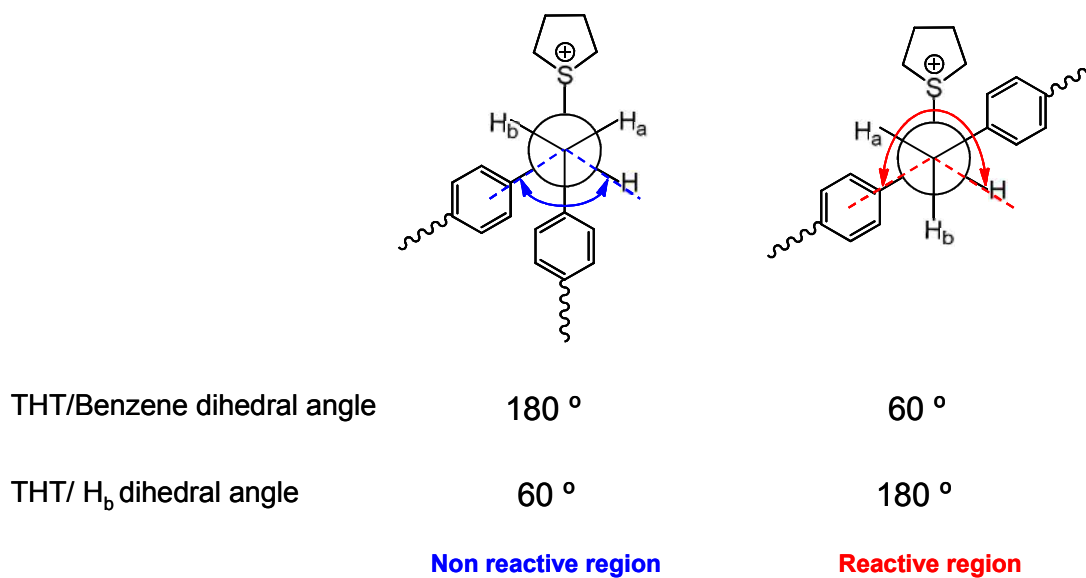
Figure 4.9 Molecular modeling of PEGNOPS in the film showing bundles formed by PEG units.

To support the idea that PXT needs to be organized in the solid state, Figure 4.10 compares UV-vis spectra of PXT-PEGNOPS thermally eliminated in solution *versus* in film at the same temperature (80 °C). PPV-PEGNOPS prepared in film form is more red-shifted in both absorption and emission spectra. The shorter fluorescence wavelength of PXT-PEGNOPS in solution is due to the shorter length of conjugation of PPV. In solution, PEG hydrogen bonds with water whereas in the PXT-PEGNOPS film PEG has the opportunity to H-bond with itself. The vibronic peaks in the fluorescence spectrum of PXT-PEGNOPS in the film are well developed and overlap with the fluorescence peak from shorter conjugated length PPV segments.[141] Thus, the PEG units in PEGNOPS appear to play a role in pre-ordering the PXT chain prior to elimination when the system is in the solid state.
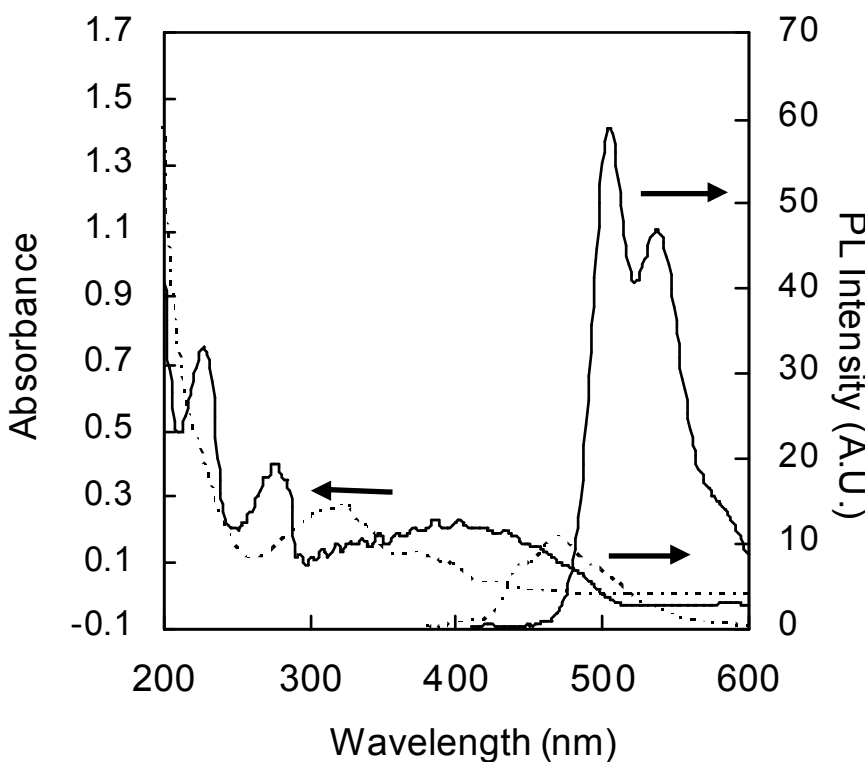
Figure 4.10 UV-vis and PL spectra of PXT-PEGNOPS film thermally annealed at 80 °C in air for 20 min (solid line) and of PXT-PEGNOPS solution thermally annealed at 80 °C for 120 min (dotted line).

4.4 Conclusion

The counterion has proven to be a convenient and versatile variable for controlling the solution properties of conjugated polymers. In the solid state, the PEGNOPS aliphatic sulfonate used here occupies most of the volume of the PXT precursor chain. The environment for thermal elimination of PXT films is now defined by the counterion and PXT chain segments are well isolated. The molecular dynamics computational study revealed partial control of the PXT backbone configuration by the polyether tails of the PEGNOPS, setting up the molecule for elimination in the preferred *trans* geometry at 80 ºC, the lowest temperature reported for efficient elimination of PXT to yield photoluminescing PPV.

CHAPTER 5

THE USE OF FT-IR TOWARDS EXPLORING THE POLYANION EFFECT ON PPV PRECURSOR ELIMINATION

5.1 Introduction

Organic light emitting diodes (OLED)s have been successfully fabricated with thin films using thermal evaporation methods, spin coating of conjugated polymers and layer-by-layer (LBL) assembly of precursors of conjugated luminescent polymers.[46,47, 132, 142-144] LBL assembly is a thin film formation method formed from alternating polycations and polyanions.[145] The LBL assembly offers the ability to fabricate different hetero-structures that fulfill different functions such as a charge injection layer at the electrodes, control over the recombination zone and the interface with the electrode.[51] The thickness of the films prepared by the LBL assembly can be controlled at the molecular level, which is an advantage that the other deposition methods lack.[132, 144] Another advantage of the LBL method is the unlimited choice of materials which can be used in the film. Films can be made from almost anything (nanoparticle, quantumn dots, polyelectrolyte, and polymers).[146] Although poly(phenylene vinylene) (PPV) insolubility in most solvent makes its processability complicated,[66] PPV is one of the most studied and promising conjugated electroluminescent polymers.[109] The processability issue of PPV was overcome by using the aqueous precursor route to PPV. The LBL thin assembly holds the promise to fabricate inexpensive, lightweight, and flexible large area OLEDs.

Many groups explored the LBL assembly of poly(xylylidene tetrahydropthiphenium) (PXT) with the two most used polyanions in the field poly(styrene sulfonate) (PSS), poly(acrylic acid) (PAA) and poly(methyacrylate) (PMA). PAA and PMA should have the same effect on the assembly because they have carboxylate as a functional group. PSS with a strong basic group (SO_3^-) is expected to enhance the elimination. Rubner and his collaborators reported assembling PPV

precursors with polyanions in LBL assembly and the ability to form PPV in these multilayer by thermal treatment.[50] Fou et. al. discussed the effect of the polyanions (PMA and PSS) and found out that PPV/PMA had a higher absorbance than that of PPV/PSS, although PPV/PMA was blue shifted.[132] The effect of ionic strength on the conjugation of PPV in LBL was explored by Cho et al., the higher the salt concentration the lower the conjugation length of PPV/PSS.[147] Recently, Ogawa et al. pointed out that PPV can be converted at low temperature (< 100 ºC) when assembled with PSS with an improved PL.[148] It is well known that polyanions play an important role in the optical properties of PXT/polyanion assembly.[50] This field lacks an explanation of how these polyanions have different effects on the optical properties of the PPV. The aim of this work is to reveal the mechanism of elimination for PXT in the assembly with PAA and PSS as polyanion using FT-IR.

5.2 Experimental Section

5.2.1 Materials

PSS (Mw 70,000, acid form), PAA (Mw 250,000, acid form) and α, ά-dichloro-*p*-xylene (98%) were purchased from Sigma-Aldrich. PXT polymer was prepared as mentioned in an earlier paper.[149]

5.2.2 Multilayer Assembly

The multilayers were deposited on polished silicon wafers <100> and quartz slides cleaned using piranha. The silicon wafers were dipped in 10 mM poly(ethylene imine) (PEI) for 20 min as a pretreatment before PEMU assembly. The substrates were dipped in the polyelectrolyte solutions for 10 min and then rinsed three times, for 1 min, with distilled water. The multilayers were dried with a gentle nitrogen stream. All multilayers were assembled from 1 mM PXT (pH 5.6) and either PSS or PAA 10 mM (based on the monomer repeat unit) at pH of 4 and 5.8, respectively. NaCl was added only to the polyanion solution not to PXT (precipitation of PXT was observed via addition of salt).

UV-vis spectra were recorded on a Varian Cary Bio 100 UV-vis double beam spectrophotometer.

Infrared (IR) spectroscopy was performed using a nitrogen purged FTIR (Nicolet Nexus 470 with a DTGS detector) spectrometer; spectra were taken at a resolution of 4 cm^{-1} with 36 averaged scans.

The PXT multilayers were eliminated under vacuum on a vacuum line equipped with an oil diffusion pump. The temperature was monitored by a thermocouple which was in direct contact with the substrate on which the film was assembled. All the multilayers were left under vacuum for 2 h prior to elimination and during the cooling process.

5.3 Results and Discussion

The simplicity of LBL assembly, compared to spin coating and vacuum deposition, is one of the reasons that the LBL technique gained popularity in OLED research. The main role of the polyanion is to serve in assembling the multilayer via electrostatic interactions with the polycation. The polyanion with its negatively charged functional group acts as a base that assists in the elimination of PXT.[132] The elimination of PXT that is compensated with small counterions yields a byproduct which is the conjugate acid of the anion (HA Figure 4.1) that has the ability to leach to the electrode and degrades it.[150] In multilayers, PXT is compensated with polyanion, the acid of which is immobile which increases lifetime of the electrode.[151] The photoluminescence intensity of the PPV thin film in such assemblies is implied by percentage of conversion of PXT to PPV where quenching sites on the backbone come into play e.g. carbonyl formation.

Table 5.1   Assignment of IR peaks for PXT, PPV, PSS and PAA.

Functional Group	IR peak wavenumber (cm^{-1})	IR modes
Trans vinylene C-H	3021-3025	Stretch
CH$_2$	2941	Stretch
Carbonyl of 6 member ring Cyclic anhydride	1800 & 1760	Asymmetric & symmetric
Aliphatic carbonyl	1721	Aliphatic carbonyl
Carboxylate COO$^-$	1553	Asymmetric stretch
Carboxylate COO$^-$	1423 & 1447	Symmetric stretch
C-O	1360	Stretch
C-O in ester	1165	Stretch
S-O-C	903-906	Stretch
Trans vinylene	961-965	Out of plane bending
Mono substituted benzene ring	700 & 732	
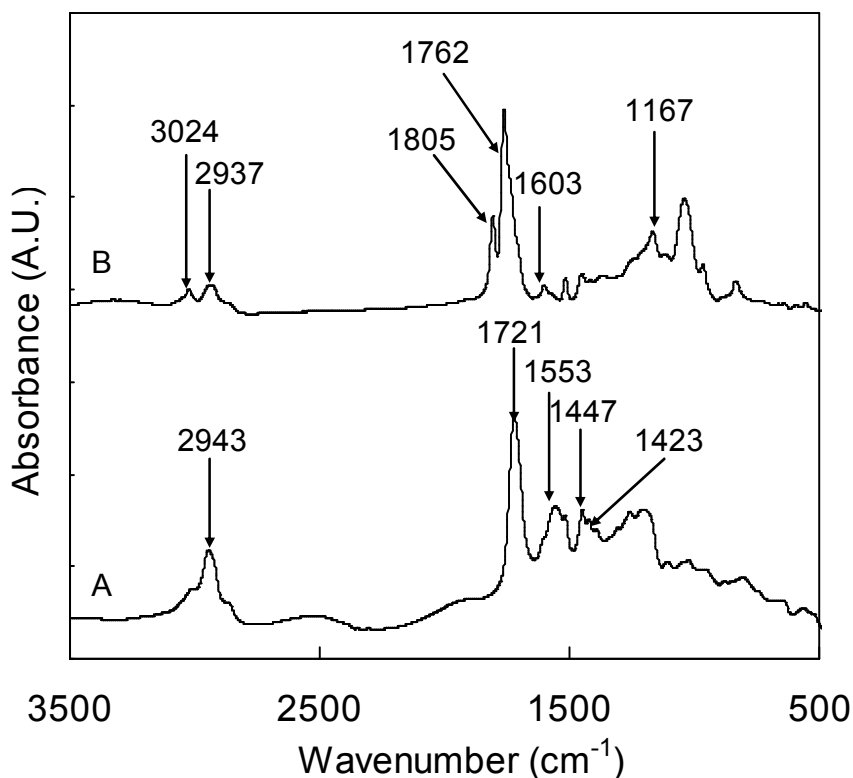
Figure 5.1 The FT-IR absorption spectrum of PEI(PXT/PAA)$_{50}$ built from 0.25M NaCl (A) before elimination (B) after elimination at 210 ºC for 10 min under vacuum.

5.3.1 Elimination in PXT/PAA Films

Experiments were performed to find the minimum number of the bilayers required to keep a track of all the significant peaks. It was found that 50 bilayers of PXT/Polyanion are required for FT-IR analysis. Figure 5.1 shows the FT-IR absorption of PEI(PXT/PAA)$_{50}$ built from 0.25 M NaCl before and after thermal annealing at 210 ºC for 10 min under vacuum. Prior to elimination, PAA in the multilayer is present in both the acidic form COOH (1721 and 2520 cm^{-1}) and carboxylate form COO$^-$ (1423, 1447 and 1553 cm^{-1}) (Figure 5.1 A) because PAA is not fully deprotonated. Table 5.1 shows the different FT-IR peak assignments. The intensity of COOH stretch is expected to increase as elimination takes place synchronized with a decrease in COO$^-$ and an increase in PPV peak at 3024 cm^{-1} reflecting the degree of elimination. Our results show that a disappearance of COOH and COO$^-$ peaks occurred after elimination. The

72

peaks at 1805 and 1760 cm^{-1} that showed up post elimination correspond to the C=O stretch in a six member ring cyclic anhydride (SMRCA). In addition to the peaks at 1165 and 1040 cm^{-1} which correspond to C-O and C-O-C stretching peak (Fig 5.1 B). Figure 5.2 shows the proposed reaction for PXT/PAA during elimination. The formation of five and six member cyclic anhydride by thermal processing without catalysis is well known.[152,153]
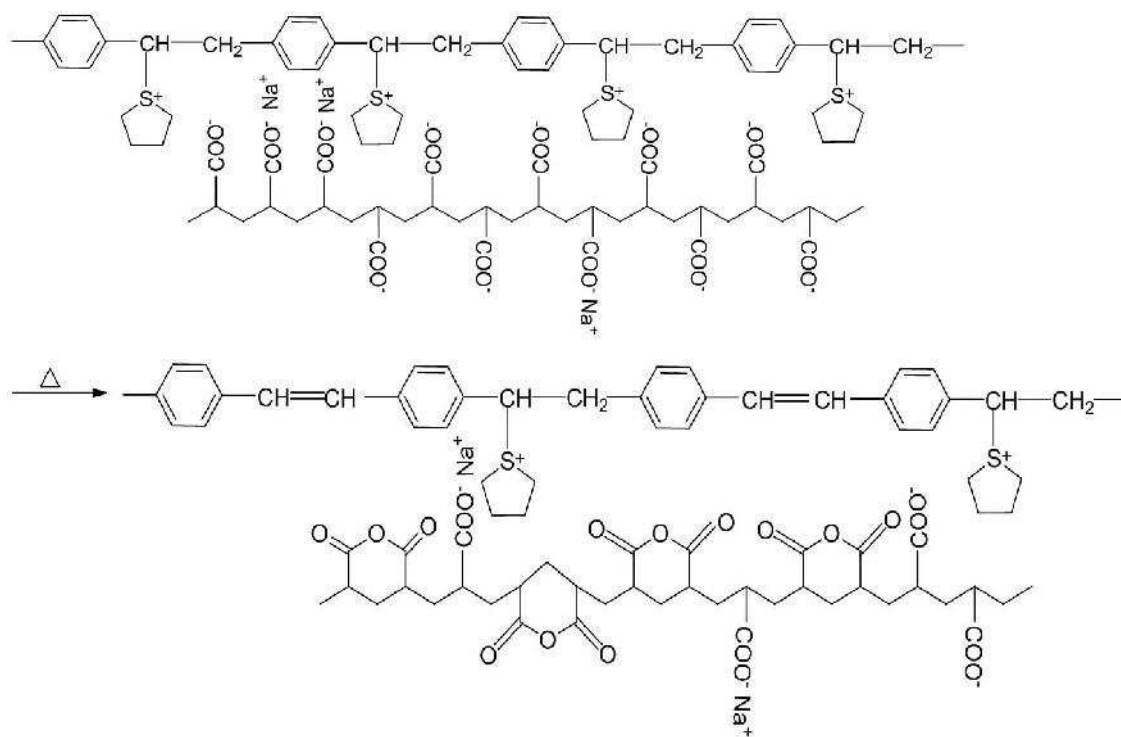
Figure 5.2   The possible reaction occurring in PXT/PAA multilayer during elimination in which a cyclic anhydride ring is formed.

5.3.2 The Kinetics of Elimination in PXT/PAA Films

The most common elimination method used for the formation of PPV in both multilayers and films requires a temperature of 210 °C for 9-11 h [115, 132] but a kinetic study of the optimum time required for elimination is not available. This long time of elimination may be an obstacle towards the commercialization of PPV multilayer in OLED application in which thermally sensitive materials are used. The optimum time that yields the highest conjugation is examined by UV-vis and FT-IR for multilayers heated at different times at 210 °C under vacuum from 10 min to 2 h. A broad

distribution of conjugation length is found for samples eliminated between 10-120 min; presented by the broad peak of absorption from 270-500 nm with a maximum at 390 nm (Figure 5.3). After 120 min of elimination the length of conjugation decreased, the absorbance was blue shifted (Figure 5.3). The FT-IR kinetic results (Figure 5.4) showed that the amount of double bond 3024 cm^{-1} (*trans* vinylene C-H stretch) and that of carbonyl in cyclic anhydride peak did not change while that of the carbonyl peak due to the oxidation of the backbone was unresolved. This is either due to oxidation not taking place or the peak being masked by the carbonyl peak of PAA.
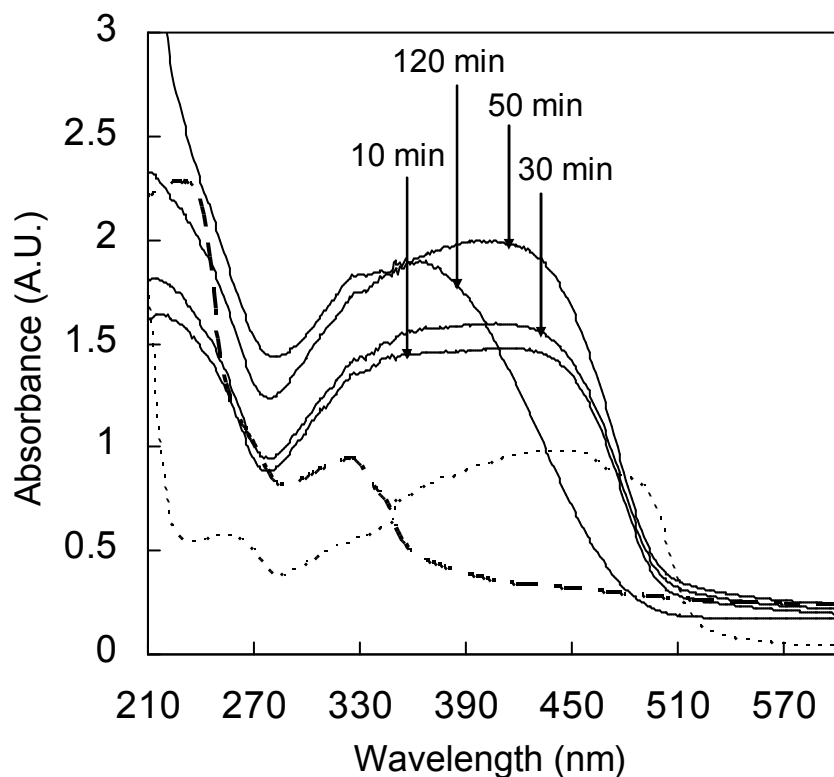
Figure 5.3   The UV-vis spectra of PEI(PXT/PAA)$_{50}$ (0.25M NaCl) at 210 ºC under vacuum for 10, 30, 50 and 120 min, (_ _) PEI(PXT/PAA)$_{50}$ (0.25 M NaCl) before elimination, and (.....) PXT-Cl after elimination at 210 ºC under vacuum.

Figure 5.4 The area of the FT-IR peaks of PEI(PXT/PAA)$_{50}$ (0.25 M NaCl) elimination at 210 °C under vacuum (dotted) of 2943 cm^{-1} (CH$_2$ stretch) , (filled) of 3024 cm^{-1} (*trans* vinylene C-H stretch) and (strips) of 1762 cm^{-1} (carbonyl stretch of 6 member ring cyclic anhydride).

5.3.3 Elimination in PXT/PSS Films

The UV-vis kinetic study of PXT-PSS at 210 °C showed that 10 min is the optimum time for elimination (Figure 5.7). The FT-IR spectra of the multilayer prior and post elimination were examined. The expected PPV peaks post elimination were observed at 962 cm^{-1} and 3024 cm^{-1} peaks (Figure 5.8B) in addition to the unexpected peaks that emerged at 902 cm^{-1}, 1358 cm^{-1} and 701 cm^{-1} which correspond to S-O-C, C-O and mono-substituted benzene ring stretch, respectively. It is well known that one of the major challenges of polystyrene sulfonation is the reversibility of the reaction (de-sulfonation) during which SO$_3$ is released and substituted by H$^+$ (Figure 5.5). Any acidic sulfonating agent e.g. H$_2$SO$_4$ can be a catalyst for desulfonation.[154] Alternatively SO$_3$ reaction with double bond to form sultones is well known especially the reaction of SO$_3$

with diphenylethylene which resembles the PPV (e.g. Figure 5.6).[155] We believe that in the PXT/PSS multilayer the SO_3, yielded from the desulfonation reaction of PSS, is reacting with the double bond formed by the elimination of PXT to form a sultone bond (Figure 5.9). The proton yielded during elimination to PPV enhanced the desulfonation. The sultone formation reduced the amount of PPV conjugation, the desulfonation and sultone formation increased as the temperature is increased.

Figure 5.5   The sulfonation/desulfonation equilibrium reaction of aromatic styrene.
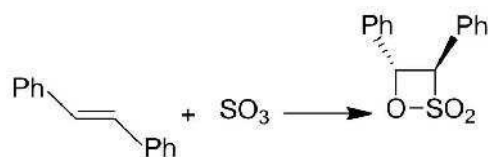
Figure 5.6   The reaction of SO_3 with *trans*-1,2-diphenylethylene to yield the corresponding sultone.
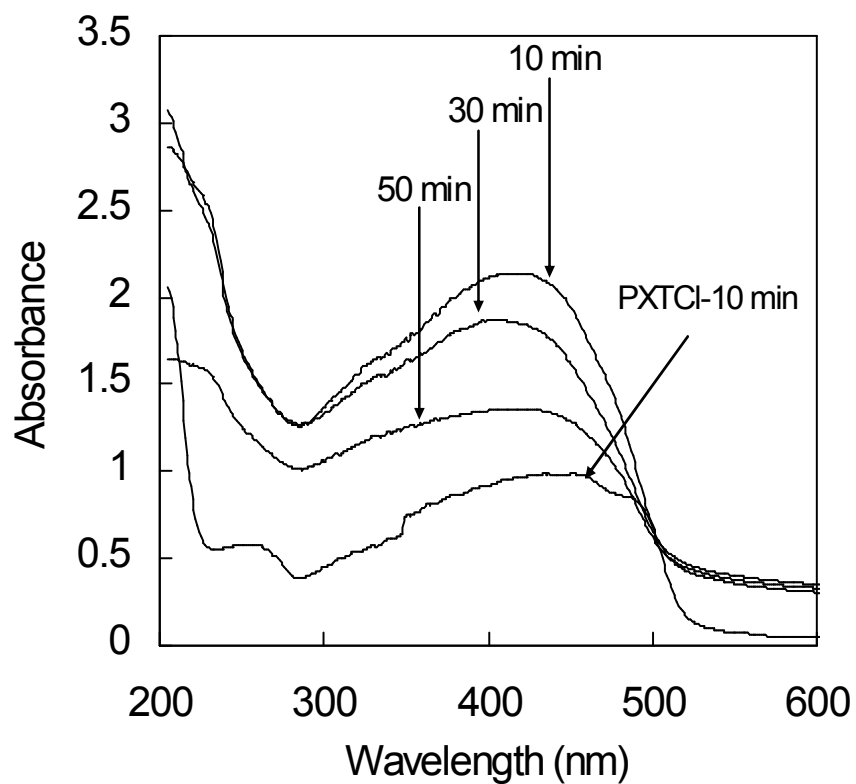
Figure 5.7 UV-vis absorbance of PEI(PXT/PSS)$_{50}$ (0.25 M NaCl) thermally annealed at 210 ºC under vacuum compared to PXT-Cl film elimination at 210 ºC under vacuum for 10 min.
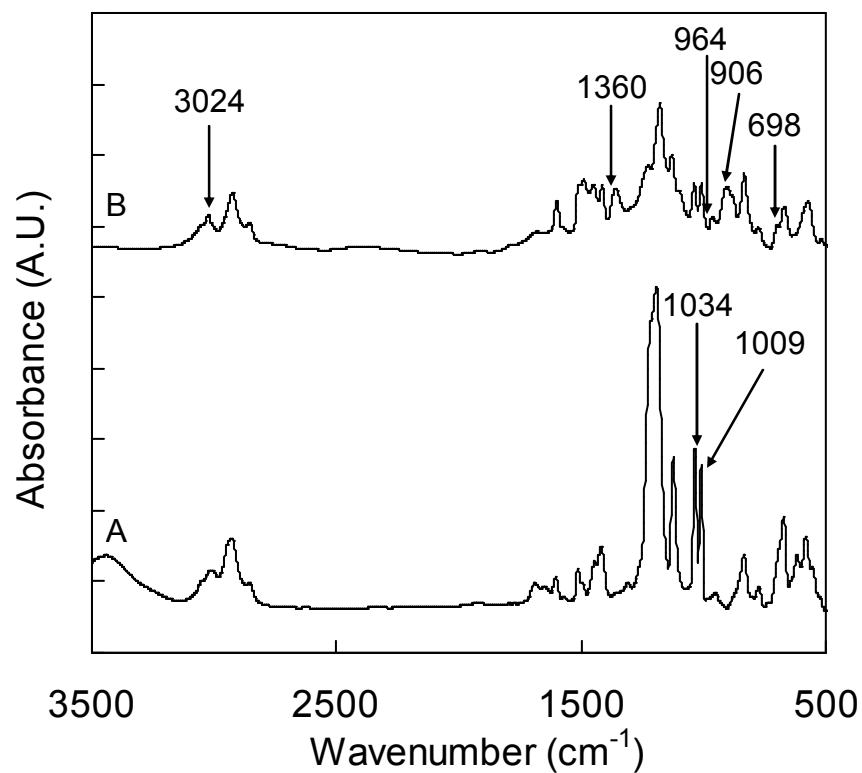
Figure 5.8 FT-IR absorption spectrum of PEI(PXT/PSS)$_{50}$ multilayer built in 0.25M NaCl (A) before thermal annealing and (B) after thermal annealing at 210 ºC under vacuum 10 min.
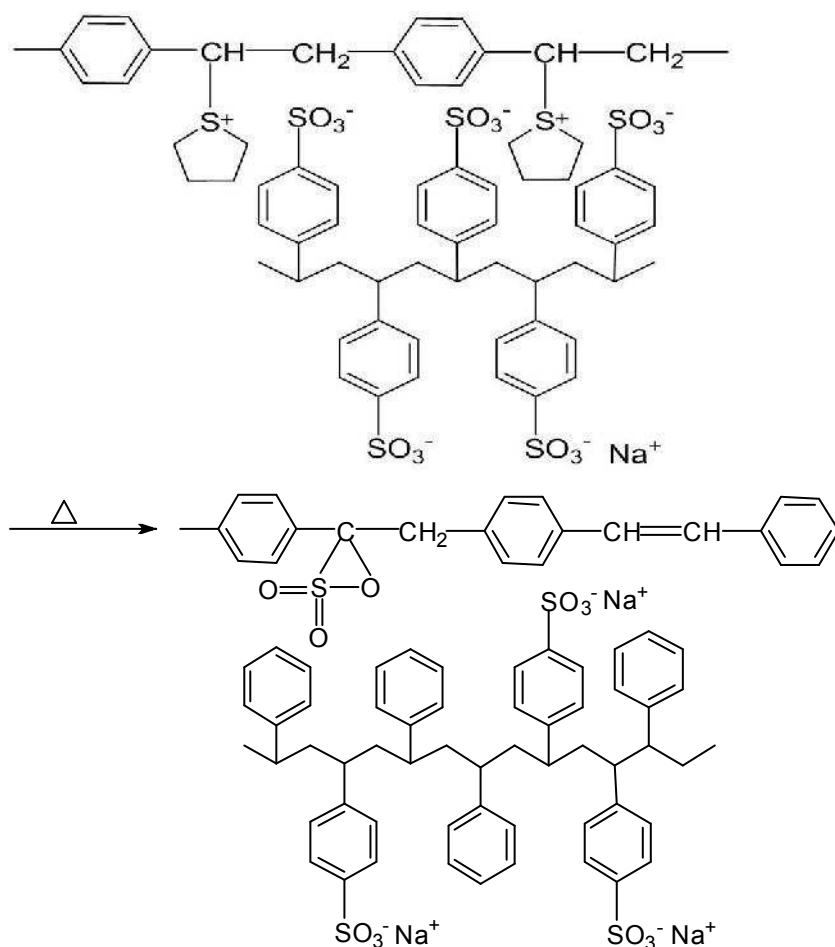
Figure 5.9 The possible reaction occurring in PXT/PSS multilayer during elimination in which sultone bond is formed.

5.4 The Optimum Temperature for the Elimination of PXT/PSS

The elimination of PEI(PXT-PSS)$_{50}$ (0.25 M NaCl) at different temperatures is monitored using FT-IR and UV-vis. Figure 5.10 shows the normalized area (to the area at 1512 cm^{-1}) of the FT-IR peak prior to elimination (25 °C), and those annealed at 100, 150, 210 °C each for 1 h. PPV and sultone formations are tracked by the ratio of the area of the significant peaks (1033 cm^{-1} SO$_3^-$, 1359 cm^{-1} C-O, 3024 cm^{-1} PPV) to the area of the benzene ring bending 1512 cm^{-1} (unchanged during thermal annealing). At 100 °C the elimination took place presented by the peaks at 962 and 3024 cm^{-1}. Despite

the 46.52% reduction of the SO$_3^-$ peak observed at 100 °C which implies that the benzene ring is losing SO$_3$, the SO$_3$ reaction with the C=C of the PPV-co-PXT backbone does not take place under these conditions (low temperature or/and low concentration of SO$_3$) indicated by the absence of 1359 and 900 cm^{-1} peak. The thermal annealing at 150 °C should be perceived as a delicate balance between the extent of elimination and sultone formation. The SO$_3^-$ peak dropped by 76.72% (from that at 25 °C) the sultone formation peak (S-O-C 1359 cm^{-1}) confirms the breakage of a part of the formed double bond of the PPV. The amount of PPV and SO$_3^-$ reduction is similar for films eliminated at 210 and 150 °C within experimental error but the sultone formation indicated by the 1359 cm^{-1} peak is higher than that eliminated at 210 °C. This can be explained by the fact that sultone formation takes place at higher temperatures.
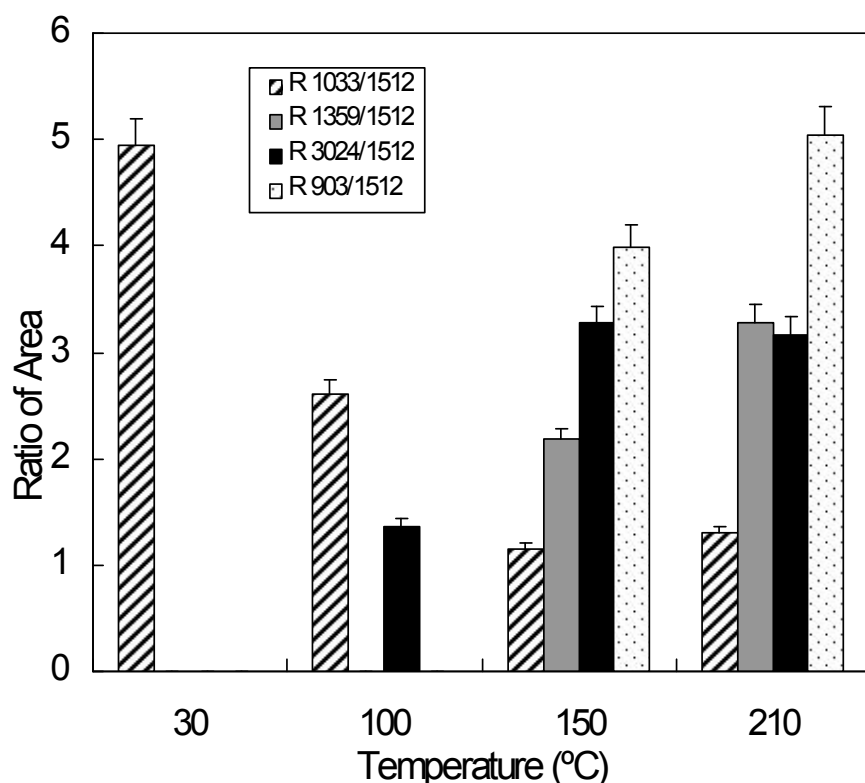
Figure 5.10 Ratio of the area under the FT-IR bands of (grey) (C-O-S) 1359, (black) (PPV) 3024 cm^{-1} and (diagonal strips) 1033 (SO$_3^-$), (dotted) 903 cm^{-1} mono substituted benzene ring to 1512 cm^{-1} (benzene ring out of plane bending) prior to thermal annealing (25 °C), 100, 150, 210 °C for 1 h of PEI(PXT/PSS)$_{50}$.

80
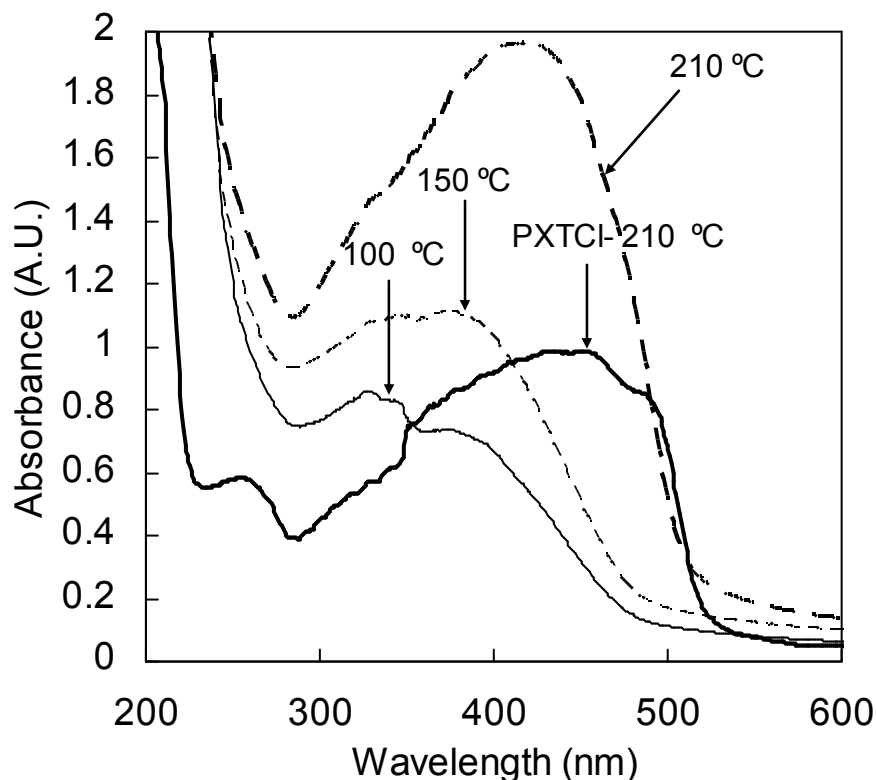
Figure 5.11 PEI(PXT/PSS)$_{50}$ (0.25 M NaCl) solid non bold line 100 °C 1 h, dashed non bold 150 °C and dotted 210 °C 1 h.

FT-IR gives an idea of the amount of the double bond in the film but it lacks the ability to give an indication about the length of conjugation which is critical for the optical properties of these films. The UV-vis of PXT/PSS films (Figure 5.11) was used as a complementary technique to gain insight into the length of conjugation. The UV-vis results support those from FT-IR. The films annealed at 150 °C compared to that at 100 °C showed not only a higher elimination degree but also a higher length of conjugation. The PXT/PSS film annealed at 150 °C is more red shifted than that annealed at 100 °C. Although FT-IR shows that both films annealed at 150 °C and 210 °C have same degree of elimination but films annealed at 210 °C have a higher length of conjugation indicated by the higher red shifting in UV-vis. At this high temperature of annealing the carbonyl formation is more probable. The effect of carbonyl formation usually is more pronounced in photoluminescence rather than UV-vis.

5.5 Conclusion

The mechanism for the elimination of PXT in the assembly of both PSS and PAA can be further complicated by the possible reaction of the polyanion with the double bond. We revealed that the effect of polyanions in such assemblies do not solely depend on the strength of the basicity of the polyanion. The PAA reacted with itself to form an anhydride without interfering with the formed double bond whereas the SO_3 released from PSS reacted with the formed double bond causing a decrease in the elimination. In light of the above results, a higher degree of elimination at lower temperature can be achieved by using a polyanion with strong base functional groups that do not react with the double bonds.

CHAPTER 6

EXPLORING THE HETEROATOM EFFECT ON POLYELECTROLYTE MULTILAYER ASSEMBLY: THE NEGLECTED POLYONIUMS

6.1 Introduction

Layer-by-layer (LBL) assembly was first described by Decher et. al. in 1991 as an alternating adsorption of oppositely charged polyelectrolytes (PE) on charged surfaces.[156] Nowadays, LBL assembly composition is extended to almost everything ranging from nanoparticles to DNA.[18, 157] LBL assembly is a technique used to control the composition and morphology of thin films for nanoassemblies.[14, 158-159] The flexibility and simplicity of this approach, and the ability to integrate diverse functionalities into the assembly, broaden the spectrum of potential applications of these films and continue to intrigue researchers in many fields such as nanotechnology, materials, and biomedical science. These nanoassemblies can be used by themselves or as coatings for other materials to improve their performance in their applications.[157, 160] The potential use of polyelectrolyte multilayers (PEMU) in optoelectronic,[14, 157] separation,[15-17, 157] anti-fouling,[13, 18] corrosion applications have been studied extensively.[13-14] Additional applications of PEMUs in drug delivery,[157, 161] biosensors,[162] tissue engineering[161] and antibacterial applications[161] have also emerged during the last decade.

The bulk and surface properties, such as the film thickness, morphology, wettability, swelling and mechanical properties, of PEMUs are dictated by many factors during build up including: the nature of the PE, molecular weight,[163] ionic strength,[164-165] pH,[35] counterion type[165] and temperature.[166] For example, the higher ionic strength of polyelectrolyte solutions used for build up leads to thicker films.[164,165] Different counterions influence the thickness, hydration and doping of multilayers.[165, 167] The charge density of PEs with weak acids or bases, as charged groups, changes with the pH leading to thicker and more swollen PEMUs when assembled at extreme pH values.[168]

While the comparison between PEs with different chemical functionality, molecular weight, and charge density has been extensively studied, a comparison between PEs of similar characteristic that differ in the nature of the heteroatom nature with tight control is rare. Laschewsky et. al. studied PEMUs built from polycations having chromophores and fluorophores to gain insight into the possibility of aggregation.[169] Schwarz et. al. compared poly(diallyldimethyl ammonium) (PDADMA)/poly(styrene sulfonate) (PSS) to poly(ethylene imine) (PEI)/PSS PEMU growth with different polycation molecular weights.[163] Boudou et. al. compared poly(l-lysine) (PLL)/ hyaluronic (HA), chitosan/HA and poly(allylamine hydrochloric acid) (PAH)/poly(L-glutamic acid) hydration, thickness and mechanical properties.[170] The effect of a blend of like-charged PEs on thickness and morphology of PEMUs was explored by Quinn et. al.[171] In most of these systems the polyelectrolytes compared showed a difference in several of the following: chemical nature of the functional group, bulkiness of the groups, stiffness, and nature of the backbone. Although molecular weight is usually considered/reported in comparing PEMUs, most of the time the PEs differ strongly in molecular weight. The influence of the nature of the charged unit, one of the most important variables in PEs, has rarely been studied for identical backbones. The question that rises up in this field is whether a different behavior is missed by using one of the heteroatoms (phosphonium, suflonium or ammonium) instead of the other.

Knowing that the charge in PEs is located on the heteroatoms, a greater variety of heteroatoms for polyanions exists compared to polycations. Main examples of the former include the sulfonate group (pH independent) and the carboxylate group (weak acid). The heteroatom for polycations used in the field is almost exclusively nitrogen which is either a quaternary ammonium cations (aromatic or not) which are either permanently charged polymers or an amine for a weak/acid base. The most commonly cited polycations are PDADMA, poly(vinyl-4-methyl pyridine) (PV4MP), PAH, PEI, and PLL (Figure 6.1). In a recent review, Jaeger et. al. presented an extensive list of quaternary ammonium polycations describing the developments and progress in their synthesis and applications.[172] Although the same (nitrogen) heteroatom is employed, a vast range of hydrophobicities and charge densities are represented,[172] resulting in an equally large range of PEMU properties. In a recent comparison of two polycations,

PDADMA and PAH, it was demonstrated that the respective association energy of PAH/PSS and PDADMA/PSS were -10 kJ/mole and 5 kJ/mole, showing that PSS associates with PAH more strongly than with PDADMA.[173] Two sulfonium polycations, poly(xylylidene tetrahydrothiophenium) (PXT) and poly(xylylidene dimethylsulfonium) (PXDMS) (Figure 6.1), important precursors for the electroluminescent conjugated polymer poly(phenylene vinylene) (PPV), have been used to make multilayers.[14, 174] PXT gave exceptionally thin PEMUs, which could be attributed to the heteroatom itself, a low charge density, or a relatively high molecular weight. Very recently, Cini et. al. illustrated some unusual and counterintuitive modes of multilayer growth depending on the selection of polyanion.[30]
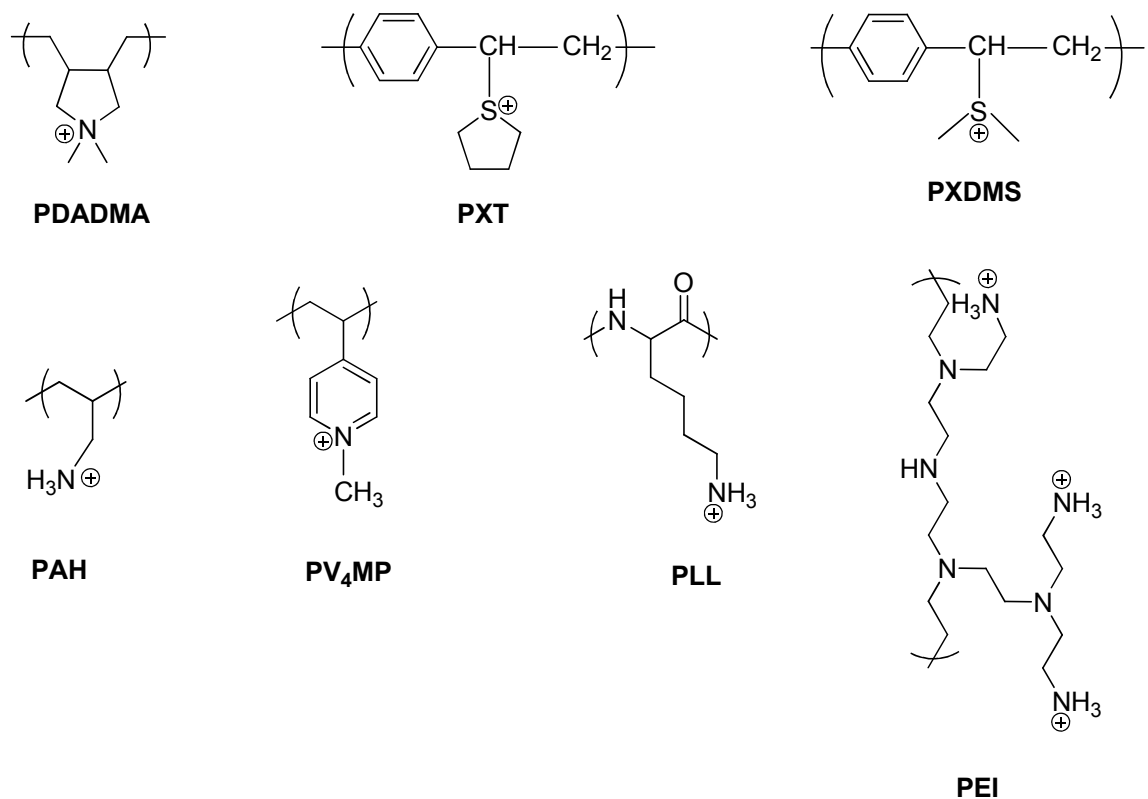
Figure 6.1   Common polycations used for multilayers: PDADMA, PXT, PXDMS, PAH, PV4MP, PLL and PEI. All shown without the counterion (usually chloride).

The goal of this work was to compare the behavior of three different multilayers assembled of three polycations, identical in every respect (i.e. molecular weight, molecular weight distribution, charge density, backbone composition), except for the

heteroatom: ammonium, phosphonium and sulfonium. To our knowledge, phosphonium PEs have not been used in PEMUs. These three polyoniums are of the type synthesized for industrial purposes in the 50s:[175-177] poly(*p*-vinyl benzyl trimethyl ammonium) (PVBTMA), poly(*p*-vinyl benzyl trimethyl phosphonium) (PVBTMP) and poly(*p*-vinyl benzyl dimethyl sulfonium) (PVBDMS). For the purpose of comparison, all three were prepared by the conversion of the same precursor *p*-vinylbenzyl chloride (PVBCl) polymer. The synthetic challenge was to achieve a high conversion from the polymer to the polyelectrolyte similar percentages of substitution for the three oniums so that it is possible to compare their PEMU properties.

6.2 Experimental Section

6.2.1 Materials

Trimethylphosphine (97%), trimethylamine (43% by weight in water), dimethylformamide (DMF) (anhydrous, 99.8%), PSS (Mw= 70,000, acid form) and PAA (Mw =100,000, acid form) were used as received from Sigma-Aldrich. Ethyl acetate (HPLC grade) and tris buffer (molecular biology grade) were purchased from Fisher Scientific. Diethyl ether (BDH, >99%), dimethyl sulfide (Alfa Aesar, 99+%), methanol (Malinckrodt, anhydrous, 99.9%), sodium chloride (EMD, >99%) and PVBCl (Scientific Polymer Products, M_w (127,900 ± 600) g/mol), were used as received. Dialysis membranes (Spectra/Pro, molecular weight cutoff 12,000 to 14,000) from Spectrum Laboratories were soaked in water for 30 min and rinsed extensively prior to use. 18 Mohm Milli-Q water was used throughout. NMR spectra were recorded on a Bruker UltraShield 400 spectrometer operating at 400 MHz for ^{1}H and at 100 MHz for ^{13}C.

6.2.2 Polymer Modification

Ammonium Polyelectrolyte: Poly(*p*-vinyl benzyl trimethyl ammonium chloride) (PVBTMA): To 0.60 g (3.9 mmol) of PVBCl and 11 mL of water were added to 5 mL of a 43 wt% solution of trimethylamine (73.6 mmol, 19 equiv.) in a sealable tube equipped with a magnetic stir bar. The tube was sealed immediately under nitrogen and the mixture was stirred for 48 h at 32 °C. After about 16 h a clear solution was obtained. The solution was dialyzed for 4 days against water and subsequently lyophilized (yield

90 %). The degree of substitution was 95 % according to ^{1}H NMR. ^{1}H NMR (D$_2$O): δ (ppm) = 7.19 (CHC*H*), 6.58 (C*H*CH), 4.37 (C*H$_2$*N), 2.95 (NC*H$_3$*), 2.30-0.80 (br m, C*H$_2$*C*H*). ^{13}C NMR (D$_2$O): δ (ppm) = 150-146 (br, *C*CH), 132.4 (*C*HCH), 128.4 (CH*C*H), 124.8 (*C*CH$_2$), 68.8 (*C*H$_2$N), 52.2 (N*C*H$_3$), 47-41 (br m, *C*H$_2$CH), 40.4 (CH$_2$*C*H), 27.1 (*C*H$_2$OH). IR (KBr) ν$_{max}$ = 3433, 3017, 2966 (ν$_{as}$ CH$_3$), 2929 (ν$_{as}$ CH$_2$), 2871 (ν$_s$ CH$_3$), 2078, 1936, 1632, 1512 (benzene ring in plane bending), 1476, 1427, 1385, 1262, 1222, 1110, 1021, 976 (ν$_{as}$ CH$_3$N), 924 (ν$_s$ CH$_3$N), 889, 858, 826, 709 cm^{-1}. Elemental analysis (Atlantic Microlab): Calculated for PVBTMA.2H$_2$O 95 % substitution C: 59.10 %, H: 8.93 %, N: 5.21 %, found C: 57.52 %, H: 8.94 %, N: 5.21 %.

Phosphonium Polyelectrolyte: Poly(*p*-vinyl benzyl trimethyl phosphonium chloride) (PVBTMP): 4.00 g (26.3 mmol) of PVBCl were dissolved in 55 mL of DMF under nitrogen in a three-neck-flask. The solution was cooled to 0 °C and 6 mL (58.0 mmol, 2.2 equiv.) of trimethylphosphine were added. The solution was stirred at room temperature under nitrogen for a total of 48 h. Portions of methanol were added whenever precipitation occurred until dissolution (total of 14 mL). Additional trimethylphosphine (total of 10 mL, 96.6 mmol, 3.7 equiv.) was added after 16 and 24 h. The reaction solution was precipitated in ethyl acetate, the solid was filtered, washed with ethyl acetate and dried under vacuum. The product was redissolved in 150 mL water and dialyzed for 3 days against water followed by lyophilization.The product was obtained as a white powder with a degree of substitution of 98 % in a yield of 90 %. ^{1}H NMR (D$_2$O): δ (ppm) = 7.04 (C*H*CH), 6.51 (CHC*H*), 4.41 (CH$_2$OH), 3.66 (C*H$_2$*P), 1.72 (PC*H$_3$*) 2.30-0.80 (br m, C*H$_2$*C*H*). ^{13}C NMR (D$_2$O): δ (ppm) = 145.6 (br, *C*CH), 129.7 (*C*HCH), 128.7 (CH*C*H), 126.0 (*C*CH$_2$), 47-41 (br m, *C*H$_2$CH), 40.3 (CH$_2$*C*H), 29.8 (d, J = 51 Hz, *C*H$_2$P), 27.4 (*C*H$_2$OH), 7.1 (d, J = 56 Hz, P*C*H$_3$). IR (KBr) ν$_{max}$ = 3443, 3024, 2969 (ν$_{as}$ CH$_3$), 2918 (ν$_{as}$ CH$_2$), 2850 (ν$_s$ CH$_3$), 2071, 1934, 1635, 1540, 1510 (benzene ring in plane bending), 1425 (CH$_2$P$^+$), 1300 (CH$_3$P$^+$), 1258, 1108, 965, 912, 889 (CH$_3$P$^+$), 835, 770, 698, 646 cm^{-1}. Elemental analysis (Atlantic Microlab): Calculated for PVBTMP.2H$_2$O 97% substitution C: 55.11 %, H: 8.4 %, found C: 55.24 %, H: 8.37 %.

Sulfonium Polyelectrolyte: Poly(p-vinyl benzyl dimethyl sulfonium chloride) (PVBDMS): 4.07 g (26.7 mmol) of PVBCl and 4.2 mL (57.5 mmol, 2.2 equiv.) of dimethylsulfide were mixed under nitrogen in a two-neck flask equipped with a reflux

condenser yielding a viscous solution. Then 200 mL of water were added and the mixture was heated to 45 °C for 6 h. A gel like phase was formed after about 2 h that gradually dissolved. The solution was filtered and extracted four times with diethyl ether. The aqueous phase was dialyzed for 48 h against water. The resulting solutions had a concentration of about 50 mM, they were stored at 4 ºC until they were used (yield 87 %). The degree of substitution was determined by ^{1}H NMR to be 93 %. ^{1}H NMR (D_2O): δ (ppm) = 7.13 (C*H*CH), 6.54 (CHC*H*), 4.53 (C*H*$_2$S), 2.68 (SC*H*$_3$), 2.30-0.80 (br m, C*H*$_2$C*H*). ^{13}C NMR (D_2O): δ (ppm) = 149-144 (br, *C*CH), 130.5 (*C*HCH), 128.8 (CH*C*H), 124.5 (*C*CH$_2$), 46.4 (*C*H$_2$S), 47-41 (br m, *C*H$_2$CH), 40.3 (CH$_2$*C*H), 27.2 (*C*H$_2$OH), 23.6 (S*C*H$_3$). IR (KBr) ν_{max} = 3417, 3017, 2998 (ν_{as} CH$_3$), 2921 (ν_{as} CH$_2$), 2854 (ν_s CH$_3$), 2339, 1193, 2062, 1926, 1628, 1610, 1510 (benzene ring in plane bending), 1425 (CH$_2$S), 1363, 1334, 1263, 1187, 1113, 1046, 1007, 933, 843, 695, 655, 629 cm^{-1}. Elemental analysis (Atlantic Microlab): Calculated for PVBDMS.2H$_2$O 92 % substitution C: 58.58 %, H: 6.61%, S: 12.95, found C: 56.23 %, H: 7.32 %, S: 11.30 %.

6.2.3 Multilayer Build up

All multilayers were built from 5 mM (based on the repeat unit) PE solutions. For the build up of PSS containing PEMUs the NaCl concentrations ranged from 0.1 M to 2 M. The pH of the PSS solution was adjusted to 7. For PEMUs built with PAA, the PEs were dissolved in Tris buffer (10 mM, pH 7.4, 0.15M NaCl) and the pH re-adjusted as needed.

Multilayers were deposited on polished Si <100> wafers cleaned using "piranha" (7/3 by volume H$_2$SO$_4$/H$_2$O$_2$). Si wafers were dipped in 10 mM PEI for 20 min as a pretreatment before PEMU assembly. Wafers were dipped in the PE solutions for 10 min and then rinsed three times for 1 min with water. The multilayers were dried with a gentle nitrogen stream, and the dry thickness was measured using a Gaertner Scientific L116B Autogain ellipsometer.

Quartz crystal microbalance (QCM) experiments were performed using a Q-Sense E4 with gold coated quartz crystals having a nominal resonance frequency of 4.95 MHz (both from Q-Sense). The crystals were cleaned using air plasma for 30 sec and extensively rinsed with water directly before use. Multilayers were built by bringing

the PE solutions (5 mM in PE, 0.25 M NaCl) into contact with the surface for 10 min followed by rinsing with water for 3 min. A viscoelastic model was used to calculate the wet thickness of the PEI(PSS/onium)$_4$ multilayers in tris buffer based on the recorded changes of the frequency and dissipation for the 3rd, 5th, 7th, 9th and 11th harmonic. Polymer molecular weights were measured using a PLgel 10 µm particle size Mixed-B SEC Column (Varian/Polymer Laboratories), tetrahydrofuran mobile phase and a DAWN EOS multi-angle static light scattering (MALS) photometer (Wyatt Technology Corp., Santa Barbara, CA, USA).

6.2.4 Multilayer Characterization

The dynamic contact angles with water, advancing and receding, of PEMU built on double-sided silicon wafers were obtained using the Wilhelmey plate technique (Cahn Instruments, DCA 300). Infrared (IR) spectroscopy was performed using a nitrogen purged FTIR (Nicolet Nexus 470 with a DTGS detector) spectrometer, spectra were taken at a resolution of 4 cm^{-1} with 36 averaged scans. Roughnesses of the multilayers were measured in air using an AFM (Asylum Research Inc., Santa Barbara, CA) equipped with Igor Pro Software. Measurements were done with a Multi75Al (Budget Sensors) silicon probe with a 225 µm length, 28 µm width and 75 kHz resonant frequency in the tapping mode. For the sake of comparison between PEMU build up the silicon wafer and gold surfaces, half of a plasma cleaned silicon wafer was coated by 100 nm gold using AUTO 306 Vacuum Coater with a turbomolecular pumping system. A comparison was made of the thickness of PEI(PSS/PVBTMP)$_4$ built on silicon and gold from 0.25M NaCl using AFM.

6.3 Results and Discussion

6.3.1 Synthesis

The two methods for synthesizing PEs are; the direct polymerization of the corresponding monomeric unsaturated salt (e.g: styrene sulfonate polymerization) and modification of a polymer (e.g: sulfonation of polystyrene). The polymer modification method has the advantage that the procedures are well established or, in some cases, the polymer is commercially available. The direct polymerization has the advantage of

yielding polymers that carry only the desired functionality and are totally charged. However, extreme control over the polymerization is necessary in order to obtain PEs with similar degrees of polymerization and polydispersity, which is a particular challenge in the case of charged monomers. In addition, the molecular weight characterization of PEs by size exclusion chromatography (SEC) is often difficult due to the dependence of their conformation on ionic strength[172] and other problems.[178,179] The polymer modification method has the advantage of starting with a polymer of fixed degree of polymerization and molecular weight distribution. The major challenge in the case of the modification method is to obtain equal (usually complete) degrees of modification using different groups. The usual problems of carrying out quantitative reactions on polymers are further complicated by the change in solubility between the uncharged starting polymer and the charged product.

Sexsmith and Frazza prepared PVBTMP by quaternizing a copolymer of styrene and chloromethyl styrene with trimethyl phosphine (TMP).[180] PVBTMA was prepared by Jones [175] in 1954 by reaction of PVBCl with trimethyl amine (TMA). PVBTMP can be prepared using either direct synthesis from the monomer or by polymer modification but the latter is usually preferred because unsaturated phosphonium salt monomers may spontaneously polymerize during purification.[181] The direct synthesis of PVBDMS from monomer is hampered by the failure to prepare unsaturated sulfonium monomers.[181] PVBDMS was prepared by Hatch and McMaster from PVBCl for use as anion exchangers, chelating resins and thickening agents for the flocculation of slimes.[176]

The starting polymer, PVBCl, had M_w =127900 ± 600 g/mol and M_w/M_n =1.624, as measured by SEC-MALS. The modification route is summarized in Figure 6.3. The percentages of substitution of Cl by TMA, TMP and dimethyl sulfide (DMS) were 95 %, 97 % and 92 %, respectively. Conditions were optimized to those presented in the experimental section. These percentages were calculated from ^{1}H NMR using the ratio of the intensities of the peaks at 2.95 ppm (NCH$_3$),1.72 ppm (PCH$_3$) and 2.68 ppm (SCH$_3$) to the intensity of those of the aromatic region around 7 ppm (corresponding to 4 H) (Figure 6.2). The substitution is nearly complete and similar enough for comparison of the influence of the nature of the charged group.
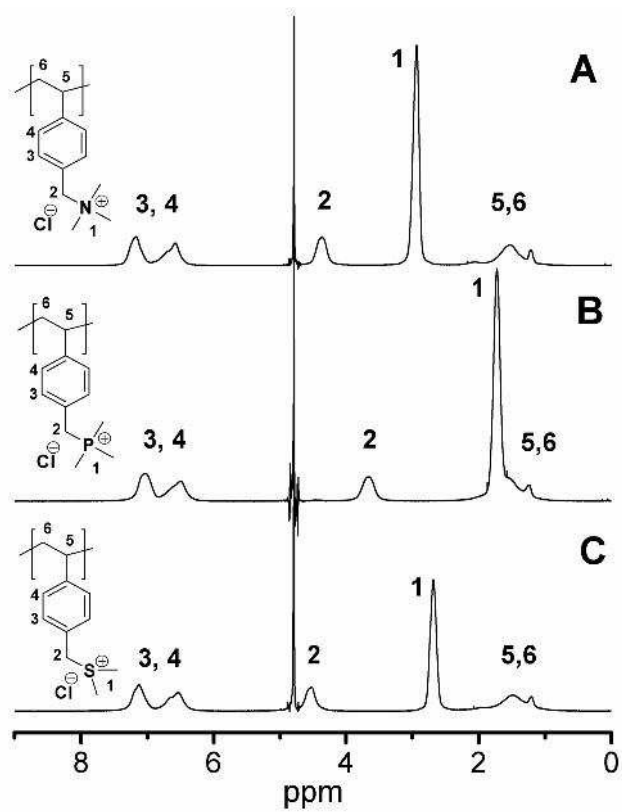
Figure 6.2 ^{1}H NMR spectra of (A) PVBTMA, (B) PVBTMP and (C) PVBDMS in D$_2$O.
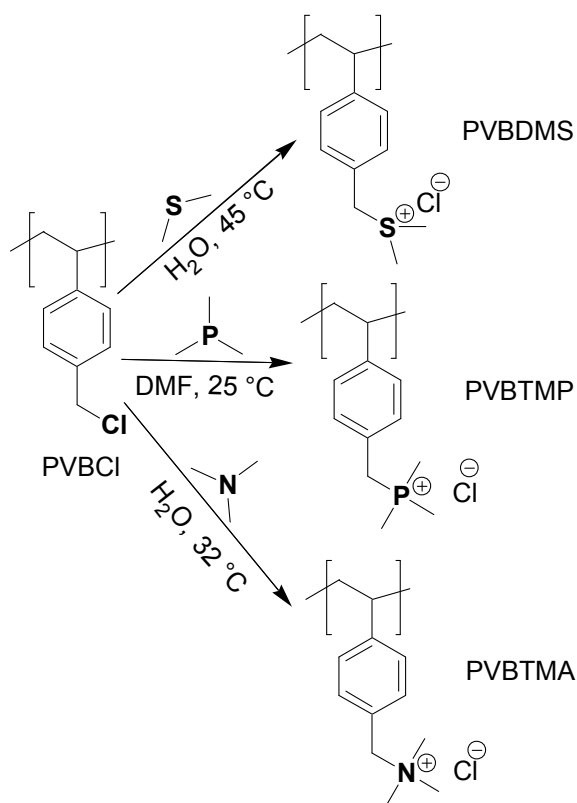
Figure 6.3 Modification reactions of PVBCl to yield PVBTMA, PVBTMP and PVBDMS.

6.3.2 Stability of Polyelectrolyte

While the phosphonium and ammonium syntheses were straightforward, the sulfonium synthesis was challenging. In fact, although sulfonium compounds are known for their instability their corresponding polycations have been subjected to more research than phosphonium polycations. This instability is due to the fact that sulfonium is a good alkylating agent and dimethyl sulfonium is a good leaving group that either eliminates or becomes substituted by small, more nucleophilic moieties. Sulfonium polycations such as PXT and PXDMS are used where an advantage of their elimination is taken to yield conjugated polymers.[14] Once it was dried, PVBDMS became partially insoluble in water over time. To overcome this problem, PVBDMS was kept as a dilute solution and stored at 4 °C. The stability of PVBDMS was assessed by recording ^{1}H NMR spectra of 50 mM PVBDMS in 1.5 M NaCl in D_2O after different times of storage. Figure 6.4 shows that PVBDMS is stable for 5 weeks, whereupon a narrow (i.e. non-

polymer) peak at 2.85 ppm corresponding to trimethyl sulfonium (SMe$_3$) appears and the intensity of the dimethylsulfonium (SMe$_2$) peak (a small amount usually remains after dialysis) at 2.20 ppm increases. Possible reactions that yield these molecules are depicted in Figure 6.5. The reverse of the modification reaction leads to the formation of dimethyl sulfide. That may be alkylated by the sulfonium to yield trimethyl sulfonium. Similar reactions can yield methyl benzyl sulfide. Reaction of the latter with benzyl chloride groups may then lead to cross-linking.
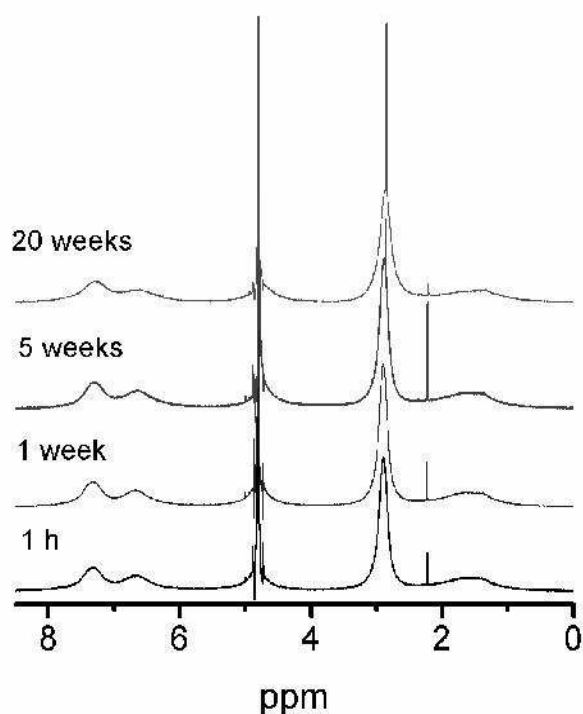
Figure 6.4 ^{1}H NMR spectra of 50 mM solution of PVBDMS in 1.5 M NaCl D$_2$O after different times of storage.
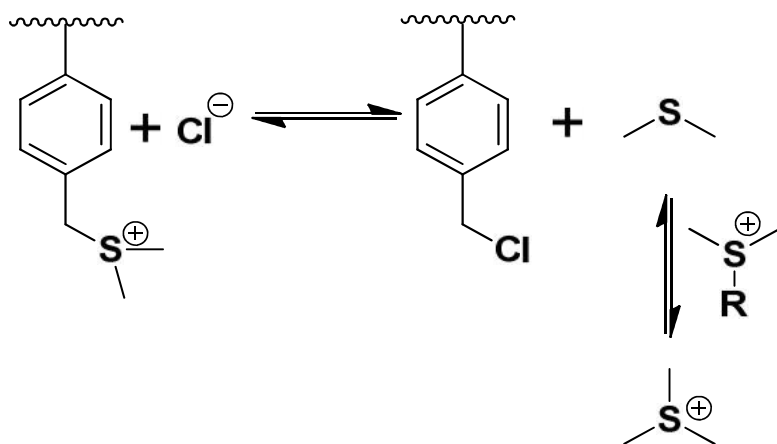
Figure 6.5   Possible reactions occurring during storage of PVBDMS.

The conditions used for the stability test ensured an enough supply of chloride ion to mimic the worst case conditions for the side reactions shown in Figure 6.5. PVBDMS stock solutions used for PEMUs assembly were stored with no salt. The stability of PVBTMA and PVBTMP was monitored by recording ^{1}H NMR spectra of 50 mM of the polycation in 1.5 M NaCl in D_2O after different times of storage. ^{1}H NMR spectra of PVBTMA and PVBTMP do not show any changes in the peaks after 20 weeks of storage (Figure 6.6/6.7, respectively) indicating that these polymers are stable over extended periods of time. It is noteworthy that the stability test described above is done in harsh condition (1.5 M NaCl) that resembles the conditions in the PEMU.
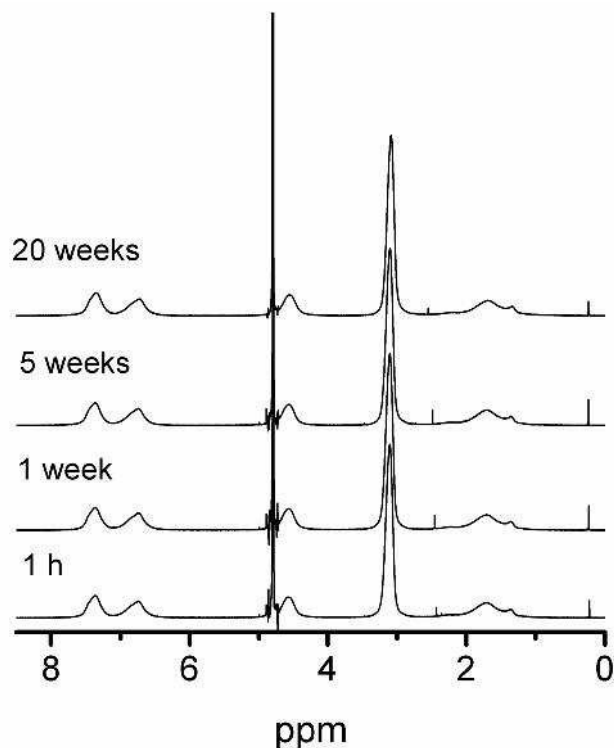
Figure 6.6 ^{1}H NMR of PVBTMA in 1.5 M NaCl in D_2O after different times of storage (from bottom to top: 1 h, 1 week, 5 weeks, 20 weeks).

6.3.3 Films Characterization

Differences between polyoniums were explored by following their LBL assembly with two polyanions. PEMU build up is generally classified under two modes of growth: linear or exponential.[18] In the former, both mass and thickness increase linearly with number of layers deposited. Typical PEMUs showing linear growth are PSS/PAH and PSS/PDADMA (at lower salt concentrations). Exponential growth is explained by diffusion of at least one of the PEs beyond its neighboring layer, where each thickness increment is a fraction of the total thickness already present.[26] PLL/alginate, PLL/HA acid and PAA-containing multilayers often grow exponentially.[18] Figure 6.8 shows the build up of PSS with polyoniums in 0.25 M NaCl as measured by ellipsometry. The three polyoniums showed linear growth of dry thickness (Figure 6.8) and (hydrated) mass with number of layers. Figure 6.9 shows that the adsorbed mass of

PEI(PSS/Polyoniums), from 0.25 M NaCl on a gold coated quartz crystals, versus number of layers measured by QCM also have a linear growth.
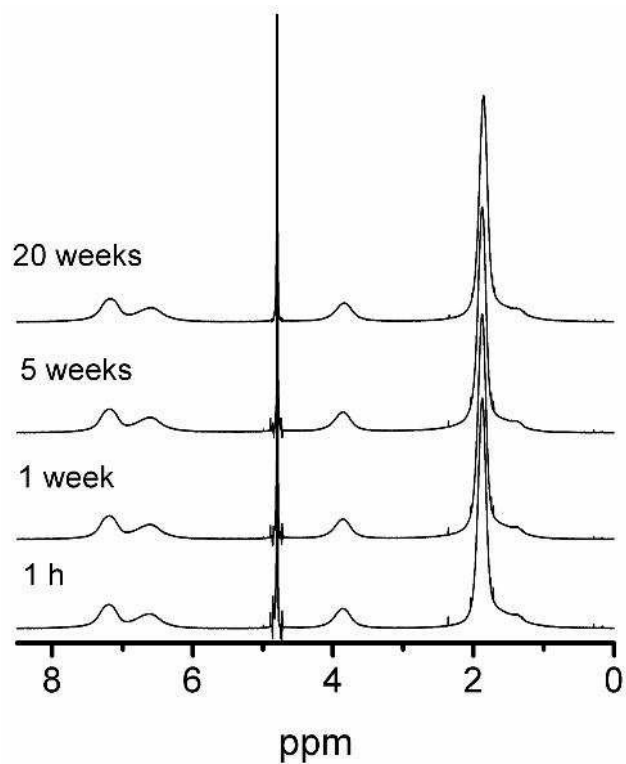
Figure 6.7 ^{1}H NMR of PVBTMP in 1.5 M NaCl in D_2O after different times of storage (from bottom to top: 1 h, 1 week, 5 weeks, 20 weeks).
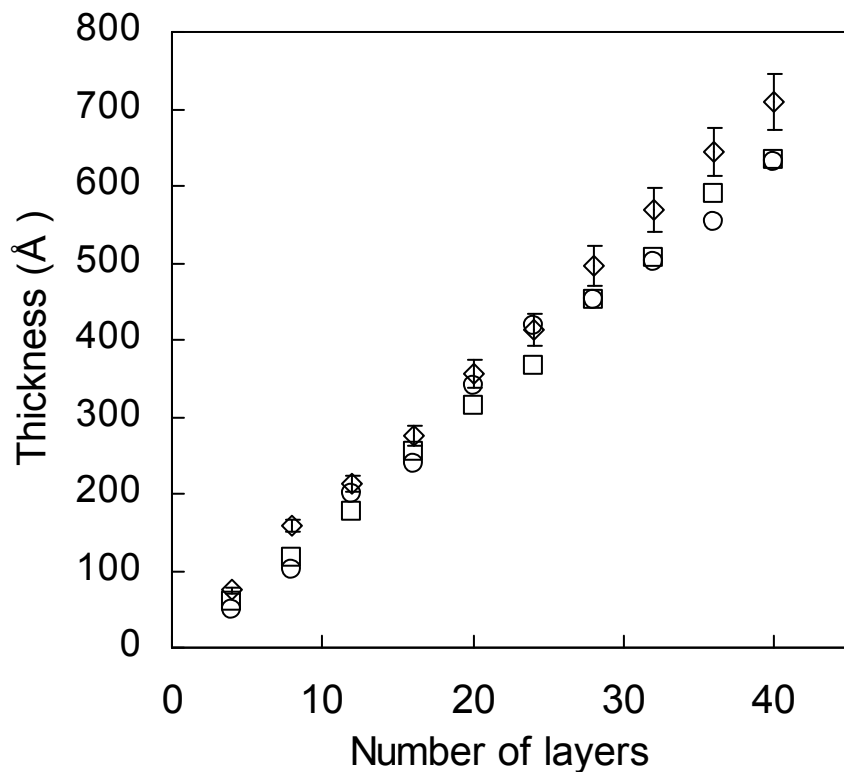
Figure 6.8 PEMU thickness versus number of layers of ($\diamond$)PEI(PSS/PVBTMA)$_n$ ($\square$)PEI (PSS/PVBTMP)$_n$ and ($\circ$) PEI (PSS/PVBDMS)$_n$ on a silicon wafer deposited from 5 mM polymer solution in 0.25 M NaCl (dipping time 10 min).

Linear growth was also observed for the other salt concentrations employed ranging from 0.25- 2 M NaCl. The thickness of the three PSS/polyonium PEMUs is almost the same at low number of layers and only slightly higher for PSS/PVBDMA above 30 layers. It was surprising to find almost identical behavior of the three polyonium in PEMU build up (within experimental error).
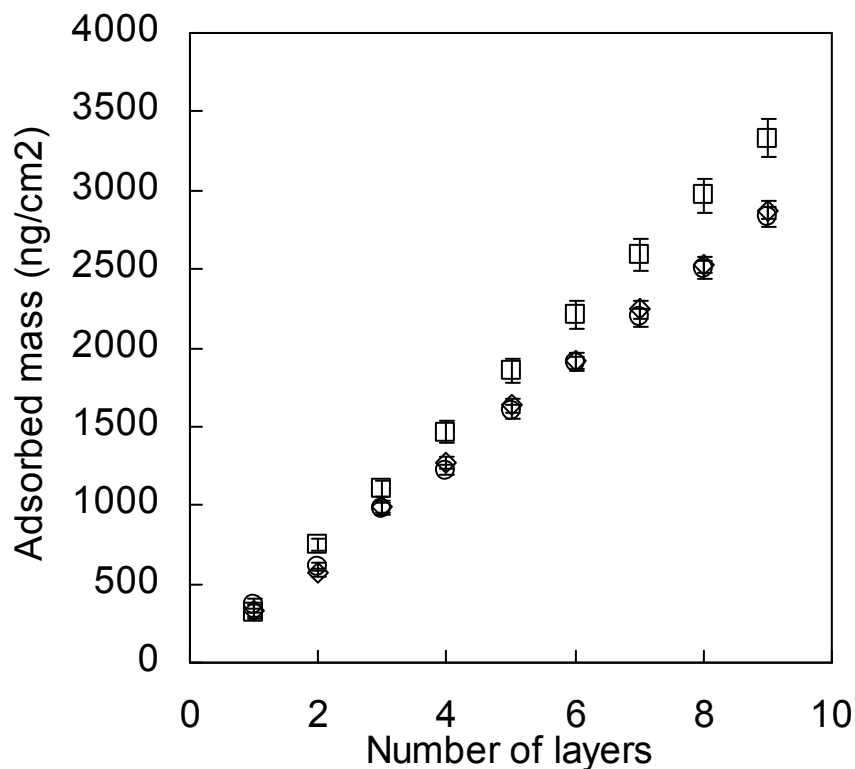
Figure 6.9 Adsorbed mass of (◊) PEI(PSS/PVBTMA)$_n$, (□) PEI(PSS/PBVTMP)$_n$ and (○) PEI (PSS/PVBDMS)$_n$ 0.25 M NaCl versus number of layers as determined by quartz crystal microbalance using the Sauerbrey equation.

6.3.4 Effect of Salt on Polyonium Films

Figure 6.10 shows the thicknesses of 40-layer PEMUs versus NaCl concentration for the same polyonium/PSS combinations (with PEI as a "primer" layer). In PEI (PSS/PVBTMA)$_n$, PEI (PSS/PVBTMP)$_n$ and PEI (PSS/PVBDMS)$_n$, multilayer thickness increases with NaCl concentration. Thickness in PEMUs as a function of salt concentration[24] is a complex dependence on the range a polyelectrolyte is able to diffuse during the formation of a layer as explained in details in Chapter 1. The energy of interaction between positively and negatively-charged units comes into play. This interaction energy is a sensitive function of the degree of hydration, for example less hydrated ("hydrophobic") PE pairs interact more strongly.[31] Despite the more significant differences in layering behavior with high salt concentrations the polyoniums show

similar multilayering properties. This similarity implies that their hydration characteristics are similar. Although the effect of NaCl in decomposition of the multilayer is more complex, it seems that the three multilayers are starting to decompose at 2.5 M NaCl as determined by the decrease in the thickness of the PEMU of the three oniums (Figure 6.10). The PVBTMA is the most affected by 2.5 M NaCl which indicates that PVBTMA/PSS has the weakest interaction between the three polyonium systems.
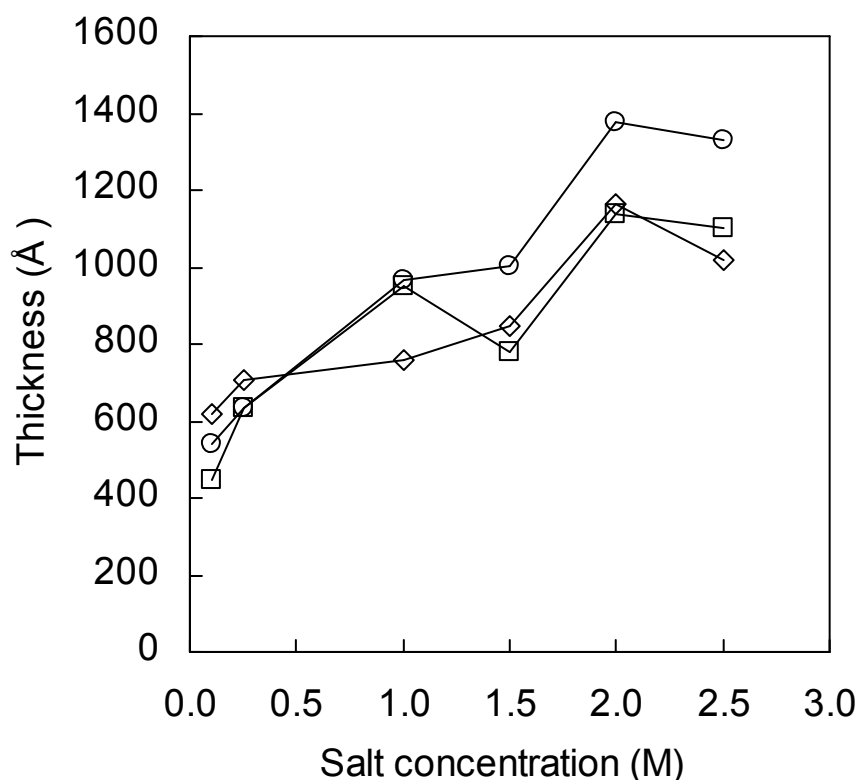
Figure 6.10 Thickness of 40-layer PEMU versus NaCl concentration (◊) PEI (PSS/PVBTMA)$_{20}$, (□) PEI (PSS/PVBTMP)$_{20}$, and (○) PEI (PSS/PVBDMS)$_{20}$ deposited on a silicon wafer. (Lines are guides to the eye).

6.3.5 Wettability of Polyonium Films

Surface hydrophilicity of the outermost layer of a PEMU controls its wettability, which has a key role in its success in applications where PEMUs are used to tailor surface interactions e.g. cell adhesion, corrosion inhibition and anti-fouling. Table 6.1

shows that the dynamic contact angles of water with multilayers terminated with the three polyoniums are very close to each other and that they are all hydrophilic. For bulk hydrophilicity, the extent of swelling of PEMUs provides further information about the degree of association of the PEs and the hydrophobicity of the complexes formed. Combinations of PEs that yield hydrophobic complexes swell less and are more strongly associated. We introduced the relative index of hydrophobicity for PE pairs defined as the ratio of the wet to dry thickness of the PEMU.[25] PAA-containing systems tend to be more hydrophilic. For example, the systems $(PAA/PDADMA)_n$ and $(PSS/PDADMA)_n$ yielded relative swelling ratios of 3.64 and 2.03, respectively [25] whereas PSS/PAH multilayers had a relative index of hydrophobicity of 1.22. The wet thickness (Table 6.1) of PSS/Polyoniums as determined by QCM implies that the three polyoniums have about the same extent of swelling. The relative indices of hydrophobicity of the PSS/PVBTMA, PSS/PVBTMP and PSS/PVBDMS are 1.9, 2.6 and 2.25, respectively, showing that the three multilayers form complexes of intermediate hydrophilicity. We did not observe differences in multilayering on gold versus silicon. For example, $PEI(PSS/PVBTMP)_{43}$ on gold and silicon wafer was 257±10 and 269±10 nm, respectively. The roughness of the three systems described in Table 6.1 was 6.5, 7.6 and 11.8 nm for ammonium, phosphonium and sulfonium, respectively. The AFM images of the topography of the three terminated polyonium multilayers are shown in Figure 6.11. The roughness of the first layers of a PEMU is usually affected by the topology of the substrate especially for the first layers. Therefore, to ensure the independency of the three systems roughness of the substrate topology, the roughness of 24 layers was measured and showed more similarities between the roughness of the three systems 13.9, 11.9 and 17.0 nm for ammonium, phosphonium and sulfonium, respectively. The same strategy was employed for the dynamic contact angle and more similarities in the advancing angle were observed.
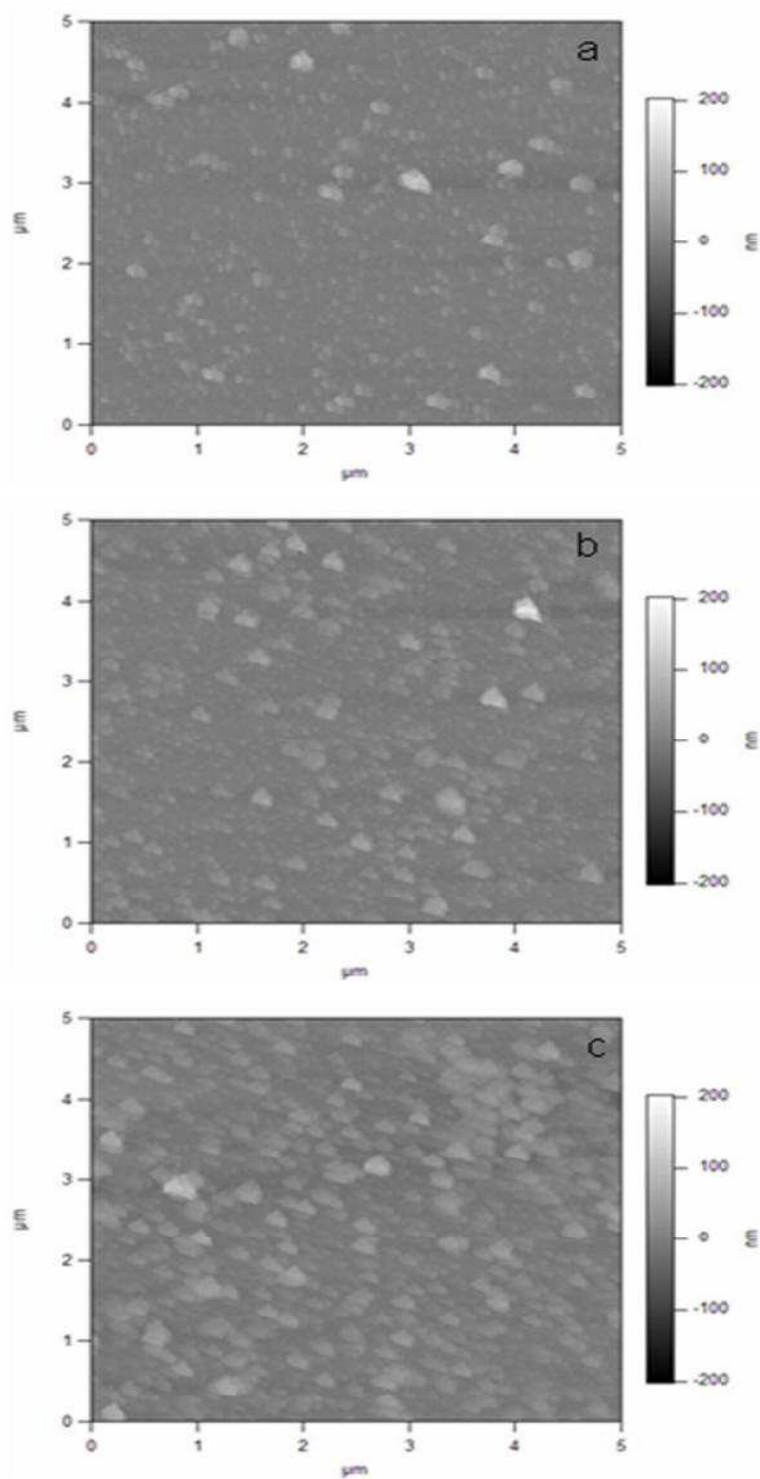
Figure 6.11 AFM images of (a) PEI(PSS/PVBTMA)$_4$ @ 0.25 M NaCl,(b) PEI(PSS/PVBTMP)$_4$ @ 0.25 M NaCl and (c) PEI(PSS/PVBDMS)$_4$ @0.25 M NaCl using the tapping mode.

6.3.6 Polyonium Exponential Growth

The assembly of the three polyoniums with PAA showed exponential growth of thickness versus number of layers (Figure 6.12). This behavior is typical for multilayers built with PAA.[18] In exponential growth the thickness as a function of the number of layers, n, is given by $a+be^{cn}$ where a is the thickness of the first layer and b and c are constants.[27] Any small differences in these constants will be amplified during growth. The three polyoniums behave in the same way for low number of layers and they have almost the same thickness. Above 15 layers PAA/PVBDMS has slightly higher thickness than PAA/PVBTMA and PAA/PVBTMP.

Table 6.1   Dynamic contact angle, wet thickness measured by QCM and dry thickness as measured by ellipsometry.

PEMU (0.25 M NaCl)	Advancing angle (degree)	Receding angle (degree)	Wet thickness(Å)	Dry thickness(Å)
PEI(PSS/PVBTMA)$_4$	66.9	23.9	270	140
PEI(PSS/PVBTMP)$_4$	63.4	25.4	320	120
PEI(PSS/PVBDMS)$_4$	57.7	23.5	270	120
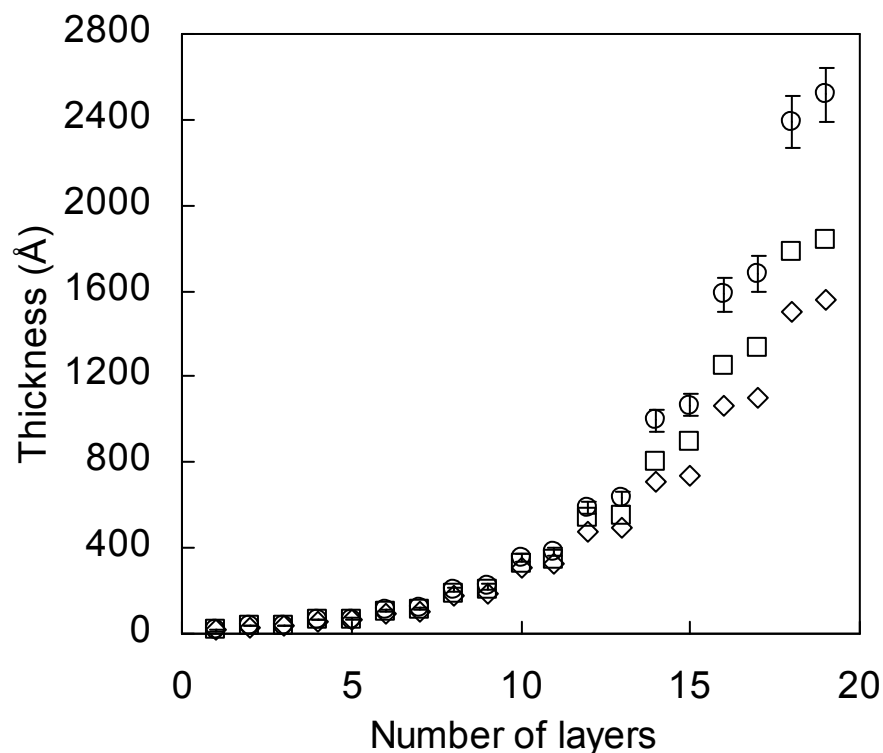
Figure 6.12 Thickness of PEMU by ellipsometry versus number of layers (◊) PEI(PAA/PVBTMA)$_n$, (□) PEI(PAA/PVBTMP)$_n$ and (○) PEI (PAA/PVBDMS)$_n$ deposited on a silicon wafer deposited from tris buffer (10 mM, pH 7.4, 0.15 M NaCl).

6.4 Conclusion

Under tight control of the prepared PE variables, the three polyoniums investigated here showed similar layer-by-layer assembly for both linear and exponential systems. Since exponential growth relies mainly on polyelectrolyte interdiffusion, it is more sensitive to small differences. Problems with long-term stability/storage of polysulfoniums were encountered, but this polymer might have a utility in reactive multilayers. In this work it was shown that chemical functionality has minimal effect on the PEMU film properties, which makes them interesting candidates for research in many fields where chemical functionality affects the properties of the film, for example in the interactions with bacteria and cells.

CHAPTER 7

CELLS AND BACTERIA RESPONSE ON HETEROATOM FILMS: A STEP TOWARDS CYTOPHOBIC FILMS

7.1 Introduction

Implants and devices ranging from catheters to artificial organs are either used or expected to be used in medicine. In addition to all the other properties that the implants should possess, to play a role in the body, a critical property for its success is the immune system response that is provoked by the body. The understanding of cell interactions with the surface of the implants is the area on which material scientists depends on to manipulate the surface characteristics of the implant. It is desirable to have control over the surface characteristics to design the required tissue-implant interaction to fulfill the increasing needs of the biomaterial field. Surfaces or factors that reduce adhesion of proteins and cells to the surface have the advantage of minimizing thrombus formation and inflammation.[182,183] These surfaces are used as coatings for implants and catheters. Cell adherent surfaces are used to promote cell and tissue growth for applications in tissue engineering.[184]

7.2 Protein Adsorption on Surfaces

Under normal conditions in the body, tissue maintains the growth and adhesion factors by secreting the extracellular matrix (ECM). The ECM is the combination of proteins and polysaccharides secreted by the cells. Fibronectin, laminin, vitronectin, elastin and collagen are constituents of ECM that may vary depending on the cell line. Both elastin and collagen form a 3D network that provides the structural support for cells whereas fibronectin and collagen are responsible for the cell adhesion. Proteins are adsorbed more on the positively charged surfaces due to the net negative charge on a protein (at pH levels higher than their iso-electric point). Although proteins acquire a net negative charge, they adsorb to a lesser extent to the negatively charged surfaces

by the aid of the positively charged side chain groups.[183] Proteins favor to adhere to hydrophobic surfaces rather than to hydrophilic. Poly(ethylene glycol) (PEG) and zwitterion polyelectrolyte multilayers PEMUs are the universal protein non adherent PEMU, due to water around the polymer that hinders protein adsorption. In the normal case fibronectin adsorbs to the surface of the device via non specific interactions. Fibronectin has an adhesion sequence that includes the arginine-glycine-aspartic acid (RGD) that binds to the transmembrane protein receptors (integrins) and triggers cell responses, which control inflammation.[185] On surfaces the protein may acquire different structure (a new energy minimum conformation) than that it has in solution that may lead to unexpected cell interactions.[183]

The first interaction between an implant in contact with the biological environment is through the proteins present on the surface of the implant. Therefore, surfaces that are protein resistant are usually cytophobic. PEMUs with their wide range of functional groups, extent of wettability,[41, 186-187] compliance,[38] charge density, charge type[188] (positively or negatively charged) and roughness can be used to tweak protein adsorption and cell behavior. PEMU applications as coating to modify the surface of biomaterials have been a focus of research for the last decade.[18, 189]

7.3 Restenosis

The re-closing of the blood vessels that have been equipped with a stent after a angioplasty, known as restenosis, is an example of undesired cell material interactions that have drawn much attention over the last decade.[190] Restenosis is associated with the adhesion and growth of vascular smooth muscle cells on the stent surface and can lead to an increase in the blood pressure or complete closure of the vessel. The A7r5 cell line is a smooth muscle that originates from the aorta of the rat and it is an adherent dependent cell line. The interaction of A7r5 with PEMU has attracted our research groups attention in an effort to find a cytophobic PEMU that can be used as a coating for the stent.[41, 186, 191, 192]

The influence of the bulk (modulus) and the surface (charge and wetability) properties on the interaction with different cell lines has been the subject of research. *Salloum et. al.* studied the effect of charge and wettability on A7r5 cells.[41] Although A7r5 adhered and spread on hydrophobic PEMUs, they were non-motile. A7r5 cells were motile on hydrophilic surfaces although cells did not adhere. *Thompson et. al.* showed that vascular endothelial cells adhesion increased on stiffer poly(allylamine hydrochloric acid) (PAH)/poly(acrylic acid) (PAA) PEMU that was tuned via pH controlling (ionic cross-linking).[38] *Francius et. al.* altered stiffness of poly(l-lysine) (PLL)/ hyaluronic acid (HA) by chemical cross-linking and showed that chodrosarcoma cells adhered and proliferated better on stiffer PEMUs.

7.4 Bacterial Adhesion

The bacterial growth on medical devices and implants is one of the reasons behind hospital-acquired infections worldwide.[193-196] Avoiding the formation of bacterial biofilms which increase resistance to antibiotics, and render the sterilization of the devices and the treatment of infections particularly difficult is of special concern. There are two major strategies that can be employed to reduce the risk of post-surgery infections and create safer biomaterial surfaces: 1- Coatings that are resistant to bacteria adhesion; 2- Surface treatment that are biocidal.

The stable adhesion of bacteria to a surface is usually irreversible and due to specific and non-specific interactions with the protein of the bacteria membrane. Designing anti-bacterial surfaces is challenging due to the complexity of the bacterial adhesion process. Ironically, it was found that highly hydrophilic and superhydrophobic PEMUs are anti-adherent bacterial surfaces. PEG terminated PEMUs have a high affinity to water due to hydrogen bonding which prevents the interaction between the bacteria membrane and the surface. Unlike the prokaryotic organisms, the eukaryotic organisms have cytoskeleton elements that are responsible for the effect of the mechanical properties of the surface on cells adherence and their behavior. Although bacteria lack to the cytoskeleton elements, changing the modulus of the PEMU is one of the effective ways to design bacterial resistant PEMUs.

The antibacterial activity of polycations and in particular ammonium, phosphonium and sulfonium monomers and their polymers is well known.[197-199] It has been shown that polycations of these functionalities have higher antibacterial activity than their monomers.[197] It is usually assumed that the polycations interact with the negatively charged cytoplasmic membrane of the bacteria which causes the disruption and release of organelles/ions from the cytoplasm resulting in the death of the bacteria.[197, 199] It has been proved that the higher the charge density of the polycation, the higher its antibacterial activity. The more hydrophobic the substituent of ammonium and phosphonium, the higher the antibacterial activity of the polycation. Kügler et. al. proposed a mechanism for the bactericidal activity of polycations as driven by entropy rather than polycation penetration into the membrane.[198] The mechanism implies that the negatively charged membrane interacts with the polycationic surface or polycation in solution. This interaction causes the release of anions from the polycation and of cations of the bacterial membrane which is entropically favorable. This release of ions causes an imbalance in the membrane and eventually its rupture.

A representative model organism used to evaluate the antibacterial activity of surfaces is the *Escherichia coli* (*E.coli*), gram negative bacteria that are usually found in the lower intestine of humans. *E.coli* is the most studied prokaryotic organism in biotechnology and microbiology because it lives outside the body. *E.coli* is more resistant because it is a gram negative bacteria which has an additional outer membrane.[200]

This work focuses on the effect of the chemical functionality of PEMUs on cell and bacteria adhesion and growth. This effect was explored by seeding A7r5 and *E.coli* on a panel of PEMUs terminated with polycations that differ only in the heteroatom on which the positive charge resided, and had the same charge density, molecular weight, and molecular weight distribution. PEMUs built from poly(styrene sulfonate) (PSS) and poly(*p*-vinyl benzyl trimethyl ammonium) (PVBTMA), poly(*p*-vinyl benzyl trimethyl phosphonium) (PVBTMP) and poly(*p*-vinyl benzyl dimethyl sulfonium) (PVBDMS) as polycation were used. The A7r5 cell line is used as a model for smooth muscle cells for *in vitro* studies.

7.5 Experimental Section

7.5.1 Materials

PSS (Mw= 70,000, acid form), poly(ethylene imine) (PEI) (Mw=10,000), PAH (Mw= 56,000) trimethylphosphine (97%), trimethylamine (43% by weight in solution), and dimethylformamide (anhydrous, 99.8%) were used as obtained from Sigma-Aldrich. Poly(p-vinyl benzyl chloride) (PVBCl) (Scientific Polymer Products, Mw 127,900 ± 600 g/mol as determined by multi angle laser light scattering), dimethyl sulfide (Alfa Aesar, 99+%), methanol (Malinckrodt, anhydrous, 99.9%), diethyl ether (BDH, >99%), ethyl acetate (Fisher Scientific, HPLC grade), sodium chloride (EMD, >99%), and tris buffer (Fisher Scientific, molecular biology grade) were used as received. Dialysis membranes (Spectra/Pro, molecular weight cutoff 12,000 to 14,000) from Spectrum Laboratories were soaked in water for 30 min and rinsed excessively prior to use. Milli-Q water with a resistivity of 18.2 mOhm was used throughout this work. The polycations PVBTMA, PVBTMP and PVBDMS (Figure 6.3) were prepared and characterized as indicated in Chapter 6.

Dulbecco's Modified Eagle Meduim (DMEM) (Sigma-Aldrich) containing 4500 mg/L glucose, L-glutamine, phenol red, 10% by volume Fetal Bovine Serum (FBS), 1% by volume gentamicin (antibacterial), 0.1% by volume gentocin (antifugal) were used for A7r5 culture. Tryptone (Bacto), yeast extract (Bacto), sodium chloride (Sigma-Aldrich), NaOH (1N) were used as purchased to prepare the Luria Bertani (LB) broth.

7.5.2 Multilayers Assembly on Cover Slips

Multilayers were assembled on circular glass cover slips (VWR, 18 mm diameter No 1) placed in 12 wells plate. The cover slips were cleaned using a slow flow of distilled water and dried by a slow flow of nitrogen followed by an air plasma treatment for 2 mins in a PDC-32G plasma cleaner. The cover slips were rinsed and dried before placing them in the well plates.

The concentration of all polyelectrolyte solutions was 5 mM (with respect to the monomer repeat unit) and 0.25 M in NaCl. The PEI concentration used for the first layer assembly was 10 mM. The PSS solution was brought up to pH 7 by using 1 N NaOH. Multilayers were assembled by the addition of the polyelectrolyte solution for 10 min to

the wells containing the cover slips. The cover slips were rinsed 3 times for 1 min each with distilled water. The process was repeated as needed until reaching the required number of layers.

7.5.3 Multilayer Assembly on Silicon Wafer and Quartz Slides

Multilayers were deposited on polished Si <100> wafers and quartz slides (GM Associates, 2 mm thick, 1 inch diameter) cleaned using piranha (7/3 by volume H_2SO_4/H_2O_2). Substrates were dipped in 10 mM PEI for 20 min as a pretreatment before PEMU build up. The substrates were dipped in the PE solutions for 10 min and then rinsed three times for 1 min each with distilled water. The multilayers were dried by a gentle nitrogen stream. The dry thicknesses of the PEMUs were measured using a Gaertner Scientific L116B Autogain ellipsometer.

7.5.4 Quartz Crystal Microbalance (QCM)

Experiments were performed using a Q-Sense E4 with gold coated quartz crystals having a nominal resonance frequency of 4.95 MHz (both from Q-Sense). The crystals were cleaned by air plasma for 30 sec and extensively rinsed with water directly before use. Multilayers were assembled by bringing the PE solutions (5 mM in PE, 10 mM PEI, 0.25 M NaCl) into contact with the surface for 10 min followed by rinsing with water for 3 min. After the last layer, rinsing was continued with tris buffer (10 mM tris, pH 7.4, 0.15 M NaCl) and the PEMU was stabilized by waiting for 30 min. A viscoelastic model was used to calculate the wet thickness of the $PEI(PSS/onium)_4$ multilayers in tris buffer based on the recorded changes of the frequency and dissipation for the 3rd, 5th, 7th, 9th and 11th harmonic. Protein adsorption is tested by bringing the surfaces, for 30 min, in contact with a 10% FBS solution in tris buffer followed by rinsing with tris buffer.

7.5.5 The Films Properties

FT-IR was performed using a nitrogen purged FTIR (Nicolet Nexus 470 with a DTGS detector) spectrometer. Spectra were taken at a resolution of 4 cm^{-1} with 36 averaged scans. UV-vis spectra were recorded on a Varian Cary Bio 100 UV-vis double beam spectrophotometer. Samples were prepared on fused quartz slides. The sterilization of PEMUs by UV was done using the UV lamp in the safety cabinet

(NUAIRE, NU 425-500, Class II, Type A_2). The multilayers were exposed to the UV light for 15 min then rinsed with distilled water. The modulus of PEI(PSS/PVBDMS)$_{60}$ before and after UV treatment were measured using an MFP-3D AFM unit equipped with an ARC2 controller (Asylum Research Inc., Santa Barbara, CA) and Igor Pro software. AC240-TS tip with a spring constant 2.11 N/m was used for indentation. The optical lever sensitivity of the tip was calibrated then immersed in 0.15 M NaCl solution. The spring constant was calibrated in air and the 0.15 M NaCl using the thermal fluctuation technique. Measurements were done by scanning a 20 x 20 μm^2 area of the sample which was immersed in 0.15 M NaCl. The distance between the tip and the sample was set to 500 nm and the tip velocity was set to 1 μm/sec. The force applied that results in the indentation is given by Equation 7.1

$$F_{Punch} = 2\frac{E}{(1-\upsilon^2)}R(z-d)$$
(7.1)

Where R is the radius of the punch; z is the distance of the tip to the surface in the z direction; K is the cantilever spring constant; d is the tip deflection, υ is the poisson ratio of the material and E is the modulus of the film.

7.5.6 Cell Culture and Cell Adhesion Tests

The A7r5 cells were cultured in DMEM in 75 cm^2 culture flasks and incubated (Water Jacket CO_2 Nu-4750, NuAire, plymart, MN, USA) at 37 °C with 8 % CO_2. The medium was changed every three days. After detachment using L-trypsin the cells were seeded onto the cover slips in 12 well plates (10,000 cells/well, volume 1 mL). The concentration and viability of A7r5 cells used (90-95%) were determined by an automated cell counting system Cedex HiRes (Roche Innovatis AG).

7.5.7 Cytotoxicity of Polyelectrolytes in Solution

The cytotoxicity of the different polyelectrolytes was assessed using the alamar blue assay (details about the assay are provided in Chapter 2). The fluorescence was measured using the Molecular Devices SpectraMax MicroPlate Reader and SoftMax Pro Software. A7r5 cells were seeded in a 96 wells plate at a density of10,000 cells/well and incubated for 24 h. The polyelectrolyte solutions with different

concentrations (0.001, 0.01, 0.1, 0.4, 0.8, 1 and 10 mM) and 1 μL of alamar blue were added to each well. The cells were incubated with the solutions for 4 h. 80 μL of the media were transferred to 96 wells plate in which the fluorescence readings were done.

7.5.8 Live Cell Imaging

The cover slips (cover glass, No. 1, 18 mm sq., Corning, plasma treated) were glued to the bottom of petri-dishes and then coated with different PEMUs as described in the multilayer assembly section. A Live Cell**TM** imaging device (Pathology devices) mounted on an inverted fluorescence microscopy (Nikon Eclipse Intensilight C-HGFI and Cool Snap HQ2 camera from Photometric, NIS-advanced software) was used to live cell imaging. An aseptic environment with 78% humidity and 8% CO_2 was maintained for the duration of imaging. A density of 1000 cells/mL was used to minimize cell/cell interaction during the 20 h of imaging. The cells were incubated for 1 h in the petri dish prior to live imaging to insure that they settled down on the surface. Every 240 secs a micrograph was taken for a period of 20 h with x20 using the differnational interference contrast (DIC) mode.

7.5.9 Bacteria Culture and Tests

The Luria Bertani (LB) broth was prepared by dissolving 10 g of tryptone, 5 g yeast extract and 10 g of NaCl in 800 mL of distilled water. The pH was adjusted to 7.5 using 1N NaOH, the solution was brought to 1000 mL, and followed by autoclaving for 45 min. The LB broth was used as a culture media for E.coli (DH5α). *E.coli* were suspended in 1 mL of LB broth incubated at 37 °C for 24 h at 100 rpm to obtain ~ 10^7 cfu/ml in the Log phase of their growth. The concentration was determined using the optical density (absorbance at 600 nm).

PEMUs were assembled in 12 wells plate on cover slips as described in the section (7.5.2). A 0.5 mL of 10^5 cfu/ml *E.coli* suspension in LB was added to each well for 4 h. After 4 h the LB was removed and only a thin film of the *E.coli.* was left there. The *E.coli* was incubated overnight with the thin film of *E.coli*. The LB broth was removed from the wells and 1 mL of 0.15 M NaCl solution with 3 μL of the dye mixture (1:1 ratio by volume SYTO9: propidium iodide) was added to each well. The plate was left in the dark for 15 mins. After the removal of the dye solution, the cover slips were

mounted on the microscope slides. The dead (red color) and live (green color) bacteria were imaged using the 41017 Endow GFP bandpass emission (400-650 nm) and Texas Red (TEXRED) (450-750 nm) (41004) filters (Chroma Technology Corp) of the inverted fluorescence microscopy. The percentages of dead and live bacteria were calculated using ImageJ software.

7.6 Results and Discussion

7.6.1 Protein Adsorption on Polyonium PEMU

The cells interact with surfaces through the protein adsorbed into the surface. Therefore, the type, amount, and conformation of proteins adsorbed onto the surface have a strong effect on the behavior of the cells. The protein adsorption from a 10 % fetal bovine serum (FBS) solution in tris buffer on PEI(PSS/PVBTMA)$_4$, PEI(PSS/PVBTMP)$_4$, and PEI(PSS/PVBDMS)$_4$ films were done using QCM (Figure 7.1). The protein adsorption on the three polyonium terminated PEMUs is the same within experimental error. The amount of protein adsorbed (around 800 ng/cm^2) corresponds to full surface coverage by protein with a 6 nm thickness.
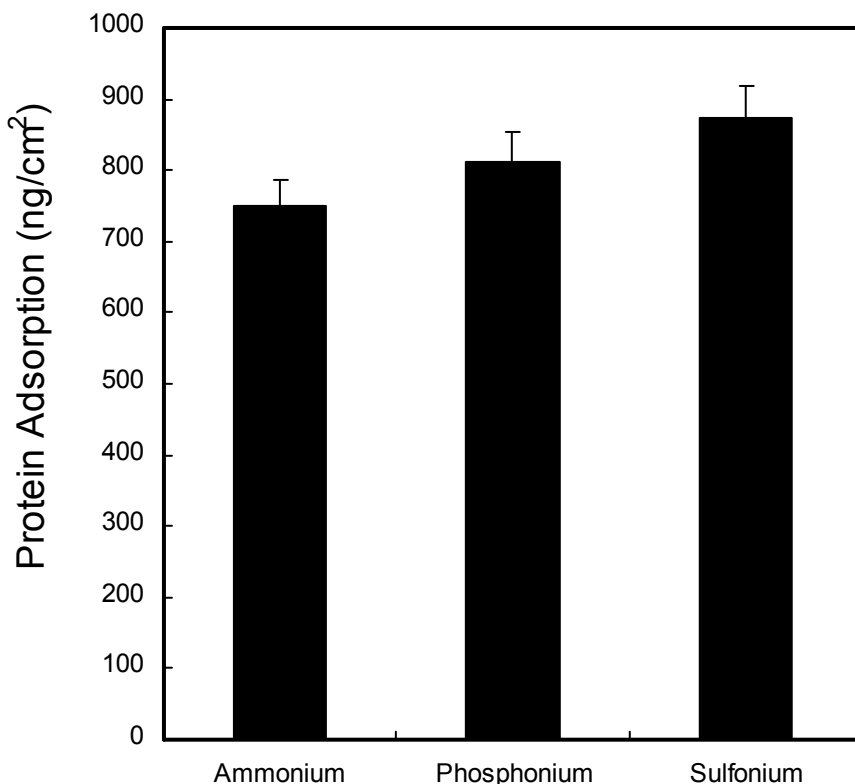
Figure 7.1 Protein adsorption on PEI(PSS/PVBTMA)$_4$ (Ammonium), PEI(PSS/PVBTMP)$_4$ (Phosphonium), and PEI(PSS/PVBDMS)$_4$ (Sulfonium) built from 0.15 M NaCl in tris buffer using Quartz Crystal Microbalance (QCM).

7.6.2 A7r5 Response to Polyonium Solution and PEMU

The cytotoxicity of polyonium solution against A7r5 cells was assessed. Although it is known that the toxicity of PE in solution is relatively different than that of the PE when it is involved in PEMU,[200] the toxicity of polyonium solutions against A7r5 were tested using alamar blue assay. Figure 7.2 depicts the relative fluorescence at 590 nm of the reduced alamar blue by A7r5 incubated with polyonium solution to the fluorescence of the reduced alamar blue by A7r5 with no PE solution. The three polyoniums have low cytotoxic activity at low concentrations where the A7r5 maintained the same metabolic activity within experimental error. The A7r5 metabolic activity dropped below the 50% viability at 1 mM concentration of the three polyonium solutions to the same extent. The three polyoniums killed all the A7r5 cells at (10 mM) judged by the disappearance of the cells activity at that concentration.
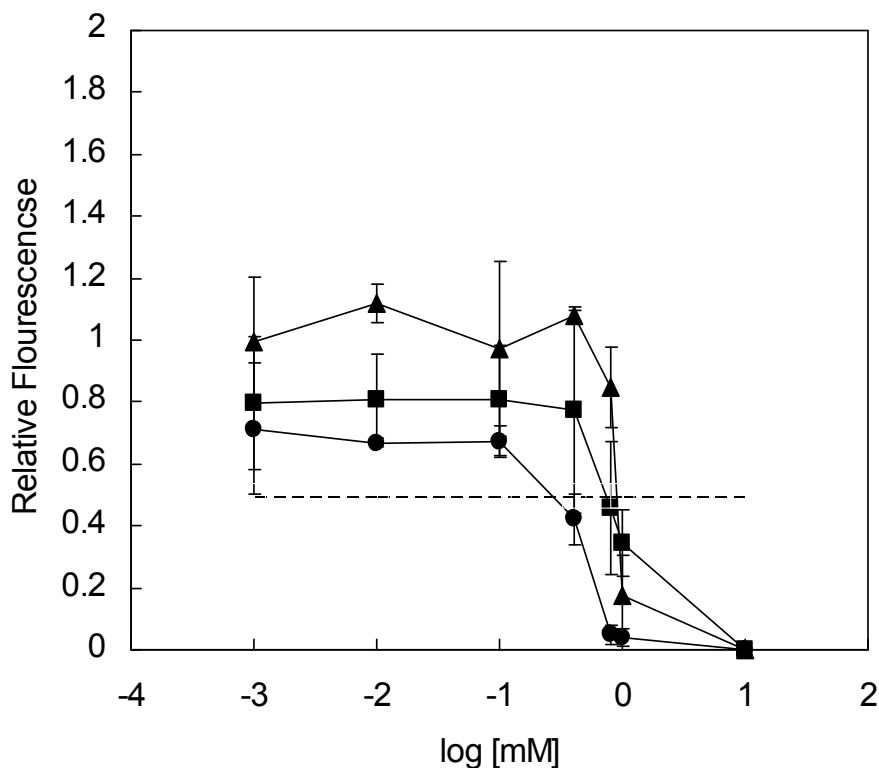
Figure 7.2 The cytoxicity of polyonium solutions with A7r5 after 4 h of exposure. The relative fluorescence at 590 nm of the A7r5 cells incubated with polyonium to the fluorescence of the A7r5 cells without polyonium solution versus the log of the polyonium concentration in mM (■) PVBTMA, (▲) PVBTMP, (●) PVBDMS and the dashed line is 50% viability line.

The effect of polyonium PEMU on A7r5 was assessed.A7r5 cells adhered strongly to the glass surface (control) and to a lesser extent the sulfonium terminated PEMU. The A7r5 showed different morphologies on the sulfonium PEMU. The cells did not adhere to phosphonium and ammonium PEMUs. The following is the chronological response of the cells on the surfaces using Live cell imaging: At t=0 min the A7r5 cells settled down on the three PEMUs and the control (glass cover slip) acquiring a round shape. On the glass surface, the cells started spreading with a relatively low motility and undergone division. On the PVBDMS film, the cells spread and divided but acquired a more elongated shape compared to that on the control. On both the PVBTMA and PVBTMP PEMUs, the cells were very motile and for the first 10 to 15 h went through

114

several cycles of extension and retraction of their cytoplasmic membrane. In the end, the cells failed to spread and adhere onto the PVBTMA and PVBTMP surfaces and became more rounded at about 800 min (no cytoplasmic extensions) and they left the surface. After 1200 min the difference between the effect of PVBTMA / PVBTMP and PVBDMS is more pronounced and it is obvious that sulfonium was a cell adhering PEMU whereas PVBTMA and PVBTMP PEMU are A7r5 cytophobic (Figure 7.3).

7.6.3 Effect of UV Treatment on Polyonium Films

During the extensive experiments, UV treatment was used as a method to sterilize the wells and the coated cover slips. Surprisingly, there was a pronounced difference in the A7r5 adherence and spreading on the UV treated PVDMS multilayer compared to the non UV treated PVBDMS. Figure 7.4 shows that the number of cells on the untreated sulfonium multilayer was relatively lower than that on the UV treated PVBDMS on which the A7r5 reached confluency. The UV treatment had no effect on the cell growth and adherence on both the PVBTMA and the PVBTMP.

The differences between polyoniums prior and post UV treatment were explored by following their UV and FT-IR spectra. Both the PVBTMA and PVBTMP showed no significant difference at the molecular level upon UV treatment. This is consistent with the no change in the A7r5 cells adherence to the ammonium and phosphonium PEMU. The UV spectra of the PEI(PSS/PVBDMS)$_5$ post UV treatment showed that the peak at 227 nm decreased and a new peak at 275 nm emerged (Figure 7.5). Slight changes in the FT-IR peaks at 1186 cm^{-1} and 637 cm^{-1} were observed for sulfonium post UV treatment with no change in the PSS peaks (1033 and 1008 cm^{-1}) which indicated that the change did not originated from PSS in the assembly.
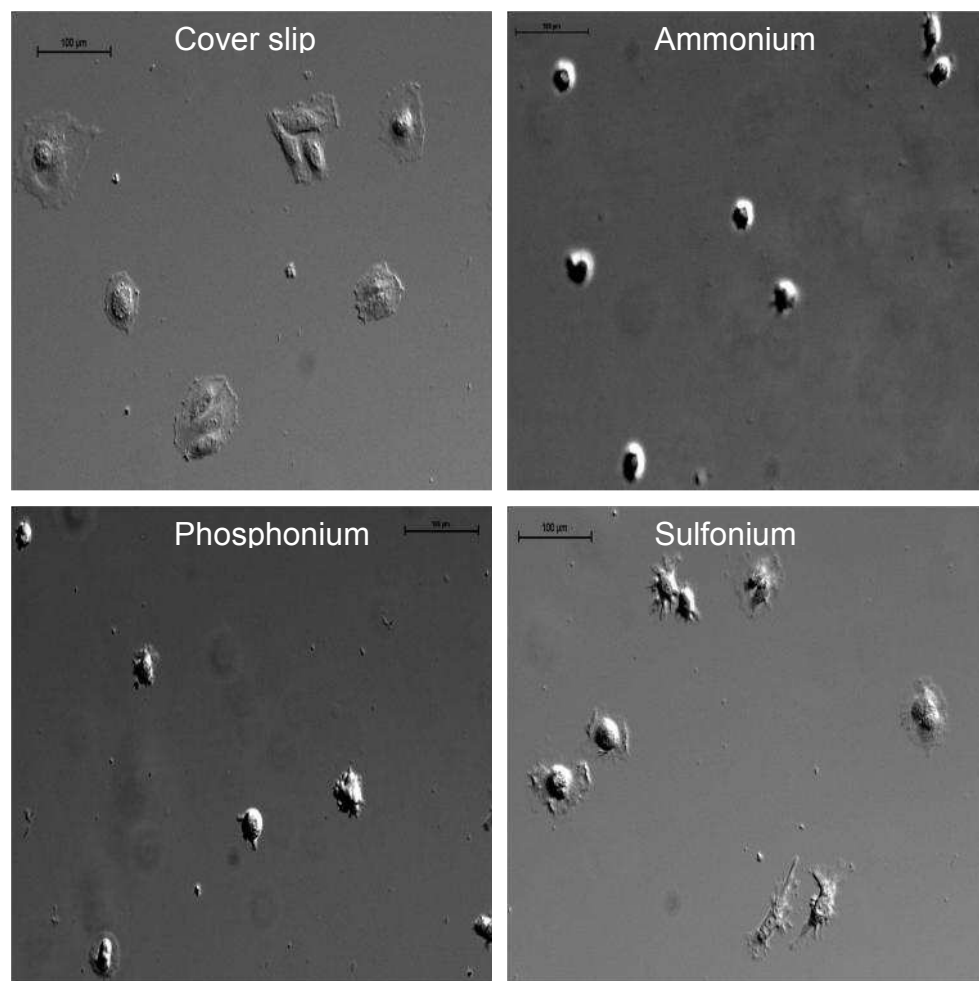
Figure 7.3 Images of live A7r5 cells after 20 h of seeding the A7r5 cells on (A) glass cover slip, (B) PEI(PSS/PVBTMA)$_5$, (C) PEI(PSS/PVBTMP)$_5$ and (D) PEI(PSS/PVBDMS)$_5$. (Scale bar is 100 µm)

Since the wettability had an effect on A7r5 cell adherence, the effect of UV treatment on the surface wettability was explored for the three polyoniums prior to and post UV treatment. Table 7.1 shows that the dynamic contact angle of water with the PEMUs terminated with the three polyoniums are all in the hydrophilic region prior and post UV treatment. The sulfonium terminated multilayer was the most to be affected by UV treatment. The dynamic contact angle post UV treatment was relatively lower for sulfonium compared to that of ammonium and phosphonium. This change in the contact angle is considered a slight change since the multilayer is still in the hydrophilic range.

116

This ensured the independency of cell behavior on the sulfonium prior and post UV treatment of the wettability of the PEMU.
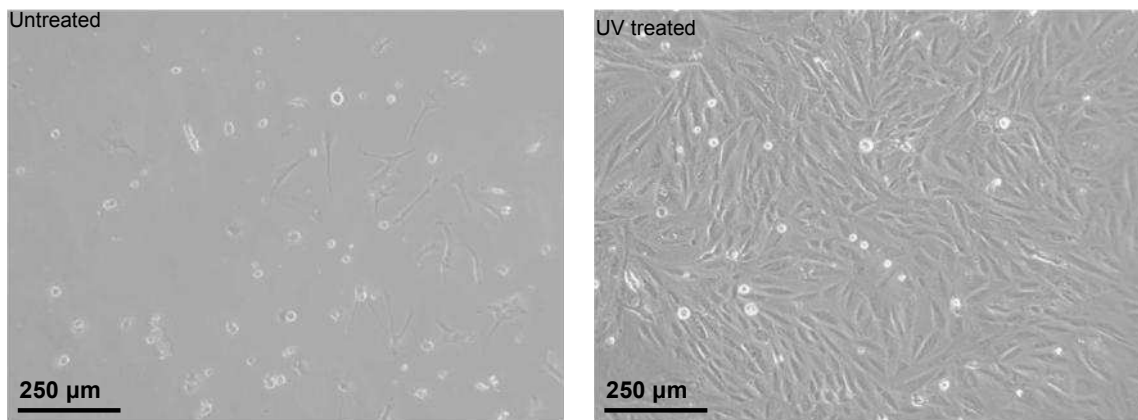
Figure 7.4 The micrographs of live A7r5 on PEI(PSS/PVBDMS)$_5$ after 5 days of seeding on UV treated coating and untreated coating.

The alkylation reaction of PVBDMS during storage in solution is discussed in Chapter 6 (Figure 6.5). The sulfonium salts are known to be widely used as cationic photoinitiators.[201] It is speculated that PVBDMS being a sulfonium salt maybe acting as an initiator resulting in cross-linking leading to an increase in the stiffness of the multilayer. Cells generally adhere and spread better on stiff substrates.[202, 203] It has been shown that A7r5 cells adhere more strongly to stiffer PEMUs.[192] The difference in the modulus of the sulfonium multilayer prior to UV treatment (91 MPa) and that after UV treatment (116 MPa) is 25 MPa. This change is considered to be a slight change on the modulus which does not explain the difference in A7r5 behavior on the UV and the non UV treated sulfonium multilayers. This excludes the hypothesis that the better the proliferation of A7r5 on the UV treated is due to the increase in the stiffness of the multilayer. The amount of protein adsorption on sulfonium PEMU is comparable to that on ammonium and phosphonium assures that protein adsorption is not the limiting factor of A7r5 spreading on sulfonium.

117
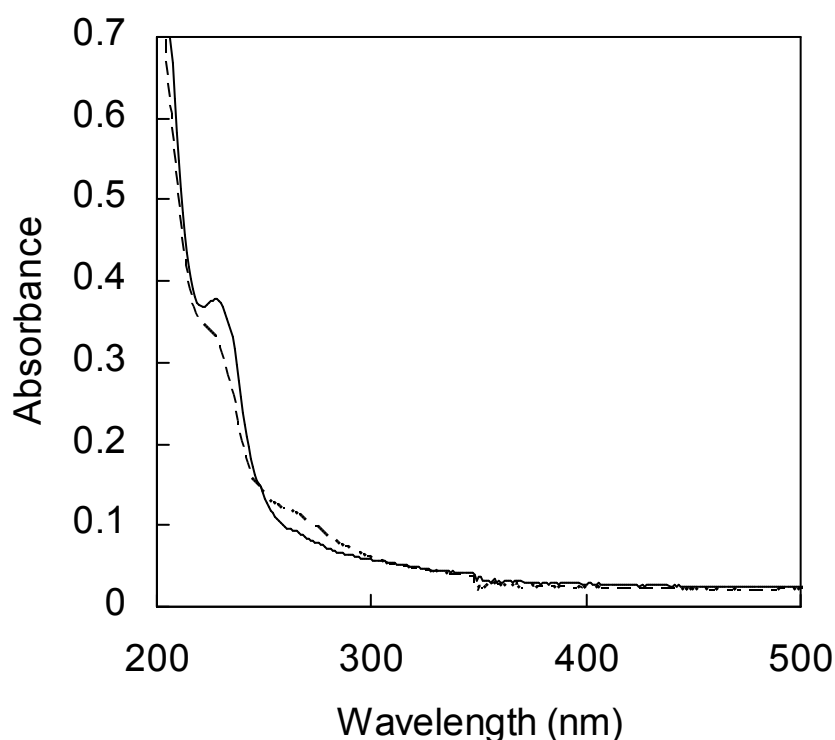
Figure 7.5 UV spectra of PEI(PSS/PVBDMS)$_5$ (0.25 M NaCl) solid line before UV treatment and dashed line after UV treatment for 15 min.

Table 7.1 Dynamic contact angle of the three polyoniums terminated PEMUs prior and post UV treatment.

PEMU (0.25 M NaCl)	Advancing/Receding angle prior UV treatment	Advancing/ Receding angle post UV treatment
PEI(PSS/PVBTMA)$_5$	65/30.5 °	64.5/30.2 °
PEI(PSS/PVBTMP)$_5$	66.3/30.7 °	72.3/30.2 °
PEI(PSS/PVBDMS)$_5$	57.7/23.9 °	37/27.9 °

7.6.4 The Polyonium Solution and PEMU Antibacterial Activity

The antibacterial activity of the polyonium solutions against E. coli is studied using the alamar blue assay after 4 h of incubation with different concentrations ranging from 0.001 mM to 10 mM (per monomer unit) (Figure 7.6). At low concentration (0.001 to 0.4 mM) the three polyonium solutions have no antibacterial activity against *E.coli*.

118

For PVBDMS, 0.8 mM is the minimum concentration at which the antibacterial activity is detected, judged by the 98.7% death of E. coli. At the same concentration PVBTMA has the lowest antibacterial activity between the three polyoniums, 41% of *E.coli* are dead whereas PVBTMP killed 82% of the *E.coli.* Therefore it is safe to conclude that PVBDMS in solution have a higher antibacterial activity than PVBTMA and PVBTMP at the minimum concentration and all polyoniums have the same extent of high antibacterial activity (97% of *E.coli* was killed) at 10 mM concentration.
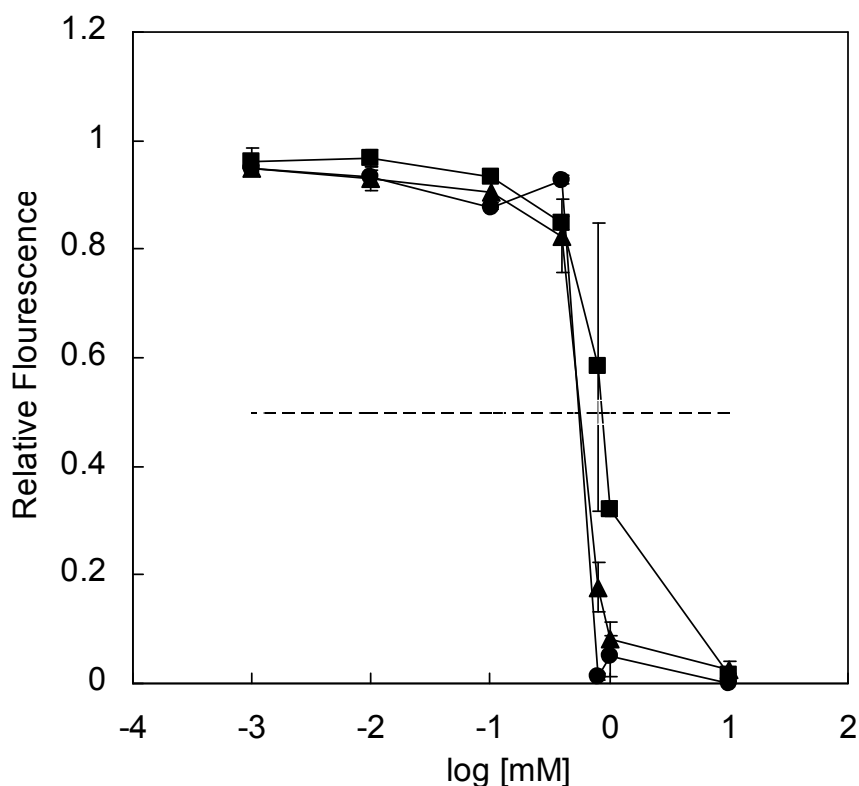
Figure 7.6 Antibacterial activity of polyonium solution with E. coli after 4 h of exposure. The relative fluorescence at 590 nm of the *E.coli* with polyonium to the fluorescence of *E.coli* with no polyonium versus the log of the polyelectrolyte concentration in mM, (■) PVBTMA, (▲) PVBTMP, (●) PVBDMS and the dashed line is 50% viability line.

PEMUs have been used as antibacterial coatings on surfaces preventing the attachment of bacteria,[204-206] by killing bacteria on contact[207-209] or by leaching antiseptic (as silver ions) or antibiotics into solution.[210] In the non adhering strategy, the bacteria biofilms cannot be formed due to the failure of the bacteria to adhere to the surface.[194]

High surface roughness, high hydrophilicity of the surface, and the film modulus have an effect on bacteria adhesion on the surface.[200] Antibiotics and silver ions are the most used biocidal reagent in the antibacterial leaching PEMUs.[200] For contact killing PEMUs, polycations possessing antibacterial activity in solutions are usually used for contact killing PEMUs. However in PEMUs, the polycation are engaged with the polyanion to different extents. The charged groups of the polycations should be available for interaction with the negatively charged membrane of the bacteria. Therefore, the antibacterial activity of polycations in solution is different from its activity in the PEMUs. For example, the antibacterial activity of chitosan and its derivatives are known to be biocidal in solution and are influenced by PEMU assembly conditions (salt and pH).[200] The contact Live/Dead assay of *E.coli* on the three polyonium terminated PEMUs showed that PVBTMA, PVBTMP and PVBDMS killed 39%, 40% and 50% of the E.coli, respectively. Therefore, the polyonium biocidal activity in PEMU is low and not sufficient enough to be used as a biocidal PEMU.

7.7 Conclusion

The difference in the behavior of the A7r5 cells on the three polyoniums terminated PEMUs ensure the effect of the heteroatom on cell adherence and growth. It is speculated that the difference in cell behavior on sulfonium compared to ammonium and phosphonium PEMUs may be due to a difference in the protein folding on the sulfonium that formed a more exposed RGD moiety. In future further research to investigate the exposed RGD on the three polyonium is needed. The three polyoniums failed to show any significant antibacterial activity in the multilayer form although they possessed antibacterial activity at 10 mM in solution.

CHAPTER 8

CONCLUSION AND FUTURE REMARKS

Polyelectrolyte multilayers can be used as coatings for other materials or as an assembly by themselves. In this work it is shown that the use of a polycation precursor to a photoluminscent polymer in optoelectronic and that of polyelectroyte multilayer in biomaterial.

In Chapter 3, a method to enhance the photoluminescence (PL) of PPV was achieved by pursing a carbonyl free route using the PEGNOPS as a counterion. The PEGNOPS suppressed formation of carbonyl by decreasing the diffusion of oxygen to the PXT backbone. The other role of PEGNOPS was undergoing oxidation in its PEG units. The PEGNOPS can be used as a preservative for PXT from photo-oxidation at room temperature in light. This PEGNOPS can be exchanged as needed with another counterion prior to use.

In Chapter 4, the effect of the intra and inter molecular interaction between the twenty PEG units and this interaction effect on restricting the PXT chain in a conformation that favors E2 elimination was revealed by a coordinated simulation and experimental results. In the future, the assembly of the PXT-PEGNOPS in an OLED assembly to study its efficiency is required.

In Chapter 5, a difference in the mechanism of elimination of PXT with different functional group polyanions (carboxylate and aromatic sulfonate) was reported. The functional group of the polyanion affected the optical properties of the films. More research is required to proof their potential use as hole and electron transport layer in an OLED assembly.

In Chapter 6, the synthesis and characterization of three polyoniums polycations by the modification of poly(vinyl benzene chloride) (PVBCl) were described. The three polyoniums showed the same characteristics (wettability, hydration, thickness) when assembled in multilayers.

In Chapter 7, the effect of the heteroatom on the A7r5 cells growth and adhesion was reported. The phosphonium and ammonium terminated multilayers exhibited

cytophobic properties. The *in vivo* studies are required to check if this cytophobic property persists in the physiological conditions (other than pH and salt).

REFERENCES

1.   Avci, D.; Mol, N.; Dagasan, L. *Polym. Bull.* **2002,** 48, 353-359.

2.   Yue, Q. Y.; Gao, B. Y.; Wang, Y.; Zhang, H.; Sun, X.; Wang, S. G.; Gu Roy, R. *J Hazard Mater* **2008,** 152, 221-7.

3.   Schanze, K. S.; Shelton, A. H. *Langmuir* **2009,** 25, 13698-13702.

4.   Ondaral, S.; Usta, M.; Gumusderelioglu, M.; Arsu, N.; Balta, D. K. *J. Appl. Polym. Sci.* **2010,** 116, 1157-1164.

5.   Langmuir, I.; Schaefer, V. J. *J. Am. Chem. Soc.* **1937,** 59, 2075-6.

6.   Blodgett, K. B. *J. Am. Chem. Soc.* **1935,** 57, 1007-22.

7.   Nuzzo, R. G.; Allara, D. L. *J. Am. Chem. Soc.* **1983,** 105, 4481-3.

8.   Tang, Z.; Wang, Y.; Podsiadlo, P.; Kotov, N. A. *Adv. Mater.* **2006,** 18, 3203-3224.

9.   Decher, G.; Hong, J. D. *Makromol. Chem., Macromol. Symp.* **1991,** 46, 321-7.

10.   Decher, G.; Schmitt, J. *Prog. Colloid Polym. Sci.* **1992,** 89, 160-4.

11.   Zhang, X.; Chen, H.; Zhang, H. *Chem. Commun.* **2007**, 1395-1405.

12.   Markarian, M. Z.; Moussallem, M. D.; Jomaa, H. W.; Schlenoff, J. B. *Biomacromolecules* **2007,** 8, 59-64.

13.   Jaber, J. A.; Schlenoff, J. B. *Curr. Opin. Colloid Interface Sci.* **2006,** 11, 324-329.

14.   Hammond, P. T. *Adv. Mater.* **2004,** 16, 1271-1293.

15.   Rmaile, H. H.; Schlenoff, J. B. *J. Am. Chem. Soc.* **2003,** 125, 6602-6603.

16.   Kapnissi, C. P.; Akbay, C.; Schlenoff, J. B.; Warner, I. M. *Anal. Chem.* **2002,** 74, 2328-2335.

17.   Graul, T. W.; Schlenoff, J. B. *Anal. Chem.* **1999,** 71, 4007-4013.

18.   Boudou, T.; Crouzier, T.; Ren, K.; Blin, G.; Picart, C. *Adv. Mater.* **2010,** 22, 441-467.

19.   Lvov, Y.; Decher, G.; Sukhorukov, G. *Macromolecules* **1993,** 26, 5396-9.

20. Trybala, A.; Szyk-Warszynska, L.; Warszynski, P. *Colloids Surf., A* **2009,** 343, 127-132.

21. Hoogeveen, N. G.; Cohen Stuart, M. A.; Fleer, G. J.; Boehmer, M. R. *Langmuir* **1996,** 12, 3675-3681.

22. Okubo, T.; Suda, M. *Colloid Polym. Sci.* **1999,** 277, 813-817.

23. Schwarz, S.; Eichhorn, K. J.; Wischerhoff, E.; Laschewsky, A. *Colloids Surf., A* **1999,** 159, 491-501.

24. Jomaa, H. W.; Schlenoff, J. B. *Macromolecules* **2005,** 38, 8473-8480.

25. Dubas, S. T.; Schlenoff, J. B. *Langmuir* **2001,** 17, 7725-7727.

26. Lavalle, P.; Gergely, C.; Cuisinier, F. J. G.; Decher, G.; Schaaf, P.; Voegel, J. C.; Picart, C. *Macromolecules* **2002,** 35, 4458-4465.

27. Jourdainne, L.; Arntz, Y.; Senger, B.; Debry, C.; Voegel, J.-C.; Schaaf, P.; Lavalle, P. *Macromolecules* **2007,** 40, 316-321.

28. McAloney, R. A.; Sinyor, M.; Dudnik, V.; Goh, M. C. *Langmuir* **2001,** 17, 6655-6663.

29. Salomäki, M.; Vinokurov Igor, A.; Kankare, J. *Langmuir* **2005,** 21, 11232-40.

30. Cini, N.; Tulun, T.; Decher, G.; Ball, V. *J. Am. Chem. Soc.* **2010,** 132, 8264-8265.

31. Schlenoff, J. B.; Rmaile, A. H.; Bucur, C. B. *J. Am. Chem. Soc.* **2008,** 130, 13589-13597.

32. Sui, Z.; Salloum, D.; Schlenoff, J. B. *Langmuir* **2003,** 19, 2491-2495.

33. Lynn, D. M. *Adv. Mater.* **2007,** 19, 4118-4130.

34. Elzbieciak, M.; Kolasinska, M.; Zapotoczny, S.; Krastev, R.; Nowakowska, M.; Warszynski, P. *Colloids Surf., A* **2009,** 343, 89-95.

35. Shiratori, S. S.; Rubner, M. F. *Macromolecules* **2000,** 33, 4213-4219.

36. Castner, D. G.; Ratner, B. D. *Surf. Sci.* **2002,** 500, 28-60.

37. Olenych Scott, G.; Moussallem Maroun, D.; Salloum David, S.; Schlenoff Joseph, B.; Keller Thomas, C. S. *Biomacromolecules* **2005,** 6, 3252-8.

38. Thompson, M. T.; Berg, M. C.; Tobias, I. S.; Rubner, M. F.; Van Vliet, K. J. *Biomaterials* **2005,** 26, 6836-6845.

39.   Chen Alice, A.; Khetani Salman, R.; Lee, S.; Bhatia Sangeeta, N.; Van Vliet Krystyn, J. *Biomaterials* **2009,** 30, 1113-20.

40.   Richert, L.; Boulmedais, F.; Lavalle, P.; Mutterer, J.; Ferreux, E.; Decher, G.; Schaaf, P.; Voegel, J.-C.; Picart, C. *Biomacromolecules* **2004,** 5, 284-94.

41.   Salloum, D. S.; Olenych, S. G.; Keller, T. C. S.; Schlenoff, J. B. *Biomacromolecules* **2005,** 6, 161-167.

42.   Lee, D.; Cohen, R. E.; Rubner, M. F. *Langmuir* **2005,** 21, 9651-9659.

43.   Guyomard, A.; De, E.; Jouenne, T.; Malandain, J.-J.; Muller, G.; Glinel, K. *Adv. Funct. Mater.* **2008,** 18, 758-765.

44.   Meng, S.; Liu, Z.; Shen, L.; Guo, Z.; Chou Laisheng, L.; Zhong, W.; Du, Q.; Ge, J. *Biomaterials* **2009,** 30, 2276-83.

45.   Chiang, C. K.; Fincher, C. R., Jr.; Park, Y. W.; Heeger, A. J.; Shirakawa, H.; Louis, E. J.; Gau, S. C.; MacDiarmid, A. G. *Phys. Rev. Lett.* **1977,** 39, 1098-101.

46.   Burroughes, J. H.; Bradley, D. D. C.; Brown, A. R.; Marks, R. N.; Mackay, K.; Friend, R. H.; Burns, P. L.; Holmes, A. B. *Nature* **1990,** 347, 539-41.

47.   Tang, C. W.; VanSlyke, S. A. *Appl. Phys. Lett.* **1987,** 51, 913-15.

48.   Hulvat James, F.; Sofos, M.; Tajima, K.; Stupp Samuel, I. *J Am Chem Soc* **2005,** 127, 366-72.

49.   Schoo, H. F. M.; Demandt, R. J. C. E. *Philips J. Res.* **1998,** 51, 527-533.

50.   Ferreira, M.; Rubner, M. F. *Macromolecules* **1995,** 28, 7107-14.

51.   Onitsuka, O.; Fou, A. C.; Ferreira, M.; Hsieh, B. R.; Rubner, M. F. *J. Appl. Phys.* **1996,** 80, 4067-4071.

52.   Cho, J.; Char, K.; Kim, S. Y.; Hong, J. D.; Kyun Lee, S.; Young Kim, D. *Thin Solid Films* **2000,** 379, 188-194.

53.   Kesters, E.; de Kok, M. M.; Carleer, R. A. A.; Czech, J. H. P. B.; Adriaensens, P. J.; Gelan, J. M.; Vanderzande, D. J. *Polymer* **2002,** 43, 5749-5755.

54.   Cho, B. R. *Prog. Polym. Sci.* **2002,** 27, 307-355.

55.   H. Bubert, H. J. *Wiley-VCH* **2002**.

56.   Arsov, L.; Ramasubramanian, M.; Popov, B. N. *Charact. Mater.* **2003,** 2, 735-744.

57.   Milling, A. J. **1999,** 87.

58.   Santos, N. C.; Castanho, M. A. R. B. *Biophys. Chem.* **2004,** 107, 133-149.

59.   Smith, B. *CRC Press LLC* **1999**.

60.   Freshney, I. **1987**.

61.   Butler, M. *IRL PRESS* **1996**.

62.   Brynda, E.; Houska, M.; Jirouskova, M.; Dyr, J. E. *J. Biomed. Mater. Res.* **2000,** 51, 249-257.

63.   Singleton, P. *Wiley* **1995**.

64.   Burroughes, J. H.; Bradley, D. D. C.; Brown, A. R.; Marks, R. N.; Mackay, K.; Friend, R. H.; Burns, P. L.; Holmes, A. B. *Nature* **1990,** 347, 539-41.

65.   Chen, L.-M.; Hong, Z.; Li, G.; Yang, Y. *Adv. Mater.* **2009,** 21, 1434-1449.

66.   Kraft, A.; Grimsdale, A. C.; Holmes, A. B. *Angew. Chem., Int. Ed.* **1998,** 37, 403-428.

67.   Herold, M.; Gmeiner, J.; Riesβ, W.; Schwoerer, M. *Synth. Met.* **1996,** 76, 109-12.

68.   Prelipceanu, M.; Prelipceanu, O.-S.; Tudose, O.-G.; Leontie, L.; Grimm, B.; Schrader, S. *Mater. Sci. Semicond. Process.* **2007,** 10, 77-89.

69.   Massuyeau, F.; Duvail, J. L.; Athalin, H.; Lorcy, J. M.; Lefrant, S.; Wery, J.; Faulques, E. *Nanotechnology* **2009,** 20, 155701-155708.

70.   Resmi, R.; Amrutha, S. R.; Jayakannan, M. *J. Polym. Sci., Part A: Polym. Chem.* **2009,** 47, 2631-2646.

71.   Bakueva, L.; Sargent, E. H.; Resendes, R.; Bartole, A.; Manners, I. *J. Mater. Sci.: Mater. Electron.* **2001,** 12, 21-25.

72.   Lee, W.-H.; Kong, H.; Oh, S.-Y.; Shim, H.-K.; Kang, I.-N. *J. Polym. Sci., Part A: Polym. Chem.* **2008,** 47, 111-120.

73.   Zou, Y.; Sang, G.; Zhou, E.; Li, Y. *Macromol. Chem. Phys.* **2008,** 209, 431-438.

74.   Yousaf, S. M.; Bower, K. E.; Sychov, M. M.; Yousaf, M. R. *Journal of Materials Science* **2005,** 40, 5507-5510.

75.   Chaieb, A.; Vignau, L.; Brown, R.; Wantz, G.; Huby, N.; Francois, J.; Dagron-Lartigau, C. *Opt. Mater.* **2008,** 31, 68-74.

76.   Wong, J. E.; Detert, H.; Brehmer, L.; Schrader, S. *Appl. Surf. Sci.* **2005,** 246, 458-463.

77.   Schoo, H. F. M.; Demandt, R. J. C. E. *Philips J. Res.* **1998,** 51, 527-533.

78.   Schlenoff, J. B.; Wang, L. J. *Macromolecules* **1991,** 24, 6653-9.

79.   Murase, I.; Ohnishi, T.; Noguchi, T.; Hirooka, M. *Polym. Commun.* **1984,** 25, 327-9.

80.   Hsieh, B. R.; Antoniadis, H.; Abkowitz, M. A.; Stolka, M. *Polym. Prepr.* **1992,** 33, 414-15.

81.   Papadimitrakopoulos, F.; Konstadinidis, K.; Miller, T. M.; Opila, R.; Chandross, E. A.; Galvin, M. E. *Chem. Mater.* **1994,** 6, 1563-8.

82.   Yan, M.; Rothberg, L. J.; Papadimitrakopoulos, F.; Galvin, M. E.; Miller, T. M. *Phys. Rev. Lett.* **1994,** 73, 744-7.

83.   Yan, M.; Rothberg, L.; Galvin, M. E.; Miller, T. M.; Papadimitrakopoulos, F. *Int. SAMPE Tech. Conf.* **1995,** 27, 694-702.

84.   Nguyen, T. P. *Mater. Sci. Semicond. Process.* **2006,** 9, 198-203.

85.   Scott, J. C.; Kaufman, J. H.; Brock, P. J.; DiPietro, R.; Salem, J.; Goitia, J. A. *J. Appl. Phys.* **1996,** 79, 2745-51.

86.   De Kok, M. M.; Van Breemen, A. J. J. M.; Carleer, R. A. A.; Adriaensens, P. J.; Gelan, J. M.; Vanderzande, D. J. *Acta Polym.* **1999,** 50, 28-34.

87.   Zoppi, L.; Calzolari, A.; Ruini, A.; Ferretti, A.; Caldas, M. J. *Phys. Rev. B: Condens. Matter Mater. Phys.* **2008,** 78, 165204-165206.

88.   Herold, M.; Gmeiner, J.; Schwoerer, M. *Polym. Adv. Technol.* **1999,** 10, 251-258.

89.   Gustafsson, G.; Cao, Y.; Treacy, G. M.; Klavetter, F.; Colaneri, N.; Heeger, A. J. *Nature* **1992,** 357, 477-9.

90.   Brown, A. R.; Bradley, D. D. C.; Burroughes, J. H.; Friend, R. H.; Greenham, N. C.; Burn, P. L.; Holmes, A. B.; Kraft, A. *Appl. Phys. Lett.* **1992,** 61, 2793-5.

91.   Bradley, D. D. C.; Brown, A. R.; Burn, P. L.; Friend, R. H.; Holmes, A. B.; Kraft, A. *Springer Ser. Solid-State Sci.* **1992,** 107, 304-9.

92.   Marletta, A.; Gonçalves, D.; Oliveira, O. N., Jr.; Faria, R. M.; Guimarães, F. E. *Adv. Mater.* **2000,** 12, 69-74.

93.   Treger, J. S.; Ma, V. Y.; Gao, Y.; Wang, C.-C.; Jeon, S.; Robinson, J. M.; Wang, H.-L.; Johal, M. S. *Langmuir* **2008,** 24, 13127-13131.

94.   Yan, M.; Rothberg, L. J.; Kwock, E. W.; Miller, T. M. *Phys. Rev. Lett.* **1995,** 75, 1992-5.

95.   Jakubiak, R.; Collison, C. J.; Wan, W. C.; Rothberg, L. J.; Hsieh, B. R. *J. Phys. Chem. A* **1999,** 103, 2394-2398.

96.   Son, S.; Dodabalapur, A.; Lovinger, A. J.; Galvin, M. E. *Science* **1995,** 269, 376-8.

97.   Cao, Y.; Yu, G.; Heeger, A. J.; Yang, C. Y. *Appl. Phys. Lett.* **1996,** 68, 3218-3220.

98.   Pei, Q.; Yu, G.; Zhang, C.; Yang, Y.; Heeger, A. J. *Science* **1995,** 269, 1086-8.

99.   Wessling, R. A.; Zimmerman, R. G. Polyelectrolytes from bis sulfonium salts. 66-591706
3401152, 19661103., 1968.

100.   Grimsdale, A. C.; Leok Chan, K.; Martin, R. E.; Jokisz, P. G.; Holmes, A. B. *Chem. Rev.* **2009,** 109, 897-1091.

101.   Cumpston, B. H.; Jensen, K. F. *J. Appl. Polym. Sci.* **1998,** 69, 2451-2458.

102.   Cheng, H.-L.; Lin, K.-F. *J. Polym. Res.* **1999,** 6, 123-131.

103.   Machado, J. M.; Schlenoff, J. B.; Glatkowski, P. J.; Karasz, F. E. *Polym. Mater. Sci. Eng.* **1987,** 57, 446-50.

104.   Raanby, B. *J. Anal. Appl. Pyrolysis* **1989,** 15, 237-47.

105.   Brown, A. R.; Greenham, N. C.; Bradley, D. D. C.; Friend, R. H.; Burn, P. L.; Kraft, A.; Holmes, A. B. *Conduct. Polym., Conduct. Polym. Conf.* **1992**, 7-15.

106.   Sauer, G.; Kilo, M.; Hund, M.; Wokaun, A.; Karg, S.; Meier, M.; Riesβ, W.; Schwoerer, M.; Suzuki, H.; et al. *Fresenius' J. Anal. Chem.* **1995,** 353, 642-6.

107.   De Kok, M. M.; Van Breemen, A. J. J. M.; Carleer, R. A. A.; Adriaensens, P. J.; Gelan, J. M.; Vanderzande, D. J. *Acta. Polym.* **1999,** 50, 28-34.

108.   Grage, M. M. L.; Wood, P. W.; Ruseckas, A.; Pullerits, T.; Mitchell, W.; Burn, P. L.; Samuel, I. D. W.; Sundstrom, V. *J. Chem. Phys.* **2003,** 118, 7644-7650.

109.   Yousaf, S. M.; Bower, K. E.; Sychov, M. M.; Yousaf, M. R. *J. Mater. Sci.* **2005,** 40, 5507-5510.

110.   Chen, L.-M.; Hong, Z.; Li, G.; Yang, Y. *Adv. Mater* **2009,** 21, 1434-1449.

111.   Feast, W. J.; Cacialli, F.; Koch, A. T. H.; Daik, R.; Lartigau, C.; Friend, R. H.; Beljonne, D.; Bredas, J.-L. *J. Mater. Chem.* **2007,** 17, 907-912.

112.   Prelipceanu, M.; Prelipceanu, O.-S.; Tudose, O.-G.; Leontie, L.; Grimm, B.; Schrader, S. *Mater. Sci. Semicond. Process.* **2007,** 10, 77-89.

113.   Grimsdale, A. C.; Leok Chan, K.; Martin, R. E.; Jokisz, P. G.; Holmes, A. B. *Chem. Rev.* **2009,** 109, 897-1091.

114.   Webster, G. R.; Whitelegg, S. A.; Bradley, D. D. C.; Burn, P. L. *Synthetic Metals* **2001,** 119, 269-270.

115.   Papadimitrakopoulos, F.; Konstadinidis, K.; Miller, T. M.; Opila, R.; Chandross, E. A.; Galvin, M. E. *Chem. Mater.* **1994,** 6, 1563-8.

116.   Marletta, A.; Gonçalves, D.; Oliveira, O. N., Jr.; Faria, R. M.; Guimarães, F. E. *Adv. Mater.* **2000,** 12, 69-74.

117.   Schlenoff, J. B.; Wang, L. J. *Macromolecules* **1991,** 24, 6653-9.

118.   Marletta, A.; Castro, F. A.; Borges, C. A. M.; Oliveira, O. N., Jr.; Faria, R. M.; Guimarães, F. E. G. *Macromolecules* **2002,** 35, 9105-9109.

119.   Kas, O. Y.; Charati, M. B.; Rothberg, L. J.; Galvin, M. E.; Kiick, K. L. *J. Mater. Chem.* **2008,** 18, 3847-3854.

120.   Moses, D.; Schmechel, R.; Heeger, A. J. *Synth. Met.* **2003,** 139, 807-810.

121.   Yaliraki, S. N.; Silbey, R. J. *J. Chem. Phys.* **1996,** 104, 1245-53.

122.   Son, S.; Dodabalapur, A.; Lovinger, A. J.; Galvin, M. E. *Science* **1995,** 269, 376-8.

123.   Nelson, J.; Kwiatkowski, J. J.; Kirkpatrick, J.; Frost, J. M. *Acc. Chem. Res.* **2009,** 42, 1768-1778.

124.   Yan, M.; Rothberg, L.; Galvin, M. E.; Miller, T. M.; Papadimitrakopoulos, F. *Int. SAMPE Tech. Conf.* **1995,** 27, 694-702.

125.   Cheng, H.-L.; Lin, K.-F. *J. Polym. Res.* **1999,** 6, 123-131.

126.   Kimura, M.; Sato, M.; Adachi, N.; Fukawa, T.; Kanbe, E.; Shirai, H. *Chemistry of Materials* **2007,** 19, 2809-2815.

127.   Schwartz, B. J. *Annu. Rev. Phys. Chem.* **2003,** 54, 141-172.

128.   Peng, K.-Y.; Chen, S.-A.; Fann, W.-S.; Chen, S.-H.; Su, A.-C. *J. Phys. Chem. B* **2005,** 109, 9368-73.

129.   Winokur, M. J.; Chunwachirasiri, W. *J. Polym. Sci., Part B Polym. Phys.* **2003,** 41, 2630-2648.

130.   Shah, H. V.; McGhie, A. R.; Arbuckle, G. A. *Thermochim. Acta* **1996,** 287, 319-326.

131. Wu, A.; Yokoyama, S.; Watanabe, S.; Kakimoto, M.-a.; Imai, Y.; Araki, T.; Iriyama, K. *Thin Solid Films* **1994,** 244, 750-3.

132. Fou, A. C.; Onitsuka, O.; Ferreira, M.; Rubner, M. F.; Hsieh, B. R. *J. Appl. Phys.* **1996,** 79, 7501-7509.

133. Tarabia, M.; Hong, H.; Davidov, D.; Kirstein, S.; Steitz, R.; Neumann, R.; Avny, Y. *J. Appl. Phys.* **1998,** 83, 725-732.

134. Abe, S.; Chen, L. *J. Polym. Sci., Part B: Polym. Phys.* **2003,** 41, 1676-1679.

135. Wessling, R. A.; Zimmerman, R. G. Polyelectrolytes from bis sulfonium salts. U.S. Patent 591706,
, November, **1968**.

136. Zheng, L.; Chen, M.; Yang, W. *Proc. Natl. Acad. Sci. U. S. A.* **2008,** 105, 20227-20232.

137. Shah, H. V.; Arbuckle, G. A. *Macromolecules* **1999,** 32, 1413-1423.

138. Garay, R. O.; Sarimbalis, M. N.; Hernandez, S. A.; Montani, R. S. *Macromolecules* **2000,** 33, 4398-4402.

139. Kesters, E.; Gillissen, S.; Motmans, F.; Lutsen, L.; Vanderzande, D. *Macromolecules* **2002,** 35, 7902-7910.

140. Pichler, K.; Halliday, D. A.; Bradley, D. D. C.; Burn, P. L.; Friend, R. H.; Holmes, A. B. *J. Phys.: Condens. Matter* **1993,** 5, 7155-72.

141. Rauscher, U.; Schütz, L.; Greiner, A.; Bässler, H. *J. Phys. Condens. Matter* **1989,** 1, 9751-63.

142. Hamada, Y.; Adachi, C.; Tsutsui, T.; Saito, S. *Jpn. J. Appl. Phys., Part 1* **1992,** 31, 1812-16.

143. Braun, D.; Heeger, A. J. *Appl. Phys. Lett.* **1991,** 59, 878.

144. Ogawa, M.; Tamanoi, M.; Ohkita, H.; Benten, H.; Ito, S. *Sol. Energy Mater. Sol. Cells* **2009,** 93, 369-374.

145. Decher, G.; Hong, J. D. *Makromol. Chem., Macromol. Symp.* **1991,** 46, 321-7.

146. Decher, G. *Science* **1997,** 277, 1232-1237.

147. Cho, J.; Char, K.; Hong, J.-D.; Kim, D. Y. *Mol. Cryst. Liq. Cryst. Sci. Technol., Sect. A* **2001,** 371, 75-78.

148. Ogawa, M.; Kudo, N.; Ohkita, H.; Ito, S.; Benten, H. *Appl. Phys. Lett.* **2007,** 90, 223107/1-223107/3.

149.   Al-Hariri, L. A.; Schlenoff, J. B. *Polymer* **2010,** 51, 2993-2997.

150.   Pocas, L. C.; Campos, K. R.; Nogueira, S. L.; Piovesan, E.; Silva, R. A.; Vega, M. L.; Marletta, A. *J. Non-Cryst. Solids* **2008,** 354, 4852-4855.

151.   Sauer, G.; Kilo, M.; Hund, M.; wokaun, A.; Karg, S.; Meier, M.; Riess, W.; Schwoerer, M.; Suzuki, H.; et al. *Fresenius' J. Anal. Chem.* **1995,** 353, 642-6.

152.   Yang, C. Q.; Gu, X. *Res. Chem. Intermed.* **1999,** 25, 411-424.

153.   Lin, S.-Y.; Yu, H.-L.; Li, M.-J. *Polymer* **1999,** 40, 3589-3593.

154.   Kučera, F.; Jančář, J. *Polym. Eng. Sci.* **1998,** 38, 783-792.

155.   Bassindale, A. R.; Katampe, I.; Maesano, M. G.; Patel, P.; Taylor, P. G. *Tetrahedron Lett.* **1999,** 40, 7417-7420.

156.   Decher, G.; Hong, J. D. *Ber. Bunsen-Ges. Phys. Chem.* **1991,** 95, 1430-4.

157.   Bertrand, P.; Jonas, A.; Laschewsky, A.; Legras, R. *Macromol. Rapid Commun.* **2000,** 21, 319-348.

158.   Mamedov, A. A.; Kotov, N. A.; Prato, M.; Guldi, D. M.; Wicksted, J. P.; Hirsch, A. *Nature Materials* **2002,** 1, 190-194.

159.   Tang, Z. Y.; Kotov, N. A.; Magonov, S.; Ozturk, B. *Nature Materials* **2003,** 2, 413-U8.

160.   Jisr, R. M.; Rmaile, H. H.; Schlenoff, J. B. *Angew. Chem., Int. Ed.* **2005,** 44, 782-785.

161.   Jiang, B.; Barnett, J. B.; Li, B. *Nanotechnol., Sci. Appl.* **2009,** 2, 21-27.

162.   Müller, M.; Meier-Haack, J.; Schwarz, S.; Buchhammer, H. M.; Eichhorn, K. J.; Janke, A.; Kessler, B.; Nagel, J.; Oelmann, M.; Reihs, T.; Lunkwitz, K. *J. Adhes.* **2004,** 80, 521-547.

163.   Schwarz, S.; Nagel, J.; Jaeger, W. *Macromol. Symp.* **2004,** 211, 201-216.

164.   Farhat, T. R.; Schlenoff, J. B. *Langmuir* **2001,** 17, 1184-1192.

165.   Dubas, S. T.; Schlenoff, J. B. *Macromolecules* **1999,** 32, 8153-8160.

166.   Salomäki, M.; Vinokurov Igor, A.; Kankare, J. *Langmuir* **2005,** 21, 11232-40.

167.   Salomäki, M.; Kankare, J. *Macromolecules* **2008,** 41, 4423-4428.

168.   Ariga, K.; Hill, J. P.; Ji, Q. *Phys. Chem. Chem. Phys.* **2007,** 9, 2319-2340.

169.   Laschewsky, A.; Mallwitz, F.; Baussard, J.-F.; Cochin, D.; Fischer, P.; Jiwan, J.-L. H.; Wischerhoff, E. *Macromol. Symp.* **2004,** 211, 135-155.

170.   Boudou, T.; Crouzier, T.; Auzely-Velty, R.; Glinel, K.; Picart, C. *Langmuir* **2009,** 25, 13809-13819.

171.   Quinn, A.; Such, G. K.; Quinn, J. F.; Caruso, F. *Adv. Funct. Mater.* **2008,** 18, 17-26.

172.   Jaeger, W.; Bohrisch, J.; Laschewsky, A. *Prog. Polym. Sci.* **2010,** 35, 511-577.

173.   Jaber, J. A.; Schlenoff, J. B. *Langmuir* **2007,** 23, 896-901.

174.   Papadimitrakopoulos, F.; Yan, M.; Rothberg, L. J.; Katz, H. E.; Chandross, E. A.; Galvin, M. E. *Mol. Cryst. Liq. Cryst. Sci. Technol., Sect. A* **1994,** 256, 663-9.

175.   Jones, G. D. Chloromethylated polystyrene and quaternary ammonium salts. **U.S. Patent** 2694702, November, 1954.

176.   Hatch, M. J.; McMaster, E. Water-soluble vinylbenzylsulfonium monomers and polymers. **U.S. Patent** 3078259, February, 1963.

177.   Garner, A. Y.; Abramo, J. G.; Chapin, E. C. Ethylenically unsaturated ionic phosphonium salts. **U.S. Patent** 3065272, November, 1962.

178.   Norwood, D. P.; Benmouna, M.; Reed, W. F. *Macromolecules* **1996,** 29, 4293-4304.

179.   Morfin, I.; Reed, W. F.; Rinaudo, M.; Borsali, R. *J. Phys. II* **1994,** 4, 1001-19.

180.   Sexsmith, D. R.; Frazza, E. J. Haloalkyl styrene-phosphine copolymers for coatings, paper sizing, and textile treatment. **U.S. Patent** 3168502, February, 1965.

181.   Hoover, M. F. *J. Macromol. Sci., Chem.* **1970,** 4, 1327-417.

182.   Gorbet, M. B.; Sefton, M. V. *Biomaterials* **2004,** 25, 5681-5703.

183.   Elbert, D. L.; Hubbell, J. A. *Annu. Rev. Mater. Sci.* **1996,** 26, 365-394.

184.   Meredith, J. C. *J. Mater. Chem.* **2009,** 19, 34-45.

185.   Morgan, M. R.; Humphries, M. J.; Bass, M. D. *Nat. Rev. Mol. Cell Biol.* **2007,** 8, 957-969.

186.   Salloum, D. S.; Schlenoff, J. B. *Biomacromolecules* **2004,** 5, 1089-1096.

187.   Mendelsohn, J. D.; Yang, S. Y.; Hiller, J. A.; Hochbaum, A. I.; Rubner, M. F. *Biomacromolecules* **2003,** 4, 96-106.

188. Lvov, Y.; Ariga, K.; Ichinose, I.; Kunitake, T. *J. Am. Chem. Soc.* **1995,** 117, 6117-23.

189. Tristan, F.; Palestino, G.; Menchaca, J. L.; Perez, E.; Atmani, H.; Cuisinier, F.; Ladam, G. *Biomacromolecules* **2009,** 10, 2275-2283.

190. Indolfi, C.; Mongiardo, A.; Curcio, A.; Torella, D. *Trends Cardiovasc. Med.* **2003,** 13, 142-148.

191. Olenych, S. G.; Moussallem, M. D.; Salloum, D. S.; Schlenoff, J. B.; Keller, T. C. S. *Biomacromolecules* **2005,** 6, 3252-3258.

192. Moussallem, M. D.; Olenych, S. G.; Scott, S. L.; Keller, T. C. S., III; Schlenoff, J. B. *Biomacromolecules* **2009,** 10, 3062-3068.

193. Boulmedais, F.; Frisch, B.; Etienne, O.; Lavalle, P.; Picart, C.; Ogier, J.; Voegel, J. C.; Schaaf, P.; Egles, C. *Biomaterials* **2004,** 25, 2003-2011.

194. Lichter, J. A.; Van Vliet, K. J.; Rubner, M. F. *Macromolecules* **2009,** 42, 8573-8586.

195. Ong, Y.-L.; Razatos, A.; Georgiou, G.; Sharma, M. M. *Langmuir* **1999,** 15, 2719-2725.

196. Vasilev, K.; Sah, V.; Anselme, K.; Ndi, C.; Mateescu, M.; Dollmann, B.; Martinek, P.; Ys, H.; Ploux, L.; Griesser, H. J. *Nano Lett.* **2010,** 10, 202-207.

197. Tashiro, T. *Macromol. Mater. Eng.* **2001,** 286, 63-87.

198. Kuegler, R.; Bouloussa, O.; Rondelez, F. *Microbiology* **2005,** 151, 1341-1348.

199. Gilbert, P.; Moore, L. E. *J. Appl. Microbiol.* **2005,** 99, 703-715.

200. Lichter, J. A.; Rubner, M. F. *Langmuir* **2009,** 25, 7686-7694.

201. Takahashi, E.; Sanda, F.; Endo, T. *J. Polym. Sci., Part A Polym. Chem.* **2003,** 41, 3816-3827.

202. Discher, D. E.; Janmey, P.; Wang, Y.-l. *Science* **2005,** 310, 1139-1143.

203. Isenberg, B. C.; Di Milla, P. A.; Walker, M.; Kim, S.; Wong, J. Y. *Biophys. J.* **2009,** 97, 1313-1322.

204. Ackart, W. B.; Camp, R. L.; Wheelwright, W. L.; Byck, J. S. *J. Biomed. Mater. Res.* **1975,** 9, 55-68.

205. Desai, N. P.; Hossainy, S. F.; Hubbell, J. A. *Biomaterials* **1992,** 13, 417-20.

206.   Arciola, C. R.; Radin, L.; Alvergna, P.; Cenni, E.; Pizzoferrato, A. *Biomaterials* **1993,** 14, 1161-4.

207.   Grapski, J. A.; Cooper, S. L. *Biomaterials* **2001,** 22, 2239-2246.

208.   Cen, L.; Neoh, K. G.; Kang, E. T. *Langmuir* **2003,** 19, 10295-10303.

209.   Tiller, J. C.; Liao, C.-J.; Lewis, K.; Klibanov, A. M. *Proc. Natl. Acad. Sci. U. S. A.* **2001,** 98, 5981-5985.

210.   Nonaka, T.; Uemura, Y.; Enishi, K.; Kurihara, S. *J. Appl. Polym. Sci.* **1996,** 62, 1651-1659.

BIOGRAPHICAL SKETCH

Lara A. Al-Hariri was born in Saida, city in South Lebanon, in September of 1982. She attended the Lebanese University of Beirut and graduated in 2004 with a *Maîtrise* degree in chemistry. In spring of 2005, Lara joined the research group of Professor Joseph B. Schlenoff at the Department of Chemistry and Biochemistry at The Florida State University. She worked on the applications of polyelectrolyte in biomaterials as well as in optoelectronics. During her work at as a graduate student, she published three papers and other two publications are still in preparation. She presented her work at national conference. Lara worked as a teaching assistant at The Florida State University during her PhD and she is a member of the American Chemical Society (ACS) and the American Association for the Advancement of Science (AAAS). Lara received her PhD on June 17, 2011.